Τεχνολογικό Πανεπιστήμιο Κύπρου
Faculty of Geotechnical Sciences and Environmental Management

Doctoral Dissertation

MECHANISTIC INSIGHTS AND DYNAMICS OF THE LIGHT-HARVESTING FUCOXANTHIN-CHLOROPHYLL A/C BINDING PROTEIN OF MARINE DIATOM FRAGILARIOPSIS SP

Charalampos Andreou

Limassol, December 2024

CYPRUS UNIVERSITY OF TECHNOLOGY

FACULTY OF GEOTECHNICAL SCIENCES AND

ENVIRONMENTAL MANAGEMENT

DEPARTMENT OF CHEMICAL ENGINEERING

Doctoral Dissertation

MECHANISTIC INSIGHTS AND DYNAMICS OF THE LIGHT-HARVESTING FUCOXANTHIN-CHLOROPHYLL A/C BINDING PROTEIN OF MARINE DIATOM FRAGILARIOPSIS SP

Charalampos Andreou

Limassol, December 2024

Approval form

Doctoral Dissertation

MECHANISTIC INSIGHTS AND DYNAMICS OF THE LIGHT-HARVESTING FUCOXANTHIN-CHLOROPHYLL A/C BINDING PROTEIN OF MARINE DIATOM FRAGILARIOPSIS SP

Presented by

Charalampos Andreou

Supervisor: Dr. Constantinos Varotsis

Signature _____

Member of the committee: Dr. Andreas Katsiotis

Signature _____

Member of the committee: Dr. Giorgos Gouridis

Signature _____

CYPRUS UNIVERSITY OF TECHNOLOGY

Limassol, December 2024

Copyrights

The approval of the dissertation by the Department of Chemical Engineering does not imply necessarily the approval by the Department of the views of the writer.

Acknowledgements

First of all, I would like to thank my supervisor Dr. Constantinos Varotsis for guiding me and supporting me through this period, called PhD.

Furthermore, I would like to thank all my fellow lab mates for cooperating and supporting me experimentally in the lab and especially, Dr Charalampos Tselios and Vasiliki Valianti who helped me with Raman Spectroscopy, Dr Aristos Ioannou and Constantinos Yiannakkos, who helped me with the isolation of FCPs and the culture of diatoms, and finally, our technician Dr Antonis Nicolaides . In addition, the transient absorption experiments were performed in the laboratory of Dr. Loukakos in the Ultraviolet Laser Facility, Foundation for Research and Technology-Hellas (FORTH), Institute of Electronic Structure and Laser (IESL) by Dr. Maria Polychronaki and Prof. Varotsis.

Last but not least, I would like to thank my parents for being next to me whenever I needed them throughout this journey.

ΠΕΡΙΛΗΨΗ

Τα θαλάσσια διάτομα εμπλέκονται σε σημαντικούς φωτοσυνθετικούς βιοχημικούς κύκλους, στην οξυγονική φωτοσύνθεση και στη σταθεροποίηση του άνθρακα. Τα διάτομα περιέχουν χλωροφύλλη και καροτενοειδή που είναι κυρίως υπεύθυνα για τη συγκομιδή φωτός και εν τέλει για τη διεξαγωγή φωτοσύνθεσης, καθώς και για τη φωτοπροστασία. Σε αυτή τη διατριβή, οι φασματοσκοπικές τεχνικές UV-Visible, fluorescence, Raman και Fourier-transform infrared spectroscopy, καθώς και η αναλυτική τεχνική της υγρής χρωματογραφίας υψηλής απόδοσης χρησιμοποιήθηκαν για τη μελέτη της απόκρισης των κυττάρων δύο διατόμων υπό διαφορετικές συνθήκες ανάπτυξης. Τα είδη του fragilariopsis sp και του phaeodactylum tricornutum έχουν επιλεγεί, τα οποία είναι και τα δύο κατηγοριοποιημένα ως πτεροειδή. Μεταβάλλοντας τις συνθήκες ανάπτυξης, παρατηρήθηκαν αλλαγές στη συγκέντρωση των παραγόμενων μορίων χρωμοφόρου καθώς και σημαντικές διαφορές στις ιδιότητες και τις αλληλεπιδράσεις που εμφανίζουν. Αυτές οι αλλαγές εξαρτώνται έντονα τόσο από την ένταση όσο και από το μήκος κύματος της πηγής φωτός που χρησιμοποιείται για την ανάπτυξη των διατομών.

Αναφέρονται τα φάσματα Raman συντονισμού των light-harvesting fucoxanthin-chlorophyll a/c binding proteins του θαλάσσιου διατόμου fragilariopsis sp. Οι μετατοπίσεις Raman του εμπλουτισμένου Διατόμου με ^{15}N-ισοτόπο παρέχει τα πρώτα φασματοσκοπικά στοιχεία για τον χαρακτηρισμό των ζωνών δεικτών C_a-N και επομένως των penta και hexa-coordinated καταστάσεων των χλωροφύλλων a/c στα FCPs. Κάτω από διεγέρσεις 405 και 442 nm raman, παρατηρούνται όλες οι ζώνες δεικτών των χλωροφύλλων a/c και οι αναθέσεις που βασίζονται σε ισότοπους παρέχουν νέες πληροφορίες σχετικά με τη δομή των χλωροφύλλων a/c στα FCPs και τις αλληλεπιδράσεις τους με το περιβάλλον πρωτεΐνης. Επομένως, το φάσμα Raman στα 405 nm προέρχεται από τις μεταβάσεις π -π* των χλωροφύλλων a/c. Με βάση τις μετατοπίσεις των ισοτόπων ^{15}N του C_a-N και σε συνδυασμό με άλλες ζώνες δείκτων, παρατηρούνται δύο ξεχωριστές διαμορφώσεις penta και hexa-coordinated καταστάσεων των χλωροφύλλων a/c. Επιπλέον, παρατηρήθηκαν δύο καρβονύλια keto σε 1679 (strong H-bonded) και 1691 cm-1 (weak H-bonded) και στα 405 και 442 nm φάσματα Raman, αντίστοιχα. Συλλογικά, τα αποτελέσματα παρέχουν σταθερά στοιχεία για τη φύση των δονητικών τρόπων των ενεργών φωτοσυνθετικών χρωστικών ουσιών χλωροφύλλων a/c

στα FCPs.

Επιπλέον, παρουσιάζονται τα εξαρτώμενα από το pH/pD φάσματα φθορισμού των FCPs του διατόμου fragilariopsis sp. Υπάρχει μια αναστρέψιμη μετάβαση 451 έως 455 nm συνοδευόμενη από μια μετάβαση 588 έως 586 nm της χλωροφύλλης c1/c2 σε εύρος pH/pD 4.9-8 με pKa = 5.4. Η ανταλλάξιμη θέση H/D της ομάδας 17-ακρυλικού της χλωροφύλλης c1/c2 χαρακτηρίστηκε από την ευαισθησία του pH/pD των ζωνών Soret και Qy και προτείνουμε ότι η χλωροφύλλες c1/c2 -ακρυλικού-H2O τμήματος μπορεί να δράσει ως αποδέκτης/δότης πρωτονίου. Υπό συνθήκες φωτός υψηλής έντασης, το τμήμα ακρυλικού του χλωροφύλλες c1/c2 πρωτονιώνεται, παρόμοιο με αυτό που παρατηρείται υπό όξινες συνθήκες. Στη φωτοπροστατευτική κατάσταση, η απορρόφηση των χλωροφύλλων c1/c2 μετατοπίζεται προς το κόκκινο και μοιάζει με την αναστρέψιμη μετάβαση από τη συγκομιδή φωτός σε κατάσταση ενεργειακής κατάστασης που συμβαίνει σε όξινο pH. Το επαγόμενο ΔpH και αυτό που δημιουργήθηκε από το φως υψηλής έντασης, είναι υπεύθυνο για την μετατοπισμένη προς το κόκκινο χλωροφύλλη c1/c2 λόγω της πρωτονίωσης της ομάδας ακρυλικού. Παρουσιάζουμε ένα μοντέλο που περιγράφει μια ανοιχτή και κλειστή μορφή της πρωτονιωμένης/αποπρωτονιωμένης χλωροφύλλης c1/c2 -ακρυλικού-H2O που ελέγχει τη θέση φόρτωσης πρωτονίων στην κατάσταση φωτοπροστατευτικής και συγκομιδής φωτός.

Επιπλέον, τα φάσματα παροδικής απορρόφησης των FCP του fragilariopsis sp και Phaeodactylum tricornutum σε διαφορετικές εντάσεις φωτός και μήκη κύματος σε συγκεκριμένα χρονικά ίχνη ερευνήθηκαν και αναλύθηκαν. Τα φάσματα παρουσιάζουν αρνητική ζώνη που βρίσκεται σε περίπου 437 nm, που αποδίδεται στο ground-state bleaching (GSB) των χλωροφύλλων και καροτενοειδών που υπάρχουν στα FCPs. Παρατηρούνται θετικές ζώνες στα 482 nm, 510 nm και 545 nm, υποδεικνύοντας τη μετάβαση απορρόφησης διεγερμένης κατάστασης (ESA) της φουκοξανθίνης, διαδινοξανθίνης και διατοξανθινής. Επιπλέον, οι ελαφρές αρνητικές κορυφές που εμφανίζονται στα 588 nm, 615 nm και 635 nm αποδίδονται στο GSB/SE των χλωροφύλλων a/c και χλωροφυλλίδιου a. Τέλος, η αρνητική κορυφή που παρατηρείται στα 672 nm αποδίδεται στη ζώνη Qy των χλωροφύλλων a και χλωροφυλλίδιου a. Η ανάλυση Global που παρουσιάζεται στα δεδομένα παρουσιάζεται εδώ με two Evolution-associated difference spectra (EADS).

Φασματοσκοπία συντονισμού Raman σε συνδυασμό με FTIR χρησιμοποιήθηκαν για τη διερεύνηση των εμπλουτισμένων με ^{13}C FCPs σε ανέπαφες θυλακοειδή μεμβράνες του Fragilariopsis sp σε φυσιολογικές συνθήκες θερμοκρασίας δωματίου. Διερευνήθηκαν δύο κλάσματα από τις διαλυτοποιημένες θυλακοειδείς μεμβράνες. Το πρώτο κλάσμα (free pigments) περιέχει φωτοευαίσθητες χλωροφύλλες a/c και σταθερές φουκοξανθίνη και διαδινοξανθίνη από αποικοδομημένα FCPs στις θυλακοειδείς μεμβράνες και το δεύτερο, σταθερά FCPs. Όλες οι ευαίσθητες δονήσεις στο ^{13}C Raman και αμίδιο I/II FTIR έχουν ταυτοποιηθεί. Οι μετατοπίσεις ^{13}C των ζωνών σήμανσης των χλωροφύλλων a/c και των καροτενοειδών φουκοξανθίνη και διαδινοξανθίνη παρέχουν τα πρώτα φασματοσκοπικά στοιχεία για τον χαρακτηρισμό όλων των χρωστικών που υπάρχουν στα FCPs, τα οποία είναι ζωτικής σημασίας για τη συλλογή φωτός και τη μεταφορά ενέργειας στην μπλε περιοχή. Η δυναμική των χρωστικών στα δύο κλάσματα συγκρίνεται και συζητείται ως προς τη διαμόρφωση και τη φωτοευαισθησία/φωτοσταθερότητά τους στις θυλακοειδή μεμβράνες.

ABSTRACT

Marine diatoms are involved in major photosynthetic biochemical cycles, in oxygenic photosynthesis and carbon fixation. Diatoms contain chlorophylls and carotenoids which are primarily responsible for light harvesting, and eventually for carrying out photosynthesis, as well as photoprotection. In this thesis, the spectroscopic techniques of UV-Visible, fluorescence, Raman and Fourier-transform infrared spectroscopy as well as the analytical technique of high-performance liquid chromatography are used to study the response of the cells of two species of diatoms under different growth conditions. The species of Fragilariopsis sp and Phaeodactylum Tricornutum has been selected which are both categorized as pennate diatoms. By varying the growth conditions, changes were observed in the concentration of the produced chromophore molecules as well as significant differences in the properties and interactions they display. These changes are strongly depended on both the intensity and the wavelength of the light source used for the growth of diatoms.

Herein, the resonance Raman spectra of the light-harvesting fucoxanthin-chlorophyll a/c binding proteins of marine diatom Fragilariopsis sp is reported. The Raman shifts in the ^{15}N-isotope-enriched diatom provide the first spectroscopic evidence for the characterization of the C_a-N marker bands and, thus, of the penta- and hexacoordinated states of chlorophylls a/c in the FCPs. Under 405 and 442 nm Raman excitations, all of the marker bands of Chl a/c are observed and the isotope-based assignments provide new information concerning the structure of Chls a/c in the FCPs and their interactions with the protein environment. Therefore, the Raman spectrum at 405 nm originates from the $\pi-\pi^*$ transitions of Chl a/c. Based on the ^{15}N isotope shifts of the C_a-N and in conjunction with other marker bands, two distinct conformations of five- and six-coordinated Chl a and Chl c are observed. In addition, two keto carbonyls were observed at 1679 (strong H-bonded) and 1691 cm−1 (weak H-bonded) in both the 405 and 442 nm Raman spectra, respectively. Collectively, the results provide solid evidence of the nature of the vibrational modes of the active Chl a/c photosynthetic pigments in the FCPs.

Moreover, the pH/pD-dependent Fluorescence-excitation spectra of the light-harvesting FCPs of the Marine Diatom Fragilariopsis sp is shown. There is a reversible 451 to 455 nm Soret transition accompanied by a 588 to 586 nm Q_x transition

of Chlorophylls c_1/c_2 in the pH/pD 4.9-8 range with a pKa =5.4. The H/D exchangeable site of the 17-acrylate group of Chlorophylls c_1/c_2 was characterized and from the pH/pD sensitivity of the Soret and Q_y bands we suggest that the Chlorophylls c_1/c_2-acrylate-H_2O moiety can act as a proton acceptor/donor site. Under high intensity light conditions, the acrylate moiety of Chlorophylls c_1/c_2 becomes protonated, resembling that observed under acidic conditions. In the photoprotective state, the absorption of Chlorophylls c_1/c_2 is red shifted and resembles that observed in the reversible transition from light-harvesting to energy-quenching state at acidic pH. The induced ΔpH and that created from the high intensity light, is responsible for the red-shifted Chlorophylls c_1/c_2 due to the protonation of the acrylate group. We present a model that describes an open and a closed form of the protonated/deprotonated Chlorophylls c1/c2-acrylate-H_2O moiety that controls the proton loading site in the photoprotective and light harvesting state.

Furthermore, the transient absorption spectra of Frag. sp and P. Tricornutum FCPs at different light intensities and wavelengths at specific time traces was investigated and analyzed. The spectra exhibit a negative band located at approximately 437 nm, attributed to the ground-state bleaching (GSB) of chlorophylls and carotenoids present in the FCPs. Positive bands at 482 nm, 510 nm, and 545 nm are observed, indicating the excited-state absorption (ESA) transition of Fx, Dd and Dt. Additionally, slight negative peaks appearing at 588 nm, 615 nm, and 635 nm are attributed to the GSB/SE of Chl c, Chl a and Chlide a. Finally, the negative peak observed at 672 nm is assigned to the Qy band of Chl a/ Chlide a. Global analysis exhibited in the data are presented in here with two Evolution-associated difference spectra (EADS).

Resonance Raman spectroscopy combined with FTIR were employed to investigate the ^{13}C- enriched light-harvesting FCPs in intact thylakoid membranes of the Marine Diatom Frag. sp at physiological room temperature conditions. Two fractions from the solubilized thylakoid membranes were investigated. The first fraction (free pigments) contains photolabile Chl a/c and stable Fx/Dd pigments from degraded FCPs in the thylakoid membranes and the second, stable FCPs. All the ^{13}C-sensitive Raman and amide I/II FTIR have been identified. The ^{13}C shifts of the marker bands of chls a/c and of the carotenoids Fx/Dd provide the first spectroscopic evidence for the characterization of all pigments present in the FCPs which are crucial for light

harvesting and energy transfer in the blue region. The dynamics of the pigments in the two fractions are compared and discussed in terms of their configuration and photosensitivity/photostability in the thylakoid membranes.

Key words: Photosynthesis, Photoprotection, Chlorophylls, Carotenoids, FCP, Fluorescence spectroscopy, Raman spectroscopy, FTIR spectroscopy.

1. Contents

Table of Figures

LIST OF ABBREVIATIONS AND MICROORGANISMS

Chl a:	Chlorophyll a
Chl c:	Chlorophyll c
Chlide a:	Chlorophyllide a
Fx:	Fucoxanthin
Dd:	Diadinoxanthin
Dt:	Diatoxanthin
β-car:	β-carotene
NPQ:	Non-Photochemical Quenching
FCP:	Fucoxanthin Chlorophyll a/c Binding Protein
FP:	Free Pigments
LHC:	Light Harvesting Complex
ROS:	Reactive Oxygen Species
OD:	Optical Density
UV:	Ultraviolet-Visible
FTIR:	Fourier-transform infrared
HPLC:	High Performance Liquid Chromatography
Rpm:	Revolutions per minute
GSB:	Ground-State Bleaching
ESA:	Excited-State Absorption

EADS:	Evolution-Associated Difference Spectra
LL:	Low Light
HL:	High Light
RL:	Red Light
Frag. sp:	Fragilariopsis sp
P. Tricornutum:	Phaeodactylum Tricornutum
C. cryptica:	Cyclotella Cryptica
C. ceratosporus:	Chaetoceros Ceratosporus
C. gracilis:	Chaetoceros Gracilis
C. Meneghiniana	Cyclotella Meneghiniana
C. calcitrans:	Chaetoceros calcitrans

2. Physicochemical Properties of Diatoms: Photosynthesis and Photoprotection

The topic of this thesis is the study of diatoms which grow in environments with different pH ranges, alternative nutrients and variable lighting conditions both in terms of intensity and wavelength. The study is carried out using spectroscopy techniques such as UV-Visible absorbance (UV), fluorescence, Raman and Fourier-transform infrared (FTIR) spectroscopy as well as the analytical technique of high-performance liquid chromatography (HPLC).

In this chapter the photosynthetic microorganisms called diatoms, will be introduced. Initially, the definition and the applications of the diatoms will be presented followed by the function of each pigment, located inside the diatoms, in terms of photosynthesis and photoprotection. Brief information about the specific diatoms studied throughout my PhD will be listed. Furthermore, insight of how light harvesting is carried out in order to produce energy through photosynthesis, as well as an extensive reference to the chromophore molecules which have a main role in these processes will be described. Additionally, the mechanism of non-photochemical quenching (NPQ) which is responsible for the protection of diatoms in environments where the radiation available for absorption can cause damage to diatom cells will be examined. Finally, the existing literature will be reviewed regarding the study of diatoms that grow in different light and wavelength, pH and nutritional conditions, which will give us background information of the light-harvesting fucoxanthin-chlorophyll a/c-binding proteins (FCPs) of diatoms.

2.1. Overview of Diatoms and Their Applications

2.1.1. Overview of Diatoms

Diatoms are unicellular eukaryotic microorganisms with a size of 1-500μm. There are more than one hundred thousand different species found all over the planet which belong to the micro-algae category. Diatoms have an envelope made of amorphous silicon (frustules) and their main distinguishing feature is their shape.[1] Diatoms constitute an important factor in the production of biomass and the sink of atmospheric greenhouse gases. Estimates indicate that these photosynthetically active organisms are responsible for 20–25% of total terrestrial primary production and about 40% of annual marine biomass production, making them the most dominant group of organisms sequestering carbon from the atmosphere.

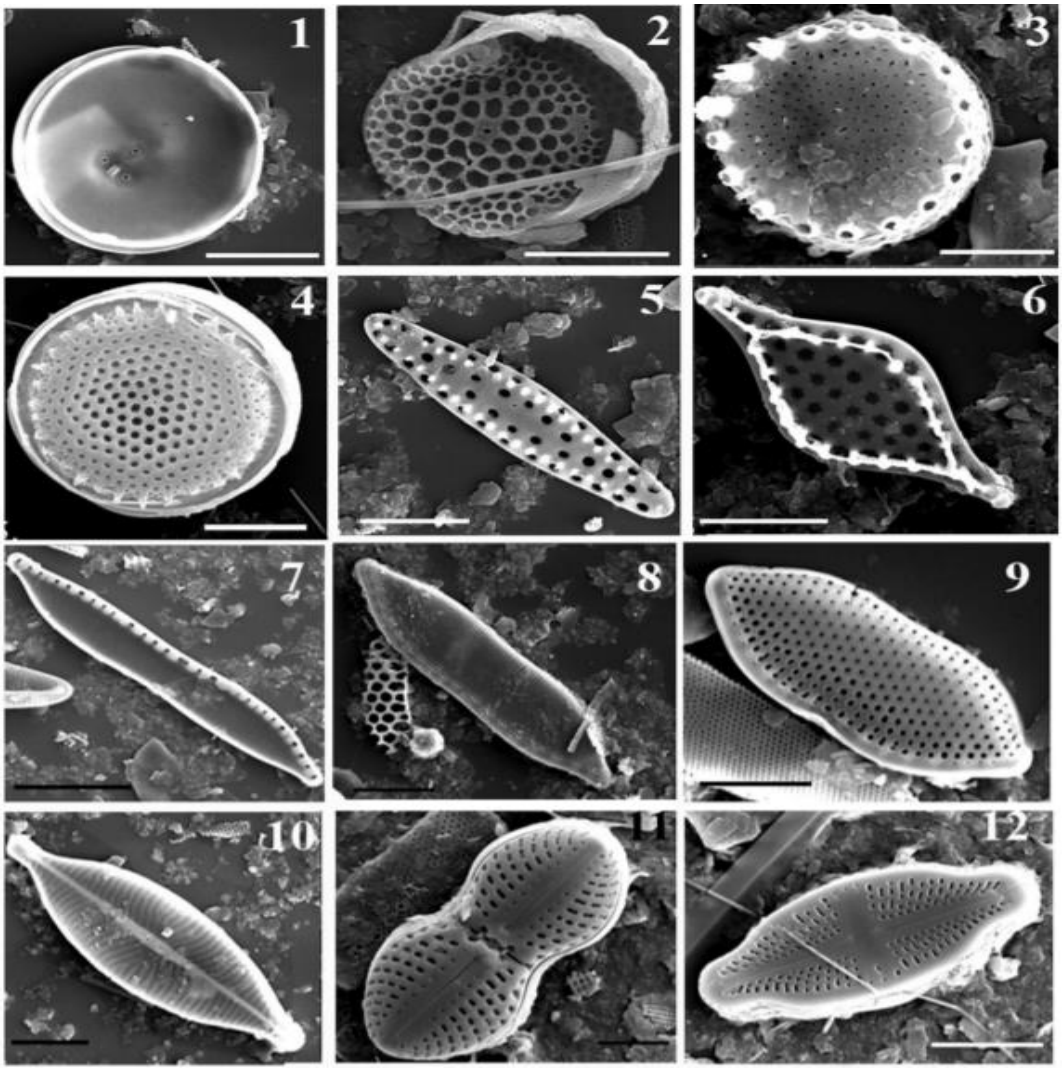

Figure 1: Scanning electron microscope (SEM) images of different diatom species.[2]

Diatoms are divided into two classes, the central diatoms (Biddulphiales or Centrales), with radial symmetry as their main characteristic, and the pennate diatoms (Bacillariales or Pennales), with bilateral symmetry as their main characteristic. The figure below shows a typical representation of the two classes and their different angles of view. [3]

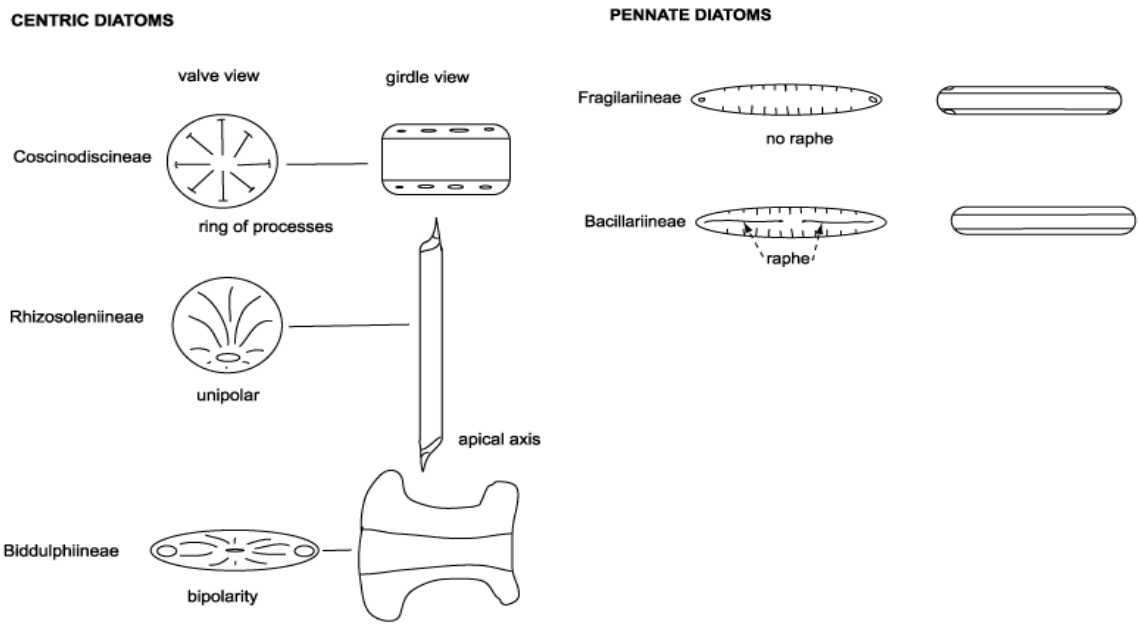

Figure 2: Schematic representation of the two basic structures of the diatom shell.[3]

Diatoms grow in moist environments, mainly marine, at a depth of up to 200m from the sea surface. Diatoms are autotrophic microorganisms, so they need sunlight to photosynthesize and produce energy. Diatoms have the ability to produce various pigments that contribute to light harvesting and photosynthesis, but also to photoprotection from the sun's radiation and its effects. The pigments, chlorophyll a (chl a), chlorophyll c (chl c) and fucoxanthin (Fx), participate cooperatively in photosynthesis, while the three carotenoids, β-carotene (β-car), diadinoxanthin (Dd) and diatoxanthin (Dt), play a key role in photoprotection. In addition, violaxanthin, antheraxanthin and zeaxanthin may be involved in the photoprotection process.[1, 4]

Diatoms are mainly autotrophic microorganisms, but heterotrophs also exist. Autotrophic diatoms utilize carbon dioxide by sequestering it in order to produce organic carbon and consequently use it for their growth. This energy is obtained from solar radiation (photo-autotrophic microorganisms). Heterotrophs utilize solar radiation to produce energy but bind carbon from organic compounds present in their

environment (amino acids, hydrocarbons, etc.) and not carbon dioxide.[4]

The main storage product of carbohydrates during diatoms photosynthesis is chrysolaminarin. A glucose polymer, composed of β-1,3-glucan with β-1,6-branched chains.[5] Unlike starch in the green lineage, chrysolaminarin is not stored in the chloroplast but externally, and therefore, transient accumulation of the storage product in the chloroplast is not observed in diatoms.[6] The photosynthesis apparatus in diatoms has the unique feature of the pigmentation of the light-harvesting apparatus and the thylakoid macrodomain. Diatoms are characterized by their brown colour which comes from the high content of Fx which is linked to Light Harvesting Complex (LHC). In green chloroplasts the most prominent LHC protein is bound to PSII which is specifically localized to grana membranes. These PSII-LHCII supercomplexes are responsible for membrane stacking and thus, these complexes form the functional basis for light-dependent grana reorganization in green chloroplasts.[7, 8] However, the thylakoids in diatoms function in zones of three-membrane, and this structure is more or less independent of light intensity.[9] These three membranes have been recently shown to have different biochemical composition than plants and can be considered as a membrane domain organization to optimize photosynthesis.[10] Therefore, this triplet structure can only be modified by applying far-red illumination during growth.[11] In general, favourable growth conditions lead to membrane lipid synthesis. However, when diatoms are exposed to abiotic stress, such as light and temperature stress, or nutrient deficiency, degradation of membrane lipids and accumulation of storage lipids can be observed.[12]

2.1.2. General Applications of Diatoms

In recent years, a great effort has been made to apply the properties as well as the produced substances of diatoms in practical applications. Attention is focused on mimicking biological processes that lead to energy production, such as photosynthesis, but also on replacing synthetic substances with biologically produced ones from diatoms. Mainly this interest is due to the economic benefit but also to the environmentally friendly practices

High quality vitamins, essential unsaturated fatty acids, amino acids and nutritional supplements are naturally synthesized by diatoms. The most relevant dietary

biomolecules produced by diatoms are the unsaturated fatty acids such as eicosapentaenoic acid, arachidonic acid, docosahexaenoic acid and other omega-3 fatty acids. They are known to reduce cardiovascular disease, are precursors to important tissue hormones, are present in 20% of the brain's gray matter, and are generally believed to be anti-carcinogenic.[13, 14, 15]

Algal biomass contains carbohydrates for ethanol production through fermentation, proteins for methane production through anaerobic gasification, and natural oils for biodiesel production.

Diatoms biomineralize a mixture of silicon, proteins and carbohydrates to form a complex inorganic silicon shell that is beyond modern engineering capabilities. These silica shells serve as a biomimetic model of micro-, meso-, and nanoscale silicon structures and are currently commonly used as diatom filters in applications ranging from liquid filtration to DNA purification for heavy metal uptake. [16,17] The ability to genetically engineer diatoms to synthesize design-specific frustules is expected to have a wide range of applications as microelectronic devices, chemical and biological sensing and diagnostics, such as drug delivery systems, catalysis, high-efficiency nanofiltration, and energy storage, including capacitors. These structures could also have potential for light-emitting display and optical storage. Additionally, frustule silicate can be completely replaced at the atomic level with magnesium oxide, engaging frustule in nanometallurgy to "cast" metal nanostructures.[18,]

When exposed to heavy metals, diatoms synthesize glutathione oligomers known as phytochelatins. Phytochelatins are intracellular and extracellular chelating agents which are important for detoxification of heavy metals. Algae exposure is caused by heavy metals found in soil and water such as Al, Ag, Cd, Co, Cr, Cs, Cu, Hg, Mg, Mn, Mo, Ni, Pb, Se, Sr and Zn. The prospect of discovering new natural or artificial phytochelatins, cation diffusion facilitators and metallothioneins would expand the range of metals available for transgenic applications. Taken together, plant, algal and fungal peptides, polypeptides and proteins expressed in diatoms could potentially bind and sequester metal pollutants in polluted waters, as transgenic plants cannot do so without soil.[19, 20]

2.2. Chlorophylls and Carotenoids

Diatoms contain pigments which are primarily responsible for light harvesting, and

eventually for carrying out photosynthesis, as well as photoprotection. These so-called pigments are the carotenoids and the chlorophylls. Chlorophylls absorb light energy mainly in the blue and red regions of the electromagnetic spectrum, which are used in photosynthesis. Carotenoids are mainly involved in photoprotection, however, Fx is also involved in light harvesting process. [1] LHCs, found in plants and green algae, play a key role in harvesting solar energy for photochemical reactions in photosynthesis. LHCs consist of hundreds of molecules of pigments, such as chlorophylls and carotenoids, bound to proteins. FCPs found in diatoms has a similar property to LHCs. Moreover, the three carotenoids, β-car, Dd and Dt, are known to play an important role in photoprotection. In addition to this, violaxanthin, antheraxanthin and zeaxanthin may be involved in the photoprotection process.[21]

2.2.1. Chlorophylls

Chlorophylls are found in living organisms that photosynthesize, such as plants and algae. There are six main classes of chls a, b, c, d, e and f which differ in their structure and are found in different organisms. In diatoms, chl a has a primary and main role where it actively contributes to the photochemical conversion of the organisms' energy. Chl c is found in various algae and functions as an auxiliary pigment in photosynthesis. chl c can be further divided into chl c_1, chl c_2, c_3 and at least eight more subclasses which are recently discovered.[22, 23, 24] The basic structure of a chlorophyll molecule is a porphyrin ring, attached to a magnesium atom in the center. The different functional groups found on the pyrrole rings are the key feature that separates the different types of chlorophyll. The differences between chl a, chl b, chl c_1 and chl c_2 are illustrated in Figure 3.

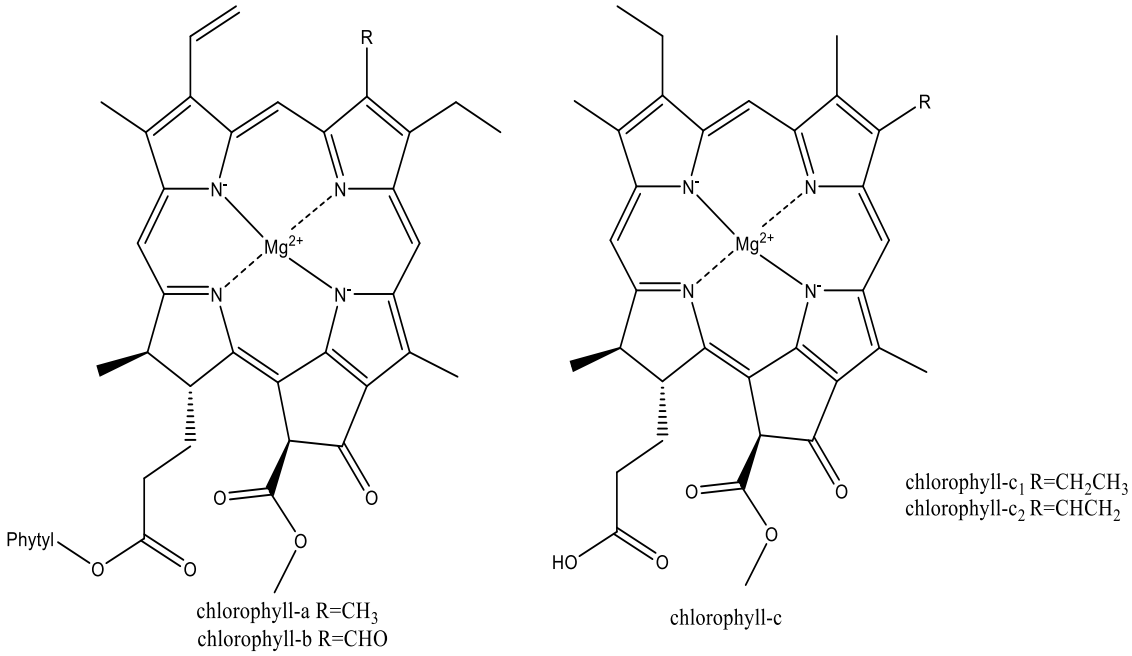

Figure 3: Chemical structure of chls a, b, c_1 and c_2.

The differences in the structure of chlorophylls affect the absorption of light in the visible part of the electromagnetic spectrum accordingly, as shown in

Figure 4. Chlorophylls absorb light around the Soret band (400 nm) and around the Q bands (600-700nm). The wavelengths at which pigments absorb light, depend on the chemical environment in which they are found. During the photosynthesis process within the cells (in vivo), chlorophylls and carotenoids, are found packed in the FCP complexes together with proteins and consequently have slightly shifted absorption bands towards longer wavelengths compared to the case where they are dissolved in organic solvents such as ethanol, methanol and acetone (in vitro).

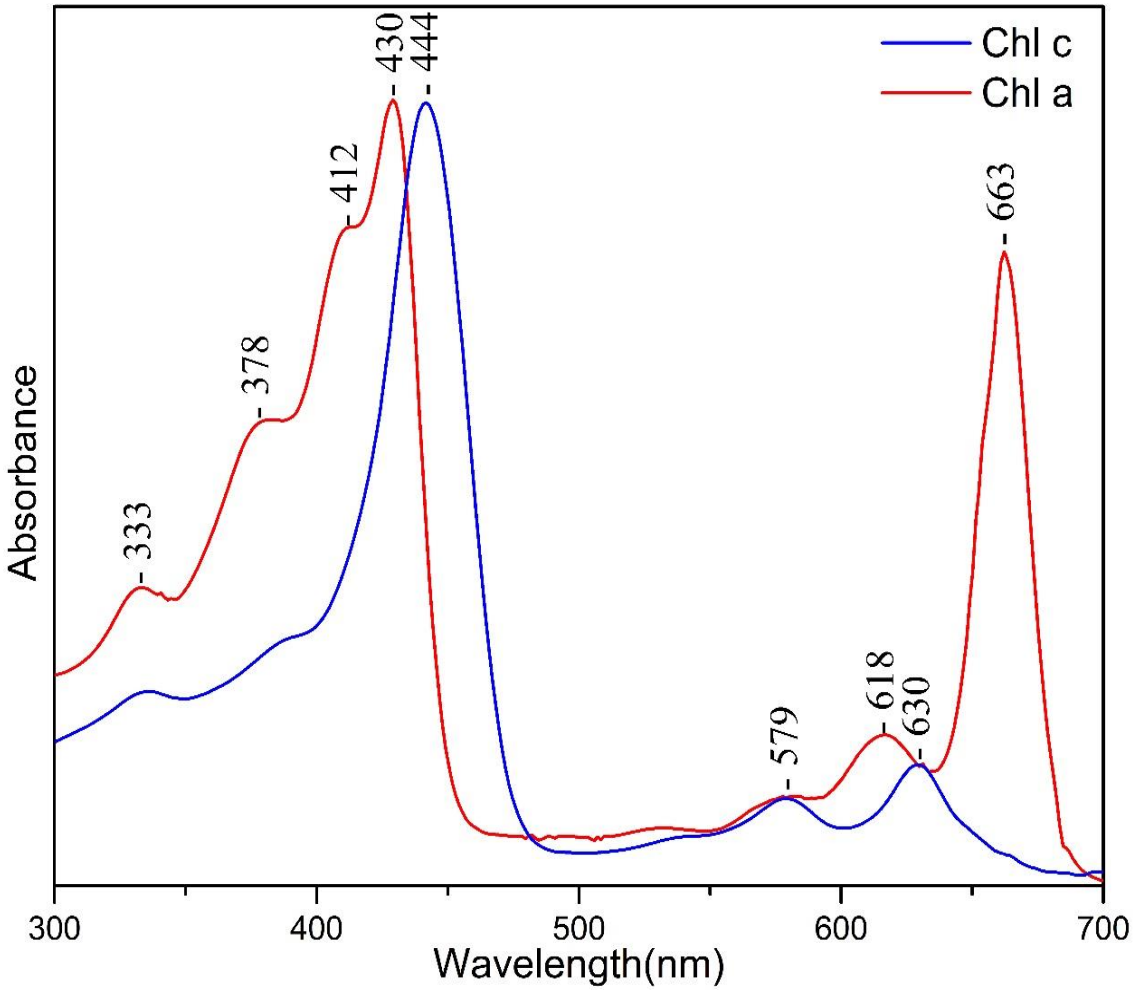

Figure 4: Absorption spectrum of chls a and c in methanol.

2.2.2. Carotenoids

Carotenoids are organic pigments with shades of yellow, orange or red and are usually produced by plants, bacteria and algae. Seven carotenoid species were identified in diatoms with β-car as an example of carotene, and Fx, Dd, Dt, violaxanthin, antheraxanthin and zeaxanthin representing the xanthophylls. The chemical structure of carotenoids is based on a conjugated polyene chain which is related to their susceptibility to oxidation, E/Z isomerization with heat, light and chemicals. The main difference between carotenes and xanthophylls is the presence of oxygen in xanthophylls while carotenes are pure hydrocarbons. The chemical structure of carotenoids is shown in Figure 5.

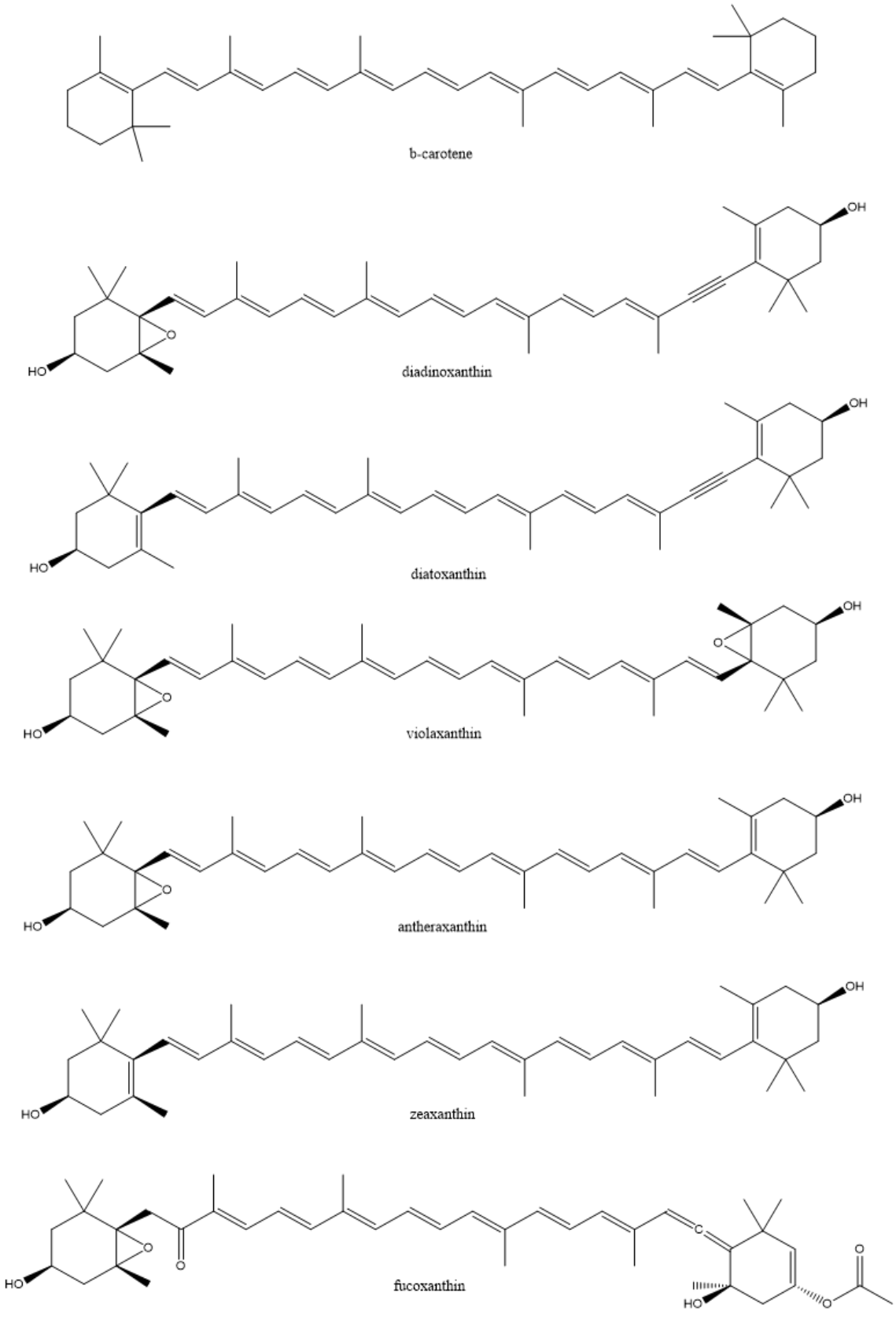

Figure 5: Chemical structure of carotenoids.

Carotenoids mainly absorb light between 350-550nm (Figure 6), where the visible part of the electromagnetic spectrum is located, but also to a lesser extent, in the ultraviolet. The conjugation length and type of functional groups attached to the ionone rings at the end of the polyene chain, determine the absorption properties of carotenoids in a great degree.[25, 26] Fx is the main light-harvesting carotenoid found in diatoms. Fx has an allenic bond, a conjugated carbonyl, a 5,6-monoepoxide, and acetyl groups that contribute to the molecule's unique structure and spectral properties. Unlike other carotenoids, Fx's broad absorption band (between 460 and 570 nm) covers much of the gap left by chlorophylls in the green region.[27]

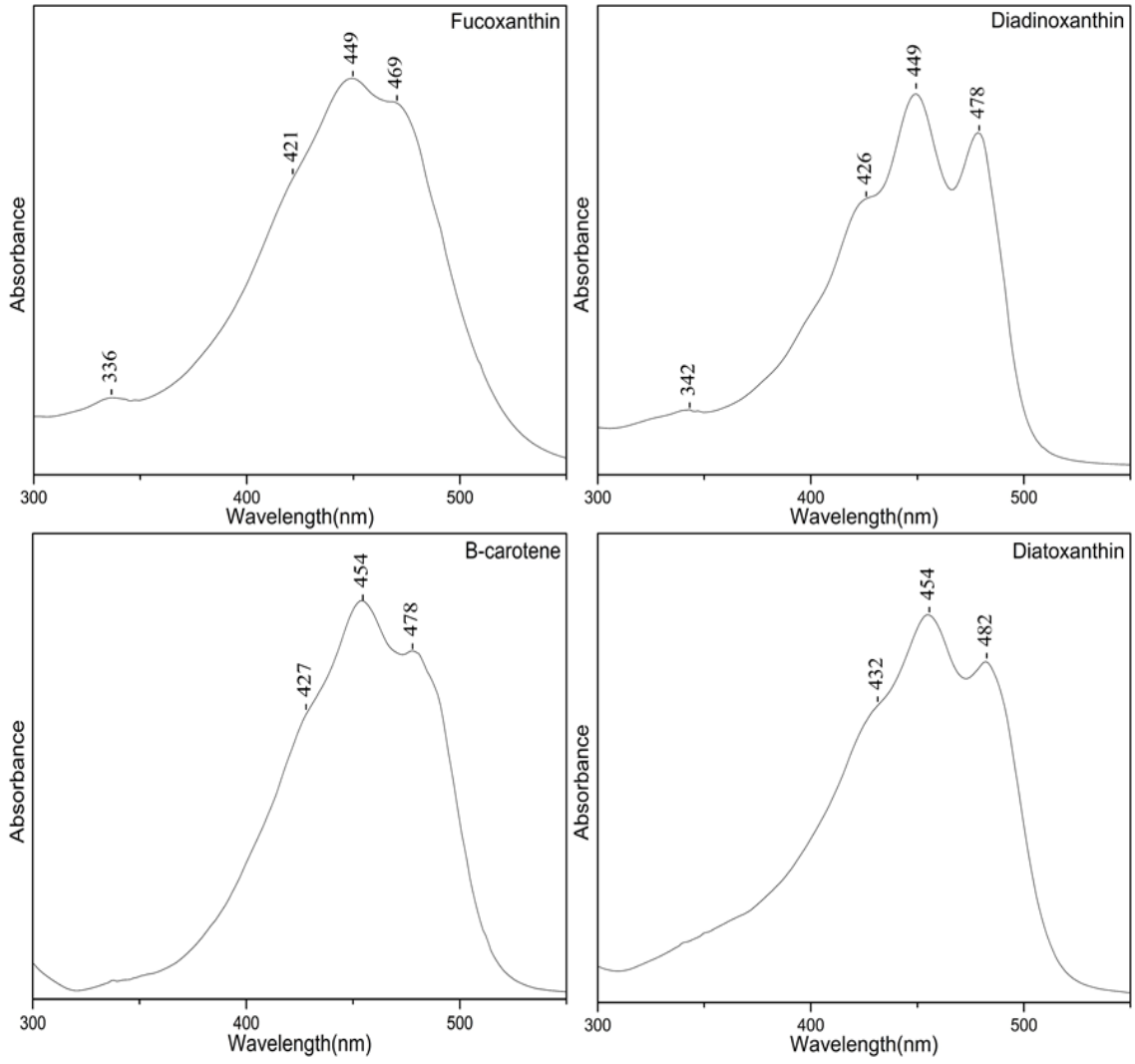

Figure 6: Absorption spectrum of Fx, Dd, β-car and Dt in methanol.

In the absorption spectrum of carotenoids, three distinct absorption peaks appear which correspond to the transitions from the ground electronic state (S_0) to the second excited electronic state (S_2). The ground electronic state and the first excited electronic state

(S_1) show the same symmetry, so the transition $S_0 \rightarrow S_1$ is forbidden. Thus, the only mode of electron transfer in this state is via de-excitation from S_2. The three characteristic peaks shown in the spectrum of Figure 7 represent the transition from S_0 to S_2 between the 0-0, 0-1 and 0-2 vibrational levels. Nevertheless, S_1 plays an important role in the transfer of energy from carotenoids to chlorophylls.[28]

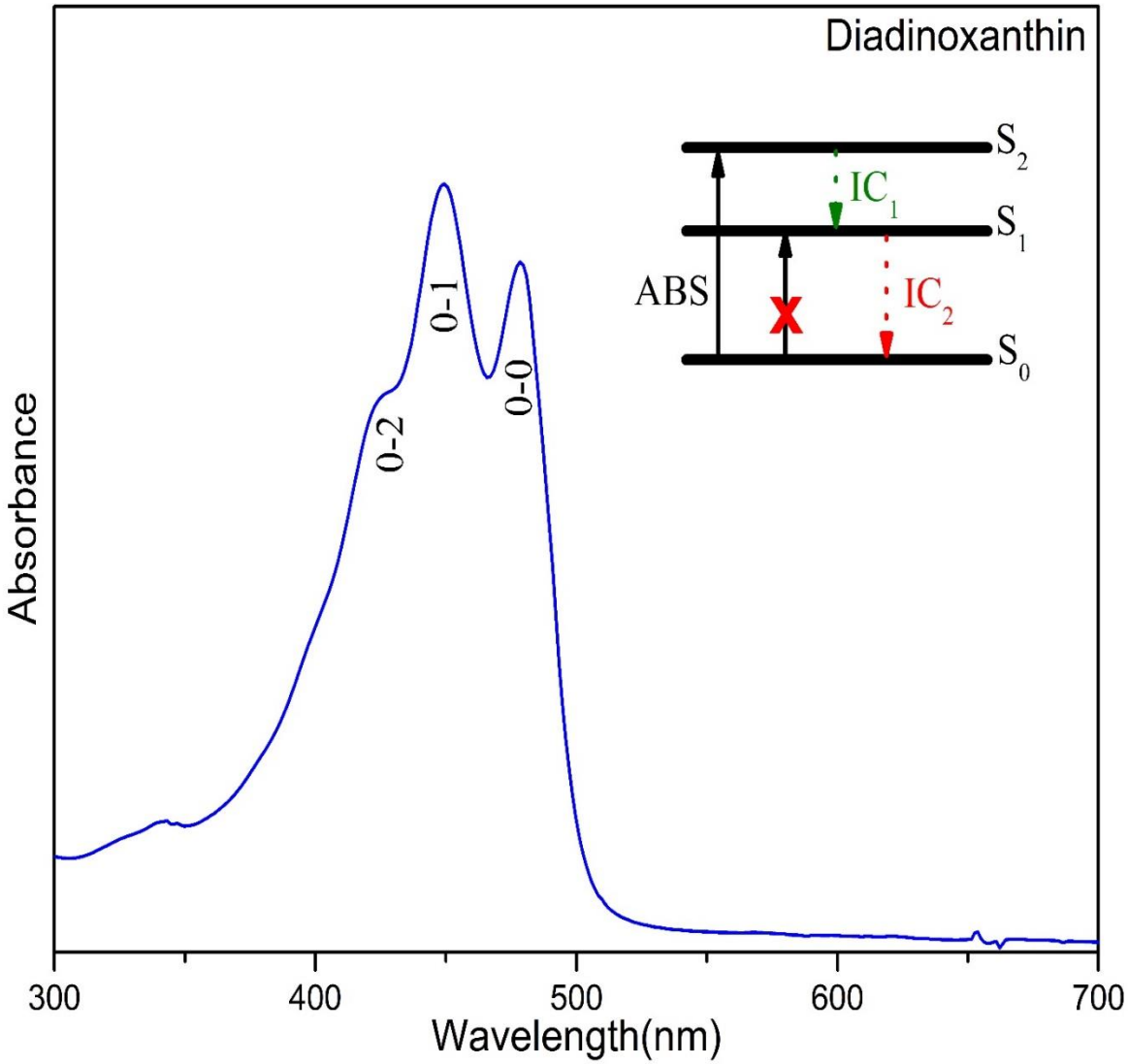

Figure 7: Absorption spectrum of Dd illustrating a simplified carotenoid energy diagram.

Excess light during photosynthesis can lead to photoinhibition, inactivation of photosystems and cause the formation of reactive oxygen species (ROS), resulting in photodamage and broad changes in cells caused by oxidative stress. To avoid this, phototrophs have developed photoprotective mechanisms such as NPQ and the xanthophyll cycle. NPQ is based on the dissipation of excess excitation energy as heat and can be detected as a quenching of chl a fluorescence. Several mechanisms have

been postulated to describe this process; however, all require structural changes in the photosynthetic antenna that allow the transition from a light-harvesting to an energy-drain state.

Two of the six types of xanthophyll cycles that have been described in photosynthetic organisms occur in diatoms. A characteristic one of these types is the Dd cycle. The two pigments involved in the Dd cycle, Dd and Dt, are normally present in diatom cells, although their amount depends on light intensity. In high light (HL), Dd, which is a monoepoxide xanthophyll, is converted to epoxide-free Dt by Dd de-epoxidase. In low light (LL) or dark conditions, the reverse reaction occurs, leading to the formation of Dd catalyzed by Dt epoxidase. Excessive light intensity leads to the formation of zeaxanthin, one of the three xanthophylls involved in the violaxanthin cycle, the second cycle appearing in diatoms.27

Violaxanthin cycle is based on a cyclic conversion of violaxanthin di-epoxide and free zeaxanthin epoxide via an intermediate product, antheraxanthin mono-epoxide. De-epoxidation of violaxanthin is catalyzed by violaxanthin de-epoxidase and epoxidation by zeaxanthin epoxidase. Although the photoprotective role of both xanthophyll rings and the ability of Dt and zeaxanthin to scavenge excited chlorophyll and free radicals are known, the reason why they exist together in diatom cells and the mechanism of activation of each remain unclear. The Dd and violaxanthin cycles are shown in Figure 8.

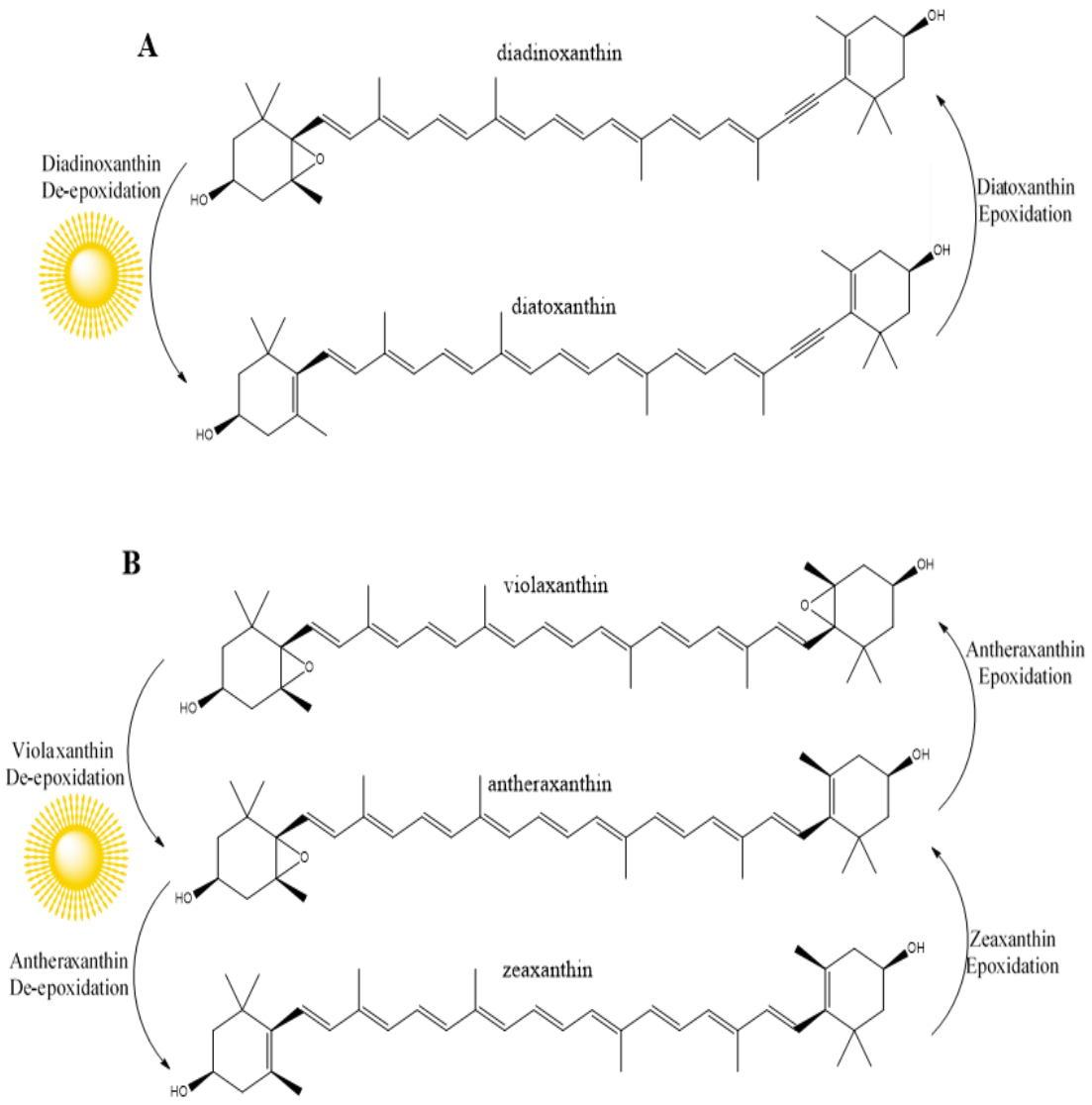

Figure 8: The Dd cycle (A) Under HL conditions, Dd with an epoxide is converted to epoxide-free Dt by violaxanthin de-epoxidase. The reverse reaction is observed in LL and darkness, and is catalyzed by zeaxanthin epoxidase. The violaxanthin cycle (B). In HL, violaxanthin is converted to zeaxanthin via the intermediate antheraxanthin, and this reaction is catalyzed by violaxanthin de-epoxidase, while in LL and darkness, two steps of zeaxanthin epoxidase-catalyzed oxidation lead to the formation of violaxanthin.

2.3. The different species of diatoms studied during my research

2.3.1. Fragilariopsis sp

The species Fragilariopsis sp (Frag. sp) belongs to the genus Fragilariopsis, family Bacillariaceae and order Bacillariophyceae, and has a cosmopolitan distribution since its range extends to all parts of the world in suitable habitats. The size of Frag. sp. ranges from 12-16 μm in length and 6-10 μm in width. They are categorized as pennate diatoms where the microscope images of the specific species reveal the symmetry of their structure as it is shown in Figure 9.[29, 30]

The cultivation of Frag. sp. in dark anoxic conditions showed large increases in lipid production but also large rates of dissolved H_2 production, suggesting the presence of fermentation. This leaves the conclusions that microalgal dark fermentation could be an important energy conservation pathway in permeable sediments.[31]

Research conducted on diatoms of different sizes and including Frag. sp. in the smaller species showed the following results: Overall, the small species showed significantly higher growth rates compared to the large species, which was related to the relatively increased light-harvesting capacity and electron transfer rates in the smaller species.[32]

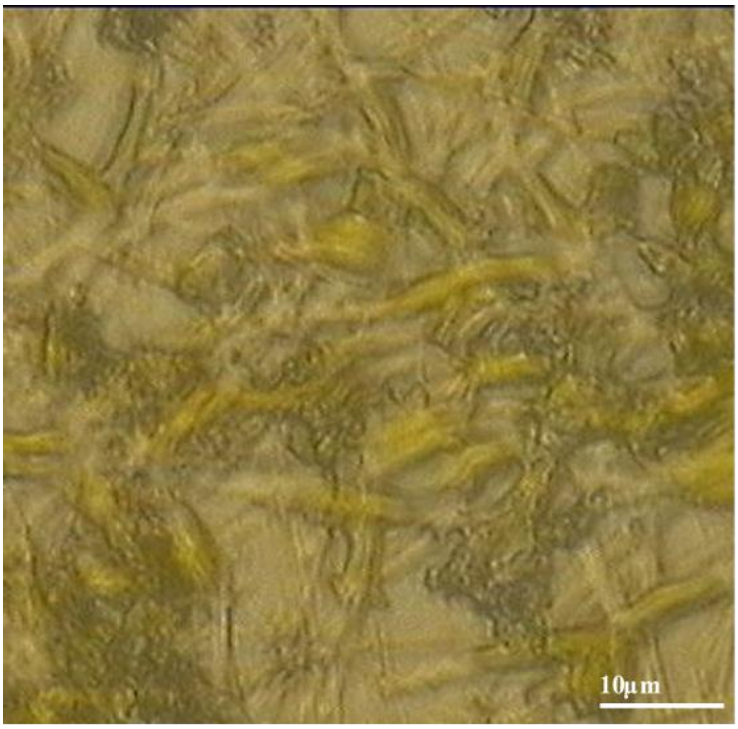

Figure 9: Microscope image of Frag. sp diatoms.

2.3.2. Phaeodactylum Tricornutum

The species Phaeodactylum Tricornutum (P. Tricornutum) belongs to the genus Phaeodactylum, family Phaeodactylaceae and class Bacillariophyceae where it is a diatom with pennate symmetry. The species P. Tricornutum is considered the most extensively studied diatom species to date which many of the researches will be discussed in the next chapter.[33]

P. Tricornutum can display different morphotypes and cell shapes which are stimulated by environmental conditions.[34] This feature can be used to explore the molecular basis of cell shape control and morphogenesis. Unlike most diatoms, P. tricornutum can grow in the absence of silicon and can survive without making silicified frustules.[35]

P. tricornutum is one of a handful of diatoms whose genome has been sequenced.[36] As of 2023, P. tricornutum is the only diatom for which a telomere-to-telomere genome assembly exists.[37] Furthermore, P. tricornutum is the first diatom where its crystal structure of an isolated LHC at high resolution was presented by Wang et al. [38]

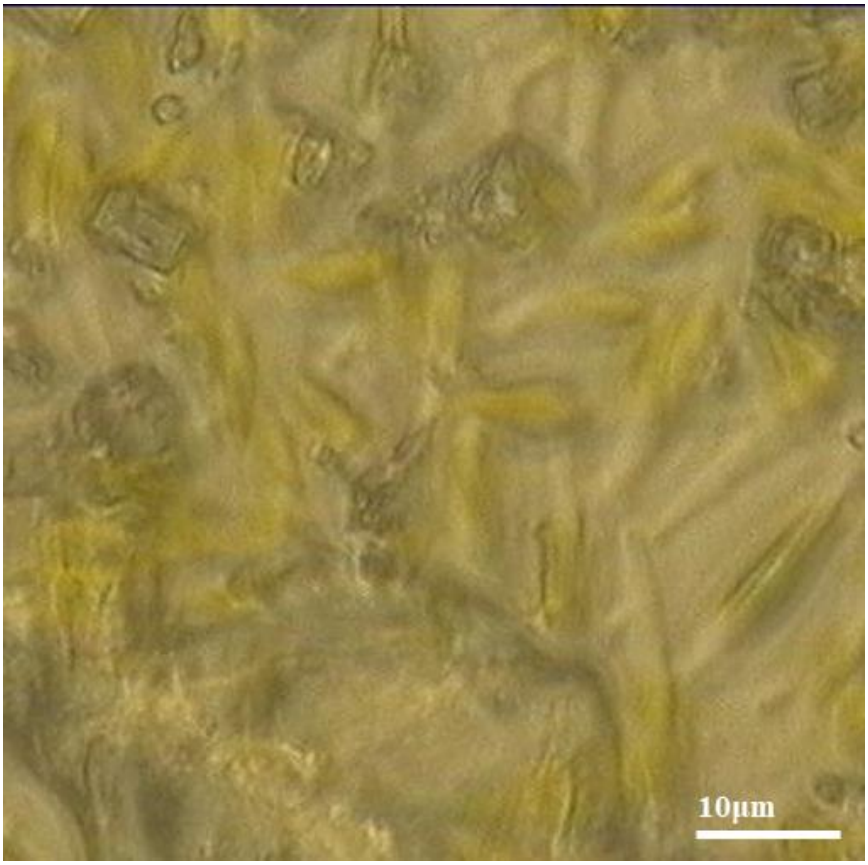

Figure 10: Microscope image of P. Tricornutum.

2.3.3. Chaetoceros ceratosporus

The species Chaetoceros ceratosporus (C. ceratosporus) belongs to the genus Chaetoceros, of the family Chaetocerotaceae and class Bacillariophyceae, which counts the most known species of diatoms on the planet. More than 400 different species have been recognized to date. They have central symmetry, which is shown in the microscope image in Figure 11: .

C. ceratosporus was the only diatom among five diatoms that has the ability to use the chemical compound bis(p-nitrophenyl) phosphate (bis-NPP) efficiently as a sole source of phosphorus. In addition, C. ceratosporus can simultaneously produce both phosphodiesterase and alkaline phosphatase at almost equal levels of activity under phosphate-deficient conditions. These results suggest that phosphodiester compounds probably play an important role as a source of phosphorus for phosphodiesterase-producing phytoplankton in coastal environments.[39,40,41]

It is worth mentioning that C. ceratosporus is an important food for several marine species.[42] Experiments carried out on shrimps, revealed that C. ceratosporus added in the feed formula, affects the increase in growth and immunity of shrimp to infection by the bacterium Vibrio harveyi.[43]

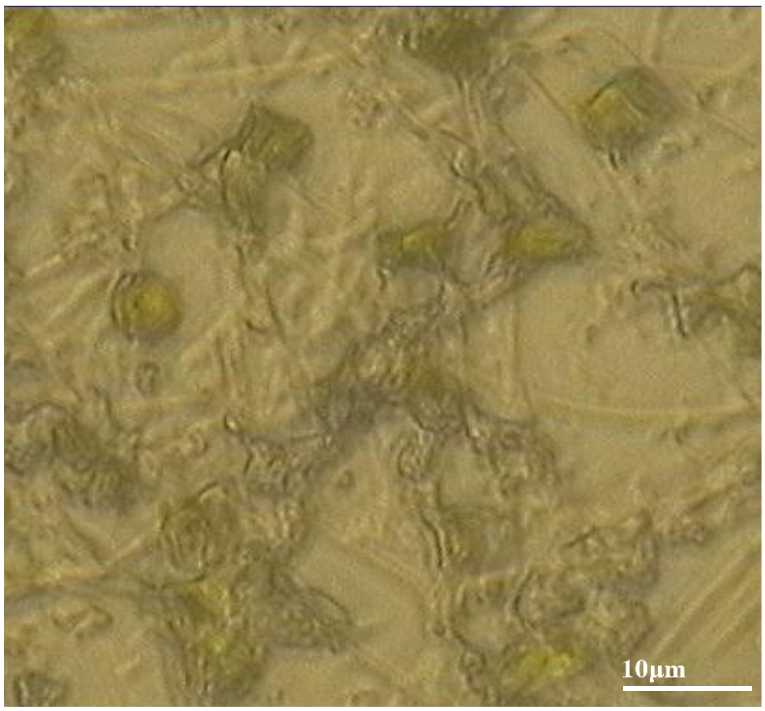

Figure 11: Microscope image of C. ceratosporus.

2.3.4. Cyclotella Cryptica

The species belongs to the genus Cyclotella, family Stephanodiscaceae and class Bacillariophyceae where it is a diatom with central symmetry.[44] C. cryptica can display different morphologies depending on salinity. The diameter of C. Cryptica can vary from 5-25 μm depending on environmental conditions.[45]

C. cryptica is a planktonic species first isolated from brackish water. It is also known to tolerate salt water. It is usually found in harbors in parts of the Great Lakes where there are unusually high concentrations of chlorine. It occurs in maximum abundance around 20°C.[46] In marine and brackish environments, C. Cryptica requires NO_3 as a nitrogen source. It also requires Ni ions to grow autotrophically. It is capable of heterotrophic growth in the dark on glucose. This suggests that it can survive for extended periods of time in deep water or glucose enriched mud. When environmental conditions improve near the shallow water, photoautotrophic growth will likely resume. It is also known to grow mesotrophically.[47,48,49]

C. cryptica produces an exudate that has the ability to suppress the growth responses of other species, such as the diatom Skeletonema costatum, in environments enriched with vitamin B-12.[50] C. cryptica is a very important specie for the growing algal biofuel industry. Roessler found that C. cryptica grown under silicon-deficient conditions had significantly higher levels of lipid production. Researchers are currently trying to genetically engineer algae that contain the enzyme acetyl-CoA carboxylase found in C. cryptica in order to increase lipid content.[51,52]

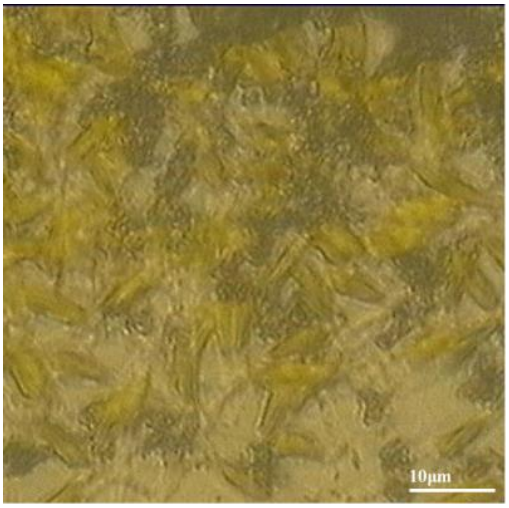

Figure 12: Microscope image of C. Cryptica.

2.4. Fucoxanthin-Chlorophyll a/c Binding Protein (FCP)

Diatom FCP proteins belong to the large family of light-harvesting proteins and thus are related to the LHC proteins of higher plants and green algae. The genes for FCP proteins are encoded in the nucleus, and thus the proteins must be imported into the chloroplast. FCP proteins have a dual function (light harvesting from blue to green regions, and quenching of excess energy) and can be divided into three groups: a) Lhcf proteins, which constitute the main, peripheral FCP complexes. These serve as the light-harvesting antenna of both Photosystem I (PSI) and II (PSII), b) Lhcr proteins, which are found in association with PSI and thus are thought to represent a PSI-specific antenna, and c) the Lhcx proteins, which are related to the Lhcsr proteins of green algae and mosses.[53, 54, 55, 56]

2.4.1. Published FCP Structures of Diatoms

Only recently, the first crystal structure of the hypercomplex form of FCPs from the marine diatom P. tricornutum was presented. Wang et al reported the crystal structure of a P. tricornutum FCP, which reveals the binding of seven chl a, two chl c, seven Fxs and possibly one Dd within the protein scaffold. Efficient energy transfer pathways can be found between chls a and c. Each Fx is surrounded by chls, thus allowing energy to be transferred and quenched through it at high efficiency. The structure provides a basis for elucidating the mechanisms of blue-green light harvesting, energy transfer and scattering in diatoms.[38]

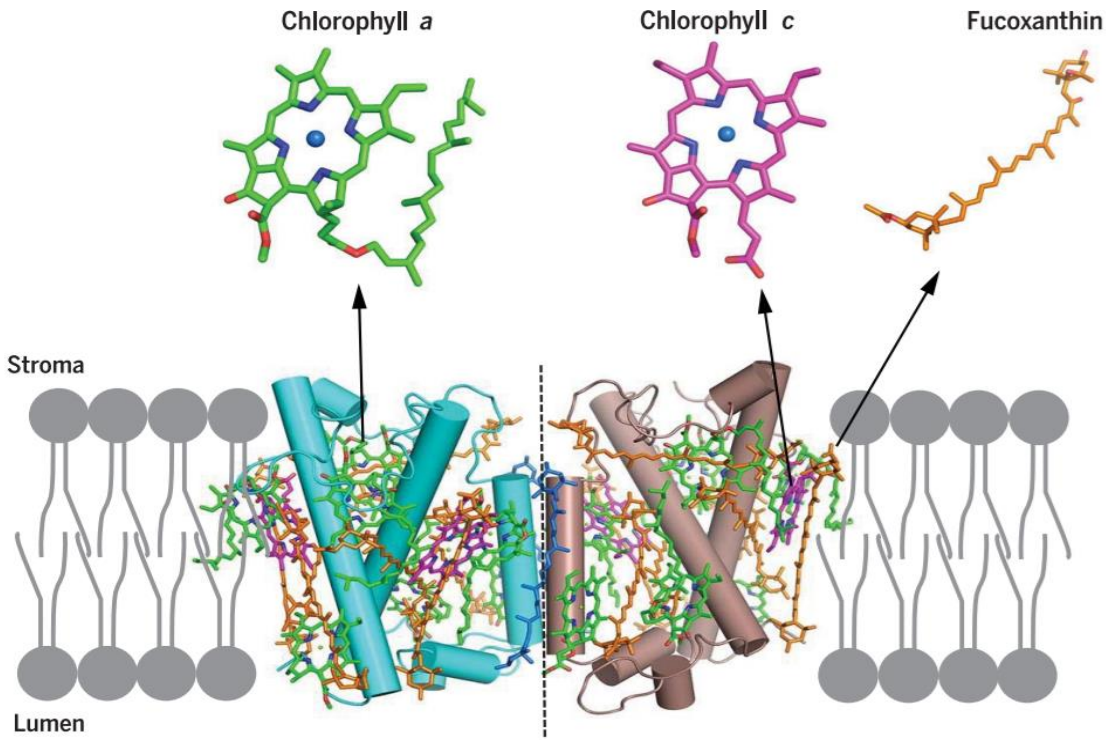

Figure 13: The structure of an FCP from the diatom P. tricornutum. The FCP was isolated as a dimer and showed that two monomers are held together by interactions between their transmembrane C helices. The structure reveals close interactions between chlorophylls and fucoxanthin, suggesting efficient energy transfer and dissipation between these pigments.38

Nagao and his team solved the structure of PSII-FCPII supercomplexes isolated from Chaetoceros gracilis (C. gracilis) by single-particle cryo-electron microscopy. PSII–FCPII forms a homodimer. In each monomer, two FCP homotetramers and three FCP monomers are associated with a PSII core. The structure reveals a highly complex protein-pigment network that differs from the green-type light harvesting apparatus. Comparing these two systems allows identification of energy transfer and quenching pathways. These findings provide structural insights not only into the excitation-energy transfer mechanisms in the PSII-FCPII diatom, but also into the light-harvesting changes between red- and green-line oxyphototrophs during evolution.[57]

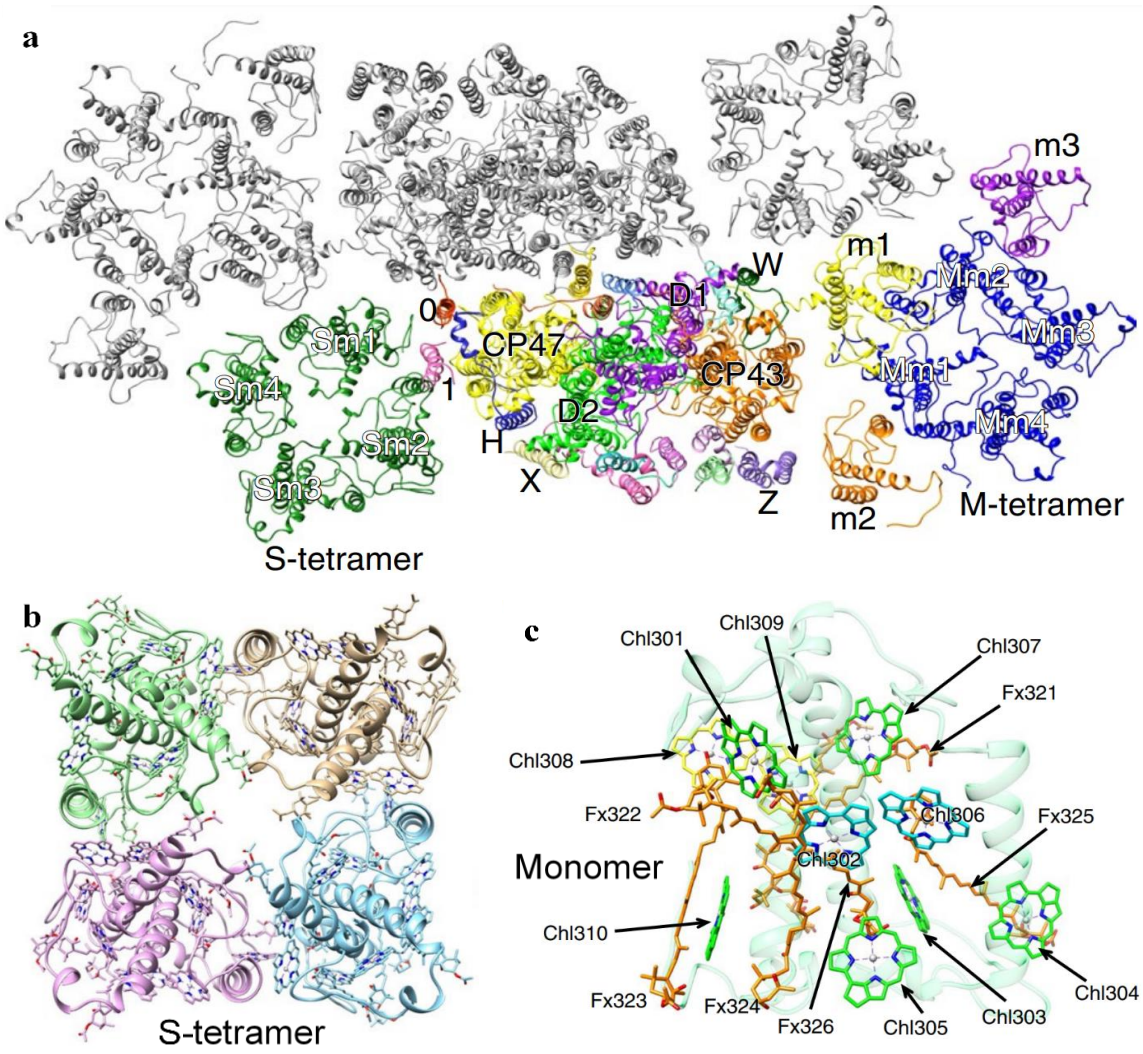

Figure 14: a) Overall structure of the PSII-FCPII supercomplex viewed across the membrane perpendicular to the stromal side. One of the PSII–FCPII modules is colored, while the other module is shown in grey. The major PSII core subunits and all FCPII subunits are labeled, with "0" and "1" indicating Unknown0 and Unknown1, respectively. b) The structure of the S-tetramer is shown across the membrane perpendicular to the stromal side. c) Arrangement of chlorophylls and fucoxanthins within a monomer of the S-tetramer.57

In another study, Nagao and his team present the structure of PSI-FCPI supercomplex from C. gracilis at a 2.40-Å resolution by cryo-electron microscopy. The supercomplex consists of 16 different FCPI subunits surrounding a monomeric PSI core. Each FCPI subunit showed different protein structures, with different pigment content and binding sites, and form a complex pigment-protein network together with the PSI core to efficiently harvest and transport light energy. In addition, two previously unknown

subunits were found in the PSI core. The structure provides numerous insights not only into the light-harvesting strategy in diatom PSI-FCPI but also into the evolutionary dynamics of light-harvesting among oxyphototrophs.[58]

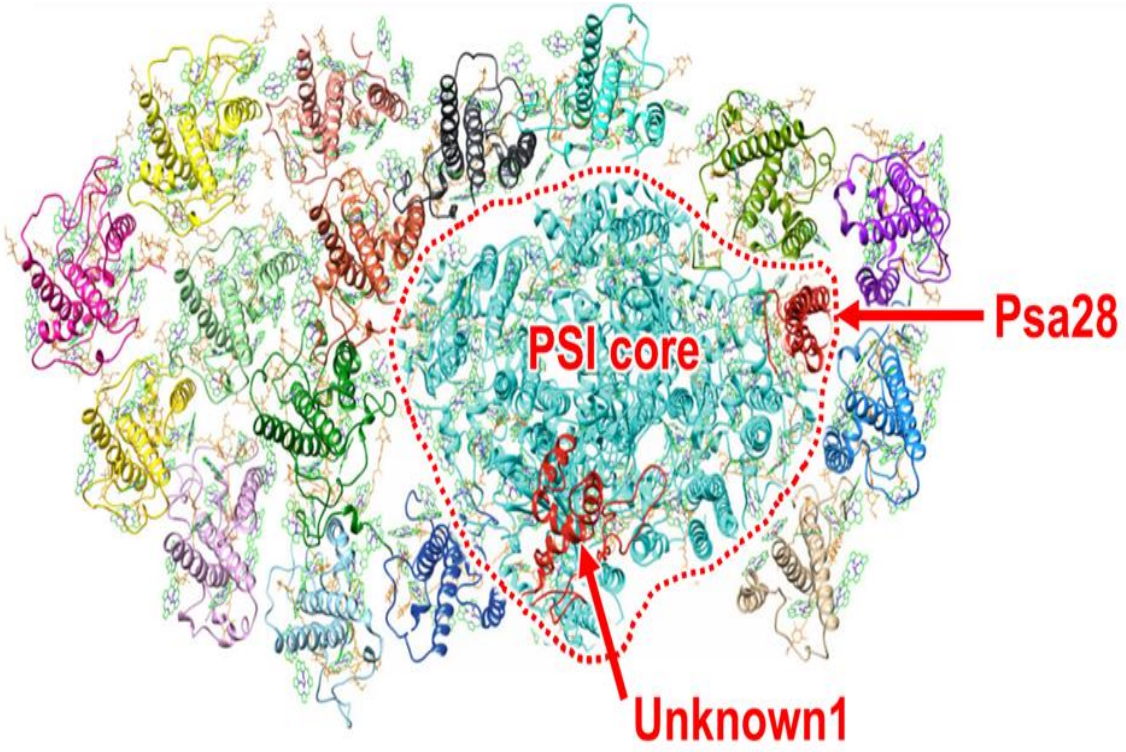

Figure 15: Overall structure of the PSI-FCPI supercomplex viewed from the stromal side. The PSI core is shown in light blue and labeled "PSI". Two previously unknown PSI core subunits are colored red and labeled "Unknown1" and "Psa28". The 16 FCPI subunits surround the PSI.58

Gelzinis evaluated how exactly the structures of Wang38 and Nagao57, 58 can account for previously published ultrafast spectroscopy results, describing excitation energy transfer in the FCP from another central diatom, Cyclotella meneghiniana (C. Meneghiniana). However, published FCP structures cannot explain several observations resulted from ultrafast spectroscopy. Using the available structures, experimental data and results from electron microscopy, they constructed a trimer FCP model for C. meneghiniana and it was used as a comparison to previous published models. Structures from diatom FCPs are observed to show greater variation among them, than plant LHCs, which may reflect species-specific adaptations or novel adaptation strategies to rapidly changing marine environments.[59]

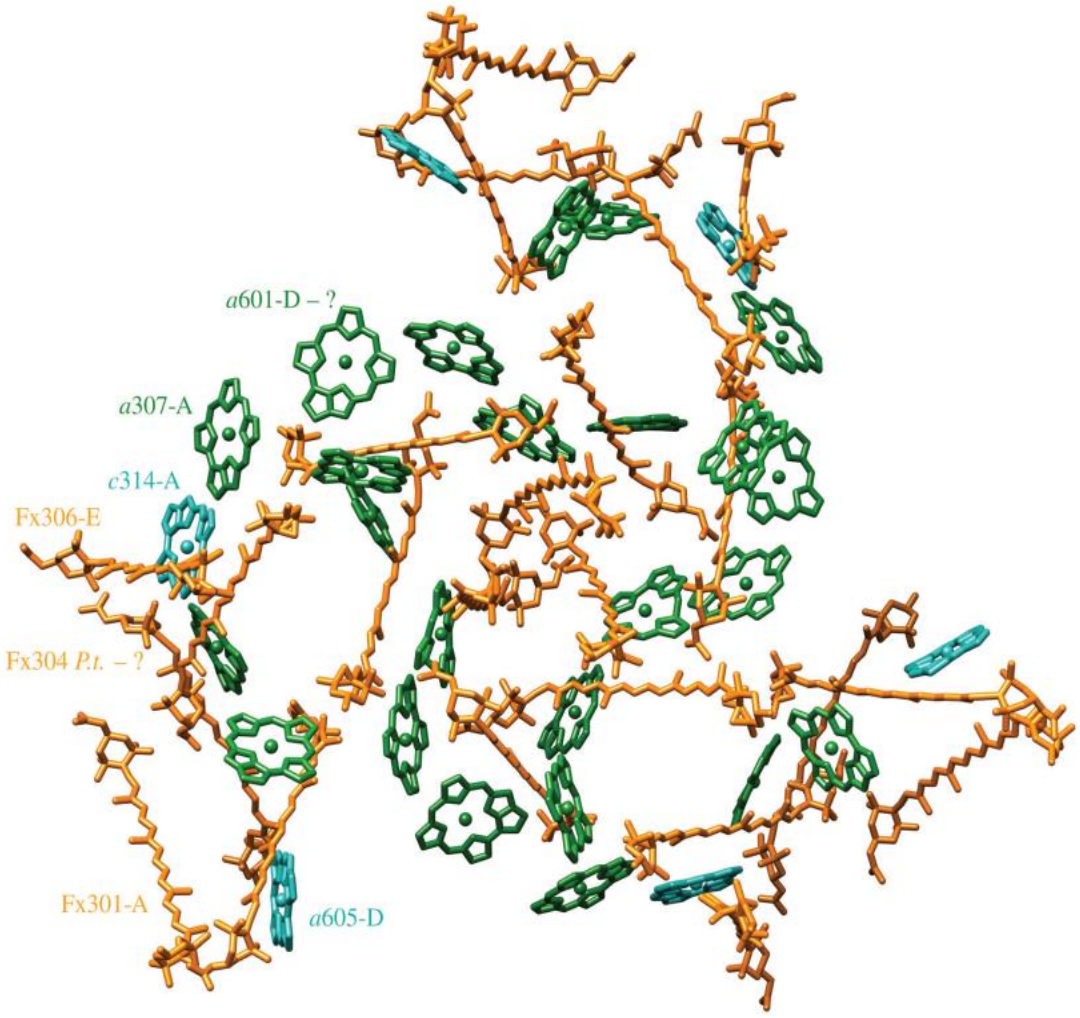

Figure 16: The proposed trimer-based FCP structure for C. meneghiniana. chl a is coloured green, chl c is blue and fucoxanthin is orange. Dd does not appear.59

2.4.2. Excitation Energy Dynamics of FCPs

Nagao and his team, have recently published several investigations surrounding the physicochemical properties of FCPs.54,58,60, They have compared the excitation energy dynamics between PSI cores and a complex between PSI and FCP I (PSI−FCPI) isolated from C. gracilis, by means of picosecond fluorescence analyses. Time-resolved spectra measured at 77 K, showed that low-energy chlorophylls in FCPI, transfer most of the excitation energy to the reaction center chlorophylls in the PSI cores, and the remaining energy to the carotenoids for quenching. Under room temperature conditions, the energy in the low-energy chlorophylls is rapidly equilibrated to chlorophylls in the PSI cores by upward energy transfer in a few tens of picoseconds. These findings provide strong evidence that low-energy chlorophylls in FCPI contribute to

photochemical reactions in PSI.[61]

Additionally, Nagao revealed the ultrafast excitation energy transfer mechanism in the PSI−FCPI complex, isolated from C. gracilis, through femtosecond fluorescence analyzes with an upconversion system. Energy transfer of chl c to chl a in FCPI was observed within hundreds of femtoseconds, and energy in FCPI was transferred to PSI in approximately 2 picoseconds. Comparative fluorescence analyzes provide physical information on the mechanism of energy transfer within FCPI and from FCPI to PSI.[62]

2.4.3. Excitation Energy Photodynamics of FCPs

In addition, Nagao and his group studied light adaptation mechanisms in the pennate diatom P. tricornutum grown at 30 μmol photons m^{-2} s^{-1} and further incubated for 24 h either in the dark, or at light intensity of 30 or 300 μmol photons m^{-2} s^{-1}. Cells grown in HL showed no detectable PSII oxygen-evolving activity, indicating the occurrence of severe photodamage. Photodamaged cells showed changes in absorbance, fluorescence, and time-resolved fluorescence spectra compared to dark- and low-light-adapted cells. In particular, the excitation-energy decay was significantly accelerated in photodamaged cells, as shown by mean lifetime analysis of chlorophyll fluorescence. Spectral changes under HL conditions may result from adjustments of pigment-protein complexes to maintain photosynthetic efficiency under excessive light. These growth-dependent spectral properties of P. tricornutum differ greatly from those of C. gracilis, thus providing insight into the different mechanisms of light adaptation between the pennate and centroid diatoms.[60]

They also demonstrated the excitation energy dynamics and relaxation of FCP complexes from P. tricornutum grown under HL conditions. Two types of FCP complexes were isolated from the diatom under HL conditions, while one FCP complex was isolated from the cells grown under LL conditions. The subunit composition and oligomeric states of FCP complexes under HL are different from those in LL. The absorption and fluorescence spectra at 77 K of the FCP complexes differ between the two conditions, indicating modifications of the pigment composition and arrangement upon HL illumination. Time-resolved fluorescence curves at 77 K of FCPs under HL showed shorter lifetime components compared to those of LL. Fluorescence decay spectra at 77 K showed distinct signs of excitation-energy quenching and changes of

energy transfer pathways in FCP complexes under HL. These findings provide insight into the molecular and functional mechanisms of the dynamic regulation of FCPs in this diatom under HL conditions.[63]

In addition, they examined the responses of P. tricornutum and C. gracilis cells to fluctuating light (FL) conditions. Excitation dynamics in cells grown under FL conditions were analyzed by time-resolved fluorescence followed by global analysis. As common responses in P. tricornutum and C. gracilis cells, quenching behaviors were observed in PSII with time constants of hundreds of picoseconds. Energy transfer from PSII to PSI was modified only in P. tricornutum cells, while quenching in FCPs was suggested only in C. gracilis cells, indicating a different strategy for dissipating excess energy under FL conditions.[64]

Furthermore, they presented the spectral profiles and excitation dynamics of novel FCP complexes isolated from C. gracilis. Under red light (RL) conditions, C. gracilis cells expressed three types of FCP complexes, two of which are very similar to the FCP complexes found in cells grown under white light and a third which is a novel FCP complex. The combination of steady-state absorption and fluorescence spectra, and time-resolved fluorescence spectra revealed that, compared to other types of FCP complexes, the new FCP complexes exhibited red-shifted absorption and fluorescence spectra and fast excitation decay. This finding will provide new insights not only into the light harvesting strategies of diatoms but also into the diversity of light adaptation machinery for photosynthetic organisms.[65]

2.4.4. Excitation Energy Dynamics of FCPs by Altered pH

Nagao reported the excitation-energy dynamics from pH changes in FCPs from P. tricornutum, investigated by time-resolved fluorescence spectroscopy at 77 K. The fluorescence curve measured at pH 5.0 showed a shorter lifetime component than the one measured at pH 8.5. The fast decay part at pH 5.0 is supported by fluorescence decay-associated (FDA) spectra, where strong fluorescence decays appear, relative to fluorescence increases, in the pH-5.0 FDA spectrum by 70 ps. These results indicate that FCPs switch their function from light harvesting to energy quenching through arrangements of energy transport pathways under acidic pH.[66]

Chrysafoudi, provides a structural basis for a remarkable pH-dependent adaptation at

the molecular level based on a computational study. Upon binding of the LHCX1 protein to the FCP complex together with a change in pH, conformational changes within the FCP protein result in a variation of the electronic coupling in a specific chlorophyllofucoxanthin pair, leading to a change in the rate of exciton transfer by nearly an order of magnitude.[67]

2.4.5. FCP Structural Adaptations to Changing Environmental Conditions

In an investigation of the effects of CO_2 concentration and temperature on photosynthetic performance in the central diatom C. gracilis, cells were grown under four different conditions: i) at 25 °C with air bubbles, ii) at 25 °C with 3% CO_2 supplementation, iii) at 30 °C with air bubbles, iv) at 30 °C with CO_2 supplementation. The growth rate of cells at 30 °C with CO_2 supplementation was faster than the other three conditions. The pigment compositions of cells grown under different conditions were varied and the fluorescence spectra measured at 77 K showed different peak positions. A new FCP complex was observed only in cells grown at 30 °C with CO_2 supplementation. Since the oxygen-growth activities of the four cell types were almost unchanged, CO_2 supplementation and growth temperature, are involved in the regulation of the light-harvesting photosynthetic system in C. gracilis to different degrees.[68]

2.4.6. Characterization of Light Harvesting Proteins and Photoprotective Mechanism of FCPs

Gundermann used the genome sequence of the central diatom C. cryptica to analyze gene sequences for potential light-harvesting proteins in C. meneghiniana, and to elucidate FCP complex composition. Two groups of FCP complexes were analyzed which were trimeric (FCPa) and nonameric (FCPb). FCPa consisted of four different trimeric subtypes. There were two different nonameric FCPb complexes. Using a milder method, two fractions from different FCP complexes were isolated. One was enriched in FCPs that incorporate the photoprotective subunit Lhcx1, such as the recently identified FCPb2 nonamer and the major ternary complex FCPa4, which have been established to be involved in energy-dependent NPQ. The other fraction contained mainly FCPs lacking Lhcx1, FCPa3 and FCPb1. Both fractions include small amounts

of trimeric FCPa complexes with the protein, Lhcx6_1 (centric diatom-specific), as a subunit. Thus, the antennal organization of central diatoms, as well as the distribution of different photoprotective Lhcx proteins, differs from that of other diatoms, as well as from plants.[69]

FCPs from C. meneghiniana were studied by means of optically detected magnetic resonance and time-resolved electron paramagnetic resonance, aiming to characterize the photoprotective mechanism based on triplet–triplet energy transfer. The spectroscopic properties of the chromophores carrying the triplet state were interpreted based on an immersion analysis of the recently solved crystallographic structures of FCP from P. tricornutum. The results point towards a photoprotective role of two Fx molecules exposed on the outside of the FCP monomers. This indicates that FCP has adopted a structural strategy different from that of related photoharvesting complexes from plants and other microalgae, in which the photoprotective role is performed by two highly conserved carotenoids within the complex.[70]

References

1. Kuczynska P, Jemiola-Rzeminska M, Strzalka K. Photosynthetic Pigments in Diatoms. Marine Drugs. 2015;13(9):5847-5881.

2. Manoylov K, Dominy Jr. J. Changes in Epipelic Diatom Diversity from the Savannah River Estuary. Journal of Environmental Protection. 2013;04(02):172-179.

3. Hasle G, Syvertsen E, Steidinger K, Tangen K. Identifying marine diatoms and dinoflagellates. San Diego: Academic Press; 1996.

4. Falciatore, A., Jaubert, M., Bouly, J. P., Bailleul, B., & Mock, T. (2020). Diatom molecular research comes of age: Model species for studying phytoplankton biology and diversity. Plant Cell. 2020; 32(3) 547-572

5. Yang YF, Li DW, Balamurugan S, Wang X, Yang WD, Li HY. Chrysolaminarin biosynthesis in the diatom is enhanced by overexpression of 1,6-β-transglycosylase. Algal Research. 2022; 66:102817.

6. Hildebrand M, Manandhar-Shrestha K, Abbriano R. Effects of chrysolaminarin synthase knockdown in the diatom Thalassiosira pseudonana: Implications of reduced carbohydrate storage relative to green algae. Algal Research. 2017; 23:66-77.

7. Ozcan Konur. Handbook of Algal Science, Technology and Medicine. Academic Press; 2020.

8. Albanese P, Melero R, Engel B, Grinzato A, Berto P, Manfredi M et al. Pea PSII-LHCII supercomplexes form pairs by making connections across the stromal gap. Scientific Reports. 2017;7(1).

9. Tanaka A, De Martino A, Amato A, Montsant A, Mathieu B, Rostaing P et al. Ultrastructure and Membrane Traffic During Cell Division in the

Marine Pennate Diatom Phaeodactylum tricornutum. Protist. 2015;166(5):506-521.

10. Flori S, Jouneau P, Bailleul B, Gallet B, Estrozi L, Moriscot C et al. Plastid thylakoid architecture optimizes photosynthesis in diatoms. Nature Communications. 2017;8(1).

11. Bína D, Herbstová M, Gardian Z, Vácha F, Litvín R. Novel structural aspect of the diatom thylakoid membrane: lateral segregation of photosystem I under red-enhanced illumination. Scientific Reports. 2016;6(1).

12. Hu C, Li M, Li J, Zhu Q, Liu Z. Variation of lipid and fatty acid compositions of the marine microalga Pavlova viridis (Prymnesiophyceae) under laboratory and outdoor culture conditions. World Journal of Microbiology and Biotechnology. 2007;24(7):1209-1214.

13. Kroth P. Molecular biology and the biotechnological potential of diatoms. Springer. Berlin 2007

14. Lebeau T, Robert J. Diatom cultivation and biotechnologically relevant products. Part I: Cultivation at various scales. Applied Microbiology and Biotechnology. 2003;60(6):612-623.

15. Meiser A, Schmid-Staiger U, Trösch W. Optimization of eicosapentaenoic acid production by Phaeodactylum tricornutum in the flat panel airlift (FPA) reactor. Journal of Applied Phycology. 2004;16(3):215-225.

16. Hildebrand M, Doktycz M, Allison D. Application of AFM in understanding biomineral formation in diatoms. Pflügers Archiv - European Journal of Physiology. 2007;456(1):127-137.

17. Lopez P, Desclés J, Allen A, Bowler C. Prospects in diatom research. Current Opinion in Biotechnology. 2005;16(2):180-186.

18. Parkinson J, Brechet Y, Gordon R. Centric diatom morphogenesis: a model based on a DLA algorithm investigating the potential role of microtubules. Biochimica et Biophysica Acta (BBA) - Molecular Cell Research. 1999;1452(1):89-102.

19. Prasad M, De Oliveira Freitas H. Metal hyperaccumulation in plants - Biodiversity prospecting for phytoremediation technology. Electronic Journal of Biotechnology. 2003;6(3).

20. Bozarth A, Maier U, Zauner S. Diatoms in biotechnology: modern tools and applications. Applied Microbiology and Biotechnology. 2009;82(2):195-201.

21. Gelzinis A, Butkus V, Songaila E, Augulis R, Gall A, Büchel C et al. Mapping energy transfer channels in fucoxanthin–chlorophyll protein complex. Biochimica et Biophysica Acta (BBA) - Bioenergetics. 2015;1847(2):241-247.

22. Dougherty R, Strain H, Svec W, Uphaus R, Katz J. Structure, properties, and distribution of chlorophyll c. Journal of the American Chemical Society. 1970;92(9):2826-2833.

23. Fookes C, Jeffrey S. The structure of chlorophyll c 3, a novel marine photosynthetic pigment. Journal of the Chemical Society, Chemical Communications. 1989;(23):1827.

24. Grimm B, Porra R, Rüdiger W, Scheer H. Chlorophylls and Bacteriochlorophylls. Dordrecht: Springer; 2006.

25. Zigmantas D, Hiller R, Sharples F, Frank H, Sundström V, Polívka T. Effect of a conjugated carbonyl group on the photophysical properties of carotenoids. Phys Chem Chem Phys. 2004;6(11):3009-3016.

26. Frank H, Cogdell R. Carotenoids in Photosynthesis. Photochemistry and Photobiology. 1996;63(3):257-264.

27. Lohr M, Wilhelm C. Algae displaying the diadinoxanthin cycle also possess the violaxanthin cycle. Proceedings of the National Academy of Sciences. 1999;96(15):8784-8789.

28. Llansola-Portoles M, Pascal A, Robert B. Electronic and vibrational properties of carotenoids: from in vitro to in vivo. Journal of The Royal Society Interface. 2017;14(135):20170504.

29. Søgaard D, Hansen P, Rysgaard S, Glud R. Growth limitation of three Arctic sea ice algal species: effects of salinity, pH, and inorganic carbon availability. Polar Biology. 2011;34(8):1157-1165.

30. Arrigo KR, Mock T, Lizotte MP, Primary producers and sea ice. In: Thomas DN, Dieckmann GS (eds) Sea ice, 2nd edn. Blackwell Science, Oxford, 2010; pp 283–325

31. Bourke M, Marriott P, Glud R, Hasler-Sheetal H, Kamalanathan M, Beardall J et al. Metabolism in anoxic permeable sediments is dominated by eukaryotic dark fermentation. Nature Geoscience. 2016;10(1):30-35.

32. Kulk G, Buist A, Poll W, Rozema P, Buma A. Size scaling of photophysiology and growth in four freshly isolated diatom species from Ryder Bay, western Antarctic peninsula. Journal of Phycology. 2019;55(2):314-328.

33. Butler T, Kapoore RV, Vaidyanathan S. Phaeodactylum tricornutum: A Diatom Cell Factory. Trends in Biotechnology. 2020 Jan;38(6).

34. Martino AD, Meichenin A, Shi J, Pan K, Bowler C. Genetic and phenotypic characterization of Phaeodactylum tricornutum (Bacillariophyceae) accessions[1]. Journal of Phycology. 2007;43(5):992–1009.

35. Chuang CY, Santschi PH, Jiang Y, Ho YF, Quigg A, Guo L, et al. Important role of biomolecules from diatoms in the scavenging of particle-

reactive radionuclides of thorium, protactinium, lead, polonium, and beryllium in the ocean: A case study with Phaeodactylum tricornutum. Limnology and Oceanography. 2014;59(4):1256–66.

36. Bowler C, Allen AE, Badger JH, Grimwood J, Jabbari K, Kuo A, et al. The Phaeodactylum genome reveals the evolutionary history of diatom genomes. Nature. 2008;456(7219):239–44.

37. Giguere DJ, Bahcheli AT, Slattery SS, Patel RR, Browne TJ, Flatley MW, et al. Telomere-to-telomere genome assembly of Phaeodactylum tricornutum. PeerJ. 2022;10:e13607

38. Wang W, Yu L, Xu C, Tomizaki T, Zhao S, Umena Y et al. Structural basis for blue-green light harvesting and energy dissipation in diatoms. Science. 2019;363(6427):1-8.

39. Yamaguchi H, Yamaguchi M, Fukami K, Adachi M, Nishijima T. Utilization of phosphate diester by the marine diatom Chaetoceros ceratosporus. Journal of Plankton Research. 2005;27(6):603-606.

40. Yamaguchi H, Sakou H, Fukami K, Adachi M, Yamaguchi M, Nishijima T. Utilization of organic phosphorus and production of alkaline phosphatase by the marine phytoplankton, Heterocapsa circularisquama, Fibrocapsa japonica and Chaetoceros ceratosporum. Plankton Biol Ecol. 2005;52(2):67-75.

41. Yamaguchi H, Arisaka H, Otsuka N, Tomaru Y. Utilization of phosphate diesters by phosphodiesterase-producing marine diatoms. Journal of Plankton Research. 2013;36(1):281-285.

42. Hawkins L, Hutchinson S, Laing I. The effects of temperature and food ration on metabolite concentrations in newly settled king scallop (Pecten maximus) spat. Aquaculture. 2005;250(3-4):841-848.

43. Ekawati A, Nursyam H, Widjayanto E, Marsoedi M. Chaetoceros ceratosporum Diatomae in Feed Formula to Increase Growth and Post Larvae Immunity of Tiger Shrimp (Penaeus monodon Fab.) to Vibrio harveyi infection. The Journal of Experimental Life Sciences. 2013;3(1):31-36.

44. Herth W, Zugenmaier P. Ultrastructure of the chitin fibrils of the centric diatom Cyclotella cryptica. Journal of Ultrastructure Research. 1977;61(2):230-239.

45. Reimann B, Lewin J, Guillard R. Cyclotella cryptica, a New Brackish-Water Diatom Species. Phycologia. 1963;3(2):75-84.

46. Liu M, Hellebust J. Effects of salinity changes on growth and metabolism of the marine centric diatom Cyclotella cryptica. Canadian Journal of Botany. 1976;54(9):930-937.

47. Oliveira L, Antia N. Evidence of nickel ion requirement for autotrophic growth of a marine diatom with urea serving as nitrogen source. British Phycological Journal. 1984;19(2):125-134.

48. Saros J, Fritz S. Nutrients as a link between ionic concentration/composition and diatom distributions in saline lakes. Journal of Paleolimnology. 2000;23(4):449-453.

49. White A. Growth of two facultatively heterotrophic marine centric diatoms. Journal of Phycology. 1974;10(3):292-300.

50. Messina D, Baker A. Interspecific growth regulation in species succession through Vitamin B12 competitive inhibition. Journal of Plankton Research. 1982;4(1):41-46.

51. Roessler P. Effects of silicon deficiency on lipid composition and metabolism in the diatom Cyclotella cryptica. Journal of Phycology. 1988;24(3):394-400.

52. Day J, Slocombe S, Stanley M. Overcoming biological constraints to enable the exploitation of microalgae for biofuels. Bioresource Technology. 2012;109:245-251.

53. Grouneva I, Rokka A, Aro E. The Thylakoid Membrane Proteome of Two Marine Diatoms Outlines Both Diatom-Specific and Species-Specific Features of the Photosynthetic Machinery. Journal of Proteome Research. 2011;10(12):5338-5353.

54. Nagao R, Takahashi S, Suzuki T, Dohmae N, Nakazato K, Tomo T. Comparison of oligomeric states and polypeptide compositions of fucoxanthin chlorophyll a/c-binding protein complexes among various diatom species. Photosynthesis Research. 2013;117(1-3):281-288.

55. Lepetit B, Volke D, Gilbert M, Wilhelm C, Goss R. Evidence for the Existence of One Antenna-Associated, Lipid-Dissolved and Two Protein-Bound Pools of Diadinoxanthin Cycle Pigments in Diatoms. Plant Physiology. 2010;154(4):1905-1920.

56. Scarsini, M., Marchand, J., Manoylov, K.M. and Schoefs, B. (2019). Photosynthesis in Diatoms. In Diatoms: Fundamentals and Applications (eds J. Seckbach and R. Gordon).

57. Nagao R, Kato K, Suzuki T, Ifuku K, Uchiyama I, Kashino Y et al. Structural basis for energy harvesting and dissipation in a diatom PSII–FCPII supercomplex. Nature Plants. 2019;5(8):890-901.

58. Nagao R, Kato K, Ifuku K, Suzuki T, Kumazawa M, Uchiyama I et al. Structural basis for assembly and function of a diatom photosystem I-light-harvesting supercomplex. Nature Communications. 2020;11,2481.

59. Gelzinis A, Augulis R, Büchel C, Robert B, Valkunas L. Confronting FCP structure with ultrafast spectroscopy data: evidence for structural variations. Physical Chemistry Chemical Physics. 2021;23(2):806-821.

60. Nagao R, Ueno Y, Yokono M, Shen J, Akimoto S. Effects of excess light energy on excitation-energy dynamics in a pennate diatom Phaeodactylum tricornutum. Photosynthesis Research. 2019;141(3):355-365.

61. Nagao R, Yokono M, Ueno Y, Shen J, Akimoto S. Low-Energy Chlorophylls in Fucoxanthin Chlorophyll a/c-Binding Protein Conduct Excitation Energy Transfer to Photosystem I in Diatoms. The Journal of Physical Chemistry B. 2018;123(1):66-70.

62. Nagao R, Kagatani K, Ueno Y, Shen J, Akimoto S. Ultrafast Excitation Energy Dynamics in a Diatom Photosystem I-Antenna Complex: A Femtosecond Fluorescence Upconversion Study. The Journal of Physical Chemistry B. 2019;123(12):2673-2678.

63. Nagao R, Yokono M, Ueno Y, Suzuki T, Kumazawa M, Kato K et al. Enhancement of excitation-energy quenching in fucoxanthin chlorophyll a/c-binding proteins isolated from a diatom Phaeodactylum tricornutum upon excess-light illumination. Biochimica et Biophysica Acta (BBA) - Bioenergetics. 2021;1862(2):148350.

64. Tanabe M, Ueno Y, Yokono M, Shen J, Nagao R, Akimoto S. Changes in excitation relaxation of diatoms in response to fluctuating light, probed by fluorescence spectroscopies. Photosynthesis Research. 2020;146(1-3):143-150.

65. Ueno Y, Nagao R, Shen J, Akimoto S. Spectral Properties and Excitation Relaxation of Novel Fucoxanthin Chlorophyll a/c-Binding Protein Complexes. The Journal of Physical Chemistry Letters. 2019;10(17):5148-5152.

66. Nagao R, Yokono M, Ueno Y, Shen J, Akimoto S. Acidic pH-Induced Modification of Energy Transfer in Diatom Fucoxanthin Chlorophyll a/c-Binding Proteins. The Journal of Physical Chemistry B. 2020;124(24):4919-4923.

67. Chrysafoudi A, Maity S, Kleinekathöfer U, Daskalakis V. Robust Strategy for Photoprotection in the Light-Harvesting Antenna of Diatoms: A Molecular Dynamics Study. The Journal of Physical Chemistry Letters. 2021;12(39):9626-9633.

68. Nagao R, Ueno Y, Akimoto S, Shen J. Effects of CO2 and temperature on photosynthetic performance in the diatom Chaetoceros gracilis. Photosynthesis Research. 2020;146(1-3):189-195.

69. Gundermann K, Wagner V, Mittag M, Büchel C. Fucoxanthin-Chlorophyll Protein Complexes of the Centric Diatom Cyclotella Meneghiniana Differ in Lhcx1 and Lhcx6_1 Content. Plant Physiology. 2019;179(4):1779-1795.

70. Agostini A, Büchel C, Di Valentin M, Carbonera D. A distinctive pathway for triplet-triplet energy transfer photoprotection in fucoxanthin chlorophyll-binding proteins from Cyclotella meneghiniana. Biochimica et Biophysica Acta (BBA) - Bioenergetics. 2021;1862(1):148310.

3. Research Methodology and Experimental Techniques

3.1. Research Methodology

In this thesis, the spectroscopic techniques of UV-Visible, fluorescence, Fourier-transform infrared and Raman spectroscopy as well as the analytical technique of HPLC are used to study the response of the cells and FCPS of diatoms under different growth conditions.

Spectroscopy is the study of the interaction between matter and electromagnetic radiation as a function of the wavelength or frequency of the radiation. In simpler terms, spectroscopy is the precise study of color as generalized from visible light to all bands of the electromagnetic spectrum.

Spectroscopy, mainly in the electromagnetic spectrum, is a fundamental research tool in the fields of physics, chemistry and astronomy, enabling the investigation of the composition, physical and electronic structure of matter at atomic, molecular, macro scales and at astronomical distances. Important applications arise from biomedical spectroscopy in the fields of tissue analysis and medical imaging.

The electromagnetic spectrum is usually categorized based on the wavelength of the radiation, as shown in the figure below.

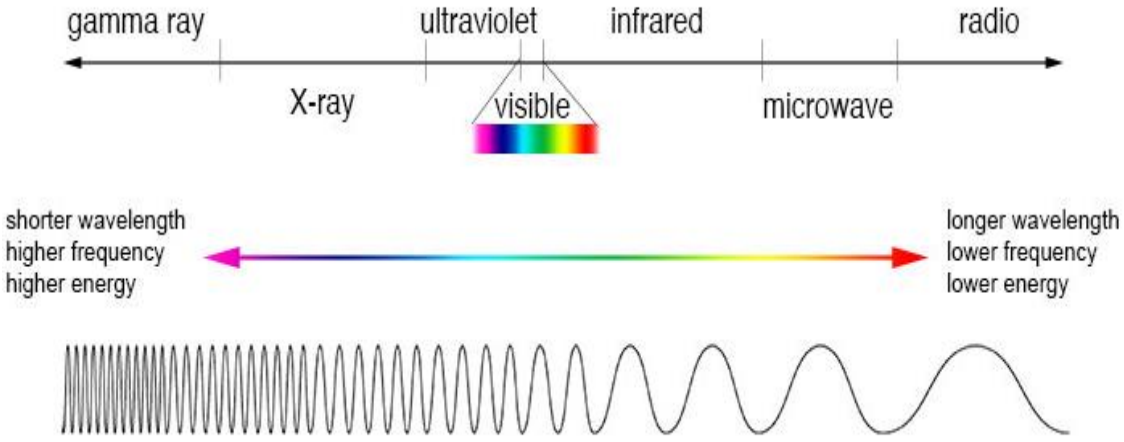

Figure 17: electromagnetic spectrum

The energy of each photon of a certain wavelength is given by the equation:

$$E = \frac{hc}{\lambda} = h\nu \qquad \text{equation (1)}$$

Where E is the energy of the photon, c the speed of light, λ the wavelength, ν the frequency and h the Planck constant (6.62607015×10−34 Js). Therefore, as the wavelength of the radiation increases, the energy that is transferred by each photon, when the specific radiation hits a body, decreases.

3.1.1. Ultraviolet – Visible Absorption Spectroscopy

Ultraviolet-Visible Spectroscopy (UV) is an analytical technique that measures the number of distinct wavelengths of UV or visible light absorbed or transmitted through a sample compared to a reference or blank. This property is affected by the composition of the sample, potentially providing information about what is present in the sample and at what concentration. UV absorption spectroscopy uses 190-800nm wavelength radiation. The region between 190-400nm is part of the ultraviolet while between 400-800nm is in the visible part of the electromagnetic field. Since this spectroscopy technique is based on the use of light, let us first consider the properties of light.

Light has a certain amount of energy which is inversely proportional to its wavelength. Thus, shorter wavelengths of light carry more energy and longer wavelengths carry less energy. It takes a certain amount of energy to excite electrons in a substance to a higher energy state which we can detect as absorption. Electrons in different bond environments in a substance require a different specific amount of energy to excite the electrons to a higher energy state. This is why absorption of light occurs for different wavelengths in different substances.

When the radiation hits the sample, the sample absorbs part of it, which is recorded by this spectroscopy. The light energy calculated by equation (1) must be equal to the energy difference of two energy states of the sample for absorption to occur. UV spectroscopy absorbs energy states such as electronic, vibrational and rotational changes. However, the very small energy difference between the vibrational and rotational states cannot be separated by this technique.[1]

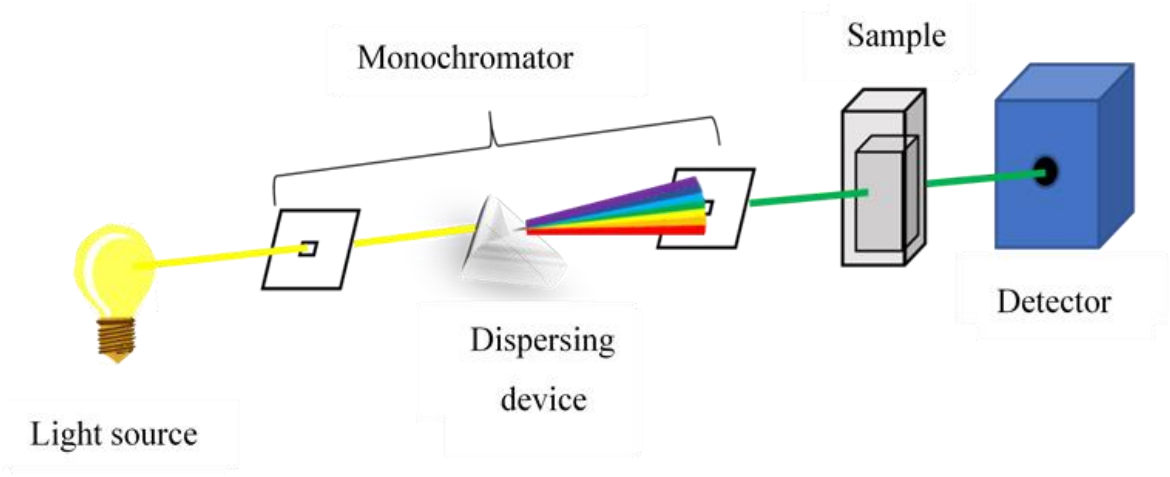

Figure 18: Schematic representation of UV-visible spectroscopy.

Radiation originates from a light source capable of emitting light in a wide range of wavelengths. A simple xenon lamp is commonly used as a high-intensity light source for both the UV and visible spectrum. Xenon lamps, however, are associated with higher costs and are less stable compared to tungsten and halogen lamps. The radiation is separated into the various wavelengths by the monochromator.

The light is passed through the sample. For all analyses, measurement of a reference sample, often referred to as a "blank", such as a vial filled with a similar solvent used for sample preparation, is imperative. If an aqueous buffer solution containing the sample is used for measurements, then the aqueous buffer solution without the substance of interest is used as the reference. The reference sample signal is automatically used by the instrument to help obtain the actual absorbance values of the analytes. It is important to know the materials and conditions used in UV-Vis spectroscopy experiments. For example, most plastic cells are unsuitable for UV absorption studies because plastic generally absorbs UV light. Glass can act as a filter, often absorbing the majority of UVC (100-280 nm)2 and UVB (280-315 nm)2, but allowing some UVA (315-400 nm) to pass through. Therefore, quartz sample holders are required for UV examination because quartz is transparent to most UV light.

After the light passes through the sample, a detector is used to convert the light into a readable electronic signal. In general, detectors are based on photoelectric coatings or semiconductors. A photoelectric coating emits negatively charged electrons when exposed to light. When electrons are ejected, an electric current proportional to the

intensity of the light is created. A photomultiplier tube (PMT) is one of the most common detectors used in UV-Vis spectroscopy. The PMT relies on the photoelectric effect to initially eject electrons upon exposure to light, followed by sequential multiplication of the ejected electrons to produce a larger electric current. PMT detectors are particularly useful for detecting very low light levels. When semiconductors are exposed to light, an electric current proportional to the intensity of the light can pass. More specifically, photodiodes and charge-coupled devices (CCDs) are two of the most common detectors based on semiconductor technology.[2, 3]

The absorption (A) of radiation by the sample is equal to the logarithm of a fraction comprising the intensity of light before passing through the sample (Io) divided by the intensity of light after passing through the sample (I). The fraction I divided by Io is also called transmittance (T), which expresses how much light has passed through a sample. However, the Beer–Lambert law (2) is often applied to obtain the sample concentration (c) after measuring the absorbance (A) when the molar absorptivity (ε) and the path length (L) are known. Typically, ε is expressed in units of L mol^{-1} cm^{-1}, L has units of cm, and c is expressed in units of mol L^{-1}. Consequently, A has no units.[4]

$$A = \varepsilon Lc = \log_{10}\left(\frac{I_0}{I}\right) = \log_{10}\left(\frac{1}{T}\right) = -\log_{10}(T) \qquad \text{equation (2)}$$

3.1.2. Fluorescence spectroscopy

Fluorescence spectroscopy is a type of electromagnetic spectroscopy that analyzes the fluorescence from a sample. Fluorescence is a type of luminescence caused by photons that excite a molecule, raising it to an electronic excited state. Molecules have various states referred to as energy levels. Fluorescence spectroscopy deals primarily with electronic and vibrational states. In general, the species under consideration has a ground electronic state (low energy state) of interest and a higher energy excited electronic state. Within each of these electronic states are various vibrational states.

In fluorescence, the sample is excited, by absorbing a photon, from its ground electronic state to one of several vibrational states in the excited electronic state. Collisions with other molecules cause the excited molecule to lose vibrational energy until it reaches a lower vibrational state than the excited electronic state. When the molecule falls back

into one of the various vibrational levels of the ground electronic state, it emits a photon. As molecules may fall into any of several vibrational levels in the ground state, the emitted photons will have different energies, and thus frequencies. Therefore, by analyzing the different frequencies of light emitted in fluorescence spectroscopy, along with their relative intensities, the structure of the different vibrational levels can be determined. Another phenomenon of similar origin is phosphorescence, where the emission of radiation originates from the molecule in ground state which has been first transferred from a singlet excited state to a triplet state via intersystem crossing.[5] Fluorescence and phosphorescence are shown in Figure 19.

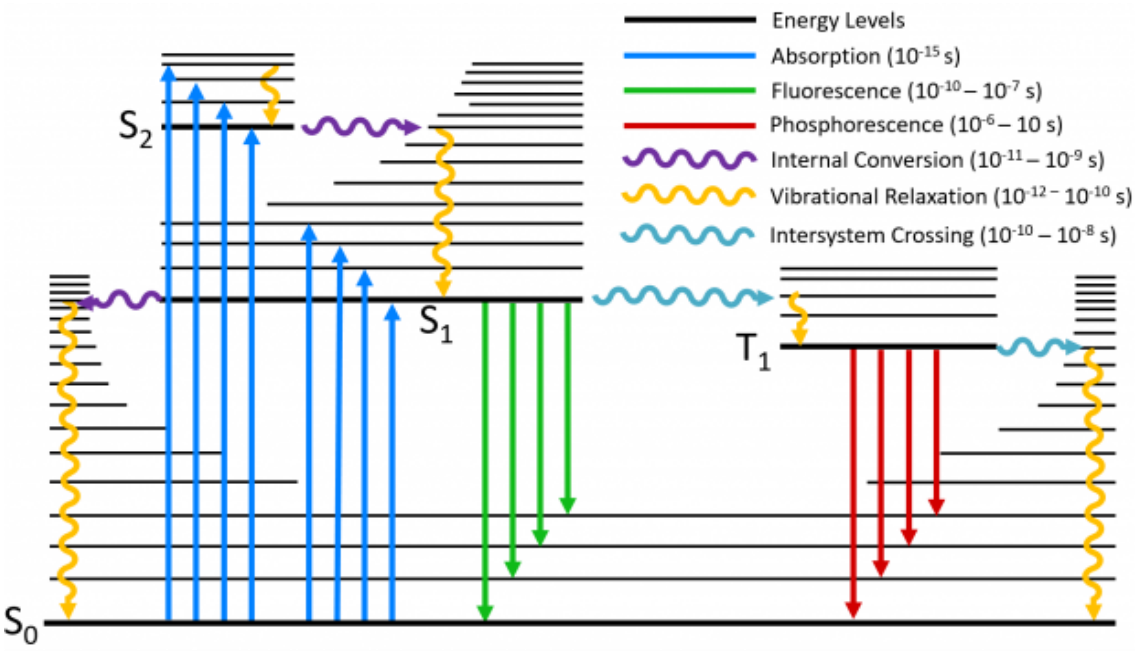

Figure 19: Schematic representation of the phenomena of fluorescence and phosphorescence.

In a standard fluorescence (emission) measurement, the excitation wavelength is fixed and the detection wavelength is varied, while in a fluorescence excitation measurement the detection wavelength is fixed and the excitation wavelength is varied over a region of interest. An emission map is measured by recording the emission spectra resulting from a series of excitation wavelengths and combining them all together. This is a 3D surface dataset. Emission intensity as a function of excitation and emission wavelengths, and is usually plotted as a contour map.

The spectrometer introduces UV or visible light using a photon source such as a laser,

xenon lamp, or LED. The light is passed through a monochromator that selects a specific wavelength, often using a diffraction grating. A diffraction grating is a plate of glass or metal with very close parallel lines, which produce a spectrum of diffraction and interference of light. The light exiting the monochromator, comes out at a certain angle depending on its wavelength. The spectrometer focuses the monochromatic wavelength onto the sample. The sample emits a wavelength, which travels to the detector. The detector is usually set at a 90-degree angle to the light source to avoid any interference from the emitted excitation light. The emitted photons strike a photo detector. Computer software connected to the detector creates a spectrum, a graphical representation that shows which wavelengths are absorbed by the sample. The emission spectrum shows which wavelengths the samples emit.[6,7]

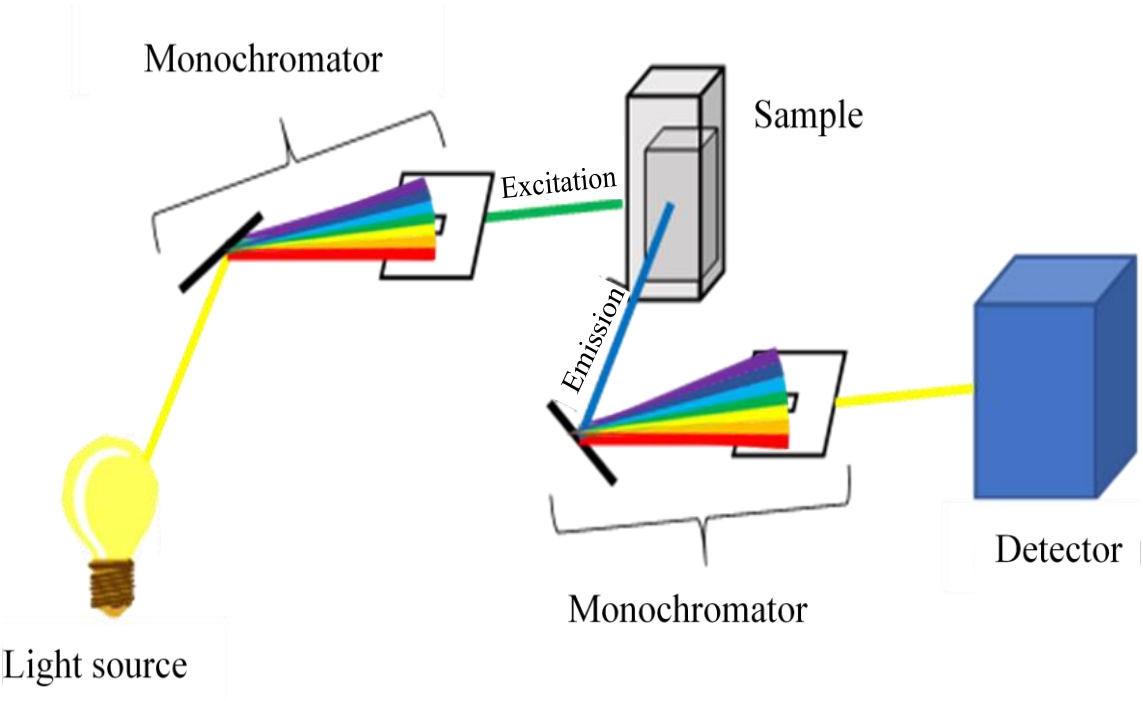

Figure 20: Schematic representation of fluorescence spectroscopy.

3.1.3. Fourier Transform Infrared Spectroscopy (FTIR)

Fourier transform infrared spectroscopy (FTIR) is a technique used to obtain an infrared absorption or emission spectrum of a solid, liquid, or gas. An FTIR spectrometer simultaneously collects high-resolution spectral data over a wide spectrum. This confers a significant advantage over a dispersive spectrometer, which measures intensity over a narrow range of wavelengths at a time. The term Fourier transform infrared spectroscopy comes from the fact that a Fourier transform (a mathematical process) is

required to convert the raw data into the actual spectrum.[8,9]

The goal of absorption spectroscopy techniques is to measure how much light a sample absorbs at each wavelength. In dispersive spectroscopy (eg, UV–Vis), a monochromatic light beam is irradiated at a sample, the light absorption is measured, and repeated for each different wavelength. FTIR spectroscopy is a less intuitive way to obtain the same information. Instead of shining a monochromatic beam of light onto the sample, this technique shines a beam containing many frequencies of light at once, and measures how much of that beam is absorbed by the sample. The beam is then modified to contain a different combination of frequencies, giving a second data point. This process is rapidly repeated many times in a short period of time. A computer then takes all the data and works backwards to deduce what the absorbance is, at each wavelength.

The beam described above is created starting with a broadband light source, containing the full range of wavelengths to be measured. The light shines on a Michelson interferometer - a certain configuration of mirrors, where it is driven by a motor. As this mirror moves, each wavelength of light in the beam is blocked and transmitted alternately by the interferometer, due to wave interference. Different wavelengths are modulated at different rates so that at each instant, or mirror position, the beam coming out of the interferometer has a different spectrum.

As mentioned, computer processing is required to convert the raw data into the desired output. The required processing turns out to be a common algorithm called the Fourier transform. The Fourier transform, transforms a domain into its inverse domain. The raw data is called a "bar graph".

As you see in Figure 21, an infrared source sends a beam of light to the beam splitter which splits the energy to a stationary mirror and a moving mirror. Both mirrors reflect the light back to the beam splitter which recombines the beam and strikes the sample. As the beam leaves the sample, it is collected by a detector that converts the signal for reading by a computer.

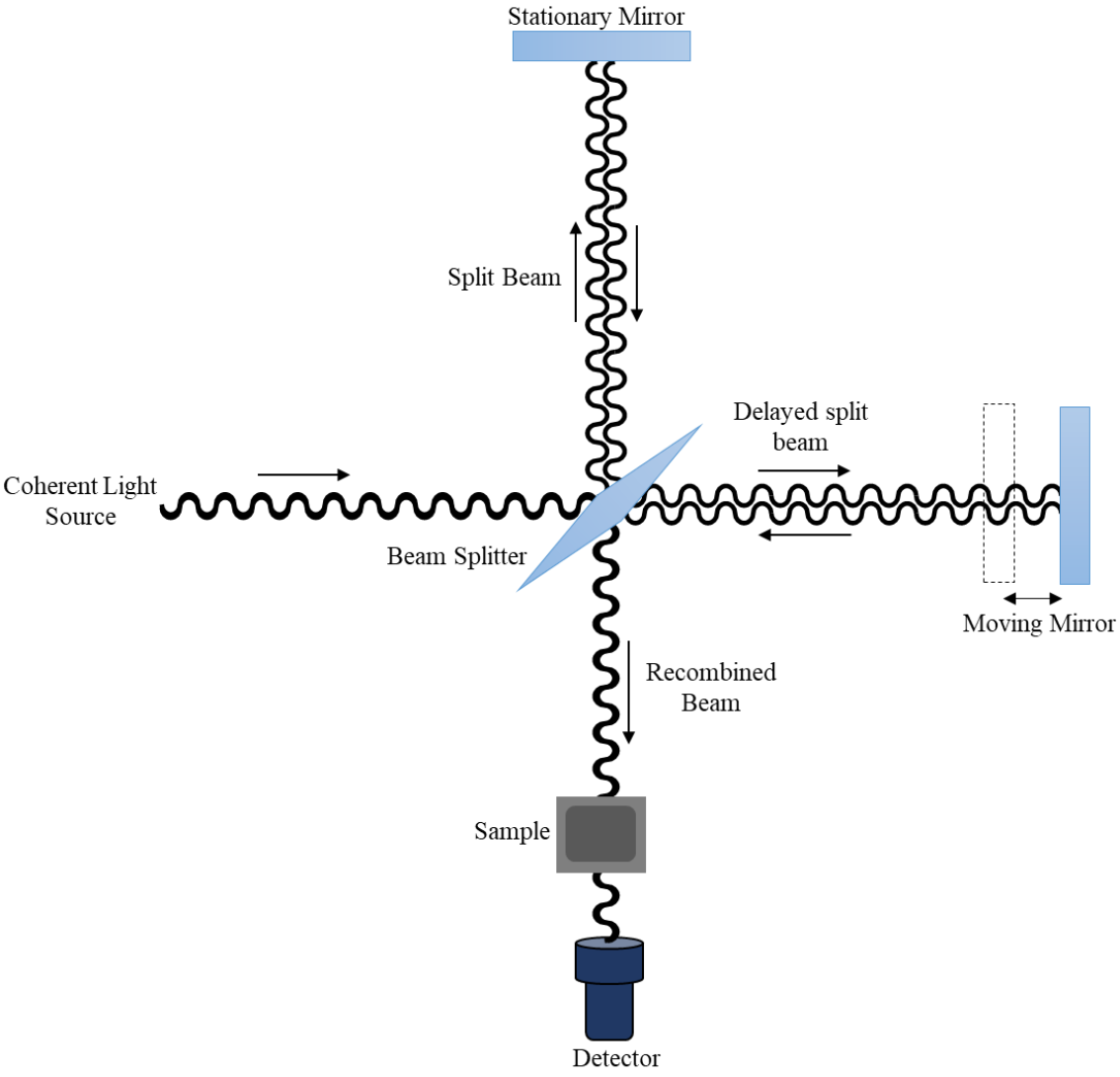

Figure 21: Schematic representation of FTIR spectroscopy.

There are four main sampling techniques in FTIR: transmission, attenuated total reflection (ATR), specular reflection, and diffuse reflection. The first techniques is transmission, in which the infrared beam is passed through the sample in a cell and then onto the detector. In ATR the infrared beam enters the crystal and interacts with the sample on the surface of the crystal and then exits the crystal and passes to the detector. In diffuse reflectance, the infrared beam interacts with the sample which is a packed powder usually mixed with other chemicals such as KBr or diamond dust. In specular reflection, the infrared beam passes through the sample lying on the surface of a reflective sample, strikes the reflective surface, and bounces through the same sample a second time and then goes to the detector.[10,11]

3.1.4. Raman Spectroscopy

The Raman method studies the scattered radiation of a solid, liquid or gaseous sample. When a photon interacts with a molecule and its energy is not sufficient to cause an electronic transition, it can be scattered in three different ways: (a) elastically, i.e. maintaining its initial energy, (b) inelastically with a decrease in its energy and (c) inelastically with an increase in its energy. In the first case, the result is that the scattered radiation has the same frequency as the incident radiation and is called Rayleigh scattering, while in the other cases, Raman Stokes and Anti-Stokes scattering occur, respectively.[5]

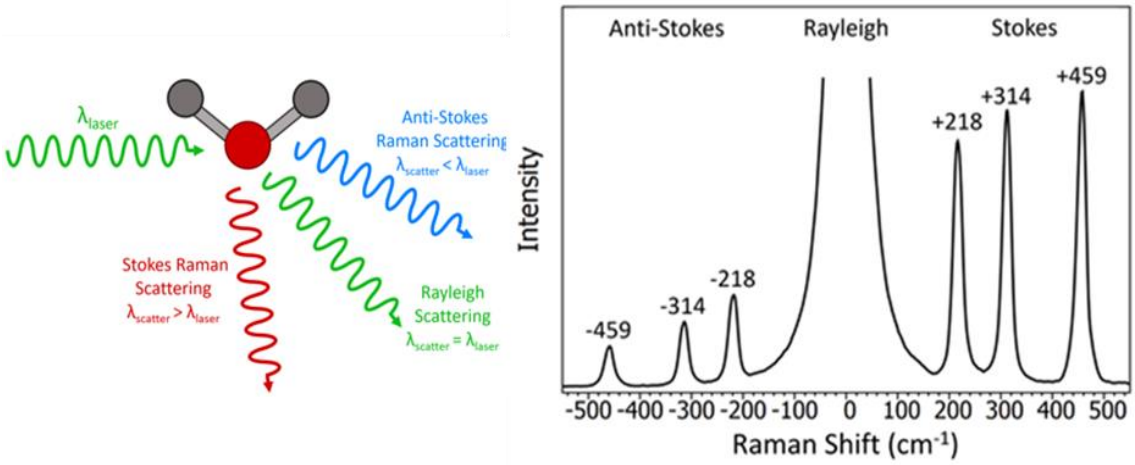

Figure 22: Schematic representation of the Raman effect.

The difference between the frequency of the incident and scattered radiation is called the Raman shift and the set of different frequencies of scattered radiation constitute the Raman spectrum. The Raman shift is usually expressed in wavenumbers $\tilde{\nu}$ (cm^{-1}) but is also referred to as frequency due to the ratio of the two quantities linked by the relationship:

$$\tilde{\nu} = \frac{\nu}{c} = \frac{1}{\lambda}$$

Where ν is the frequency, c is the speed of light and λ is the wavelength. Accordingly, the Raman shift depends on the wavelength of the incident (λ_0) and scattered (λ_i) radiation as follows:

$$\text{Raman shift}(\text{cm}^{-1}) = \frac{10^7}{\lambda_{0(\text{nm})}} - \frac{10^7}{\lambda_{\iota(\text{nm})}}$$

Raman scattering is a weak process and thus, many times the intensity of the signal due to certain vibrations is not enough to allow its observation. Phenomena such as fluorescence also contribute to this. However, it has been observed that if the wavelength emitted by the laser is identical to or close enough to the energy required by a molecule to make an electronic transition in it, then the intensity of the scattered Raman radiation is amplified by 10 to 100,000 times. This amplification is more intense in chromophore molecules due to the greater absorption of radiation by them. The resonance phenomenon is mainly due to the rapid increase in polarizability during radiation absorption.[12]

Due to the resonance phenomenon mentioned earlier, chromophore molecules are ideal for study with Raman spectroscopy. Carotenoids and chlorophylls are two classes of chromophore molecules that have been extensively studied with this technique. Figure 23 shows a characteristic Raman spectrum of the diatom P. Tricornutum cells, showing the origin of the most important vibrations between carotenoids and chlorophylls.

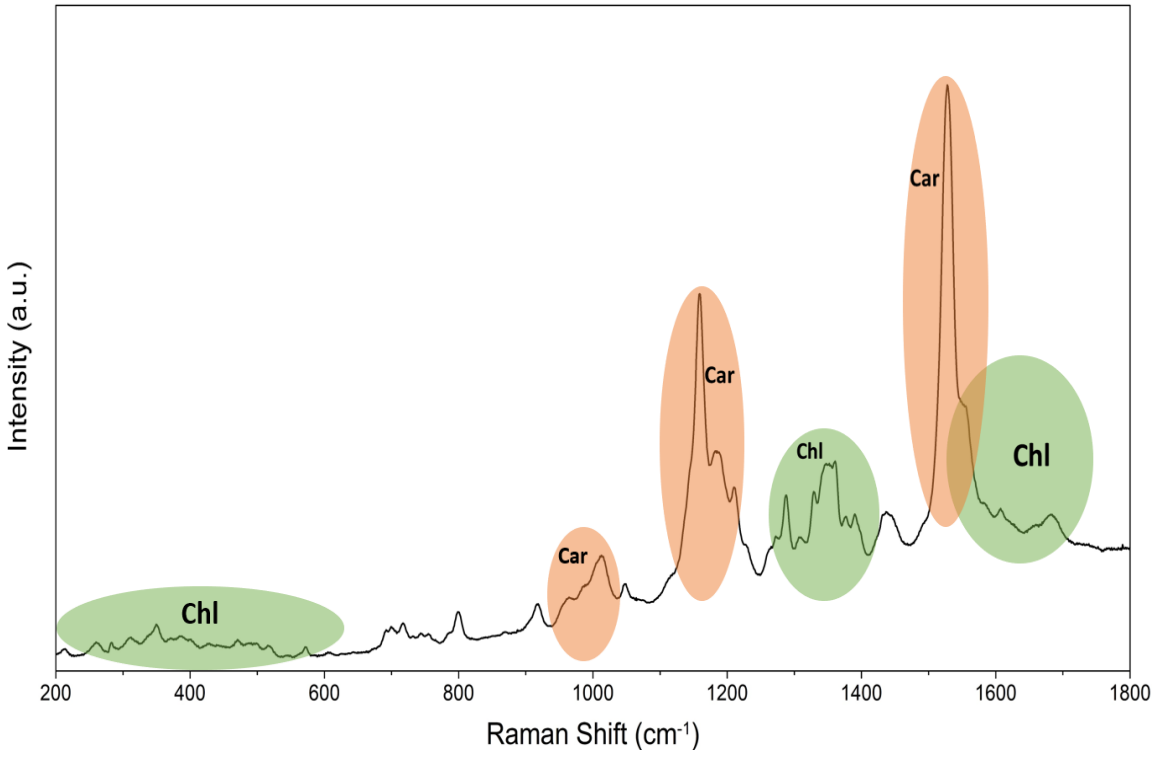

Figure 23: Raman spectrum of the diatom P. Tricornutum cells.

The spectrum of carotenoids is characterized by four groups of vibrations (ν1-ν4) which have the highest intensity. ν1 appears at approximately 1520 cm^{-1} and is attributed to stretching vibrations of the C=C double bonds.[13,14]

However, the position of appearance can be influenced by other factors such as temperature and the chemical environment in which the polymer is located, so the identification and separation of the different carotenoids cannot be done with this information alone.[15] The full width at half maximum of the peak corresponding to a particular vibration can provide information about the number of different carotenoids present in a cell. When the sample consists of a single species, the expected width is about 12 cm^{-1}, when the width is larger it is usually due to the overlap of peaks originating from vibrations of more carotenoids.[13]

The ν2 appears at approximately 1160cm^{-1} and is due to the stretching vibrations of the C-C single bonds. Around the main vibration, satellite vibrations appear which can be correlated with the arrangement of the carotenoids.[14,15]

The ν3 is due to the in-plane stretching vibrations of the methyl groups attached to the polymer chain in combination with the in-plane C-H bending vibrations and appears at approximately 1005cm^{-1}. This region provides information about the structure and orientation of the polymer chain ends.

The ν4 appears at about 960cm^{-1} and is due to the out-of-plane C-H wagging vibrations in combination with the C=C twisting vibrations. When the "structure" of the carotenoid is planar, these vibrations are not visible due to the non-coupling of the orbitals with electronic transitions. This has the effect that these vibrations are not amplified by the resonance effect and thus are not visible in the spectrum obtained.[13,14]

Regarding the vibrations originating from chlorophyll molecules, the most important ones can be divided into 3 regions. The first is located between 200-600 cm^{-1} and concerns vibrations that are directly related to the central magnesium atom of their structure. The second region is between 900-1600 cm^{-1} where vibrations sensitive to the geometric configuration of the molecules appear, such as the C-N vibrations and finally the region 1600-1710 cm^{-1} where the stretching vibrations of the conjugated vinyl and carbonyl groups are present. These vibrations offer information about the coordination number of the central magnesium atom as well as more generally about the interactions

of the molecules with the environment in which they are found.[13]

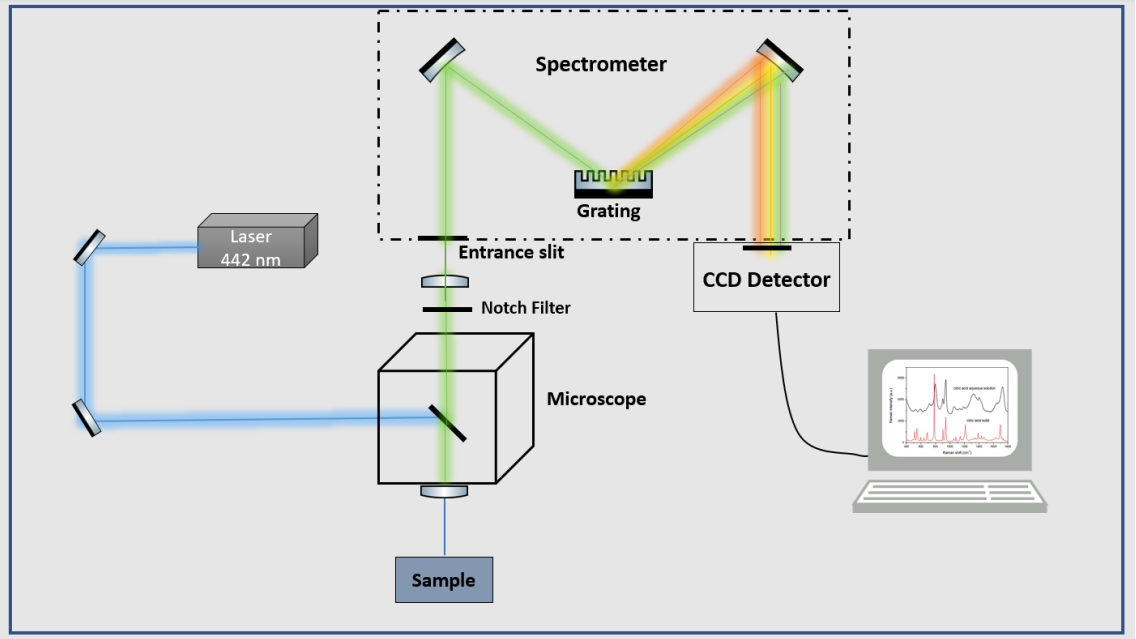

Figure 24: Schematic experimental setup of Raman spectroscopy.

The above image shows a typical experimental setup for Raman spectroscopy. In summary, the excitation radiation comes from a laser source and is directed using mirrors to the sample where, using a suitable lens, the beam is focused on the sample. Subsequently, the scattered light is directed to the detector where, using a suitable optical filter, the radiation is cut off from Rayleigh scattering and then enters the monochromator where, using mirrors and diffraction gratings, the analysis of the scattered radiation is carried out by separating it into parallel beams depending on their energy. After being analyzed, the light is collected by the CCD (Charge Coupled Device) detector and transferred to the computer where, with appropriate software, the signal can be processed.

3.1.5. High Performance Liquid Chromatography

The HPLC technique is used to identify and quantify the components of a sample. Its operation is based on the interactions between the sample and the packing material located within a special column used in chromatography and leads to the separation of the components. A representation of the operation of the technique is shown in the image below.

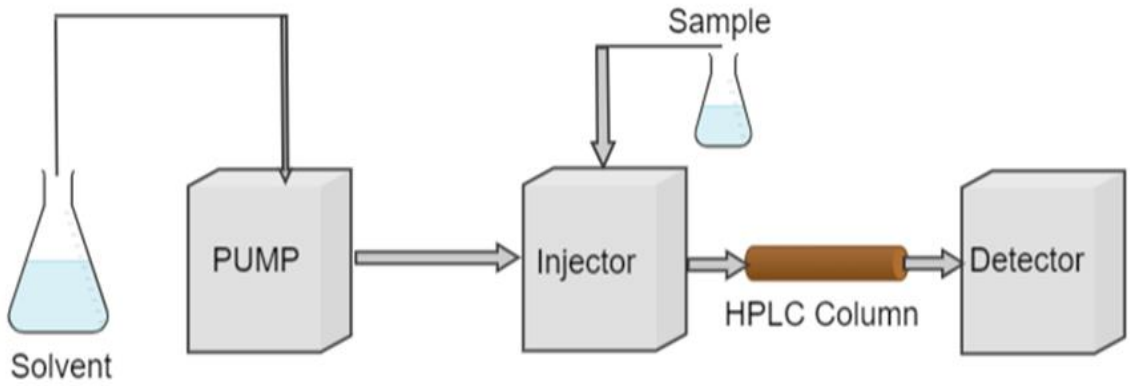

Figure 25: Schematic representation of the liquid chromatography technique

The appropriate solution or mixture of solutions used as the mobile phase enters the system through the pump. Subsequently, the sample is introduced and directed to the selected chromatography column which has the appropriate packing material. The interactions of the sample with the packing material of the column in combination with the type of mobile phase mixture lead to separation of the components of the sample through the different retention time of each component and consequently different elution time. When the parameters that determine the characteristics of the mobile phase, such as composition, pH, flow and temperature, remain constant, then the elution is called isocratic, while when they change, it is called gradient. Then the components of the sample are directed to the detector through which identification can be made depending on its type. In the context of this thesis, two types of detectors have been used, the first is a visible-ultraviolet detector, which can detect the presence of a substance that exhibits absorption at a specific wavelength, while the second is a photodiode array detector (PDA) which can detect the absorption of the sample in a wide range of wavelengths in the visible and ultraviolet regions, essentially offering the absorption spectrum of each component of the sample. After the detector, there is the option of discarding or collecting the sample depending on the capabilities of the system.

There are several variations of liquid chromatography, but herein reference will be made to two basic ones that were used in the thesis. Reversed-phase chromatography uses the polarity of the samples as a means of separation. The column packing material in this method is non-polar, while polar solvents are used in the mobile phase, with

methanol and acetonitrile being the most common. A second category of liquid chromatography is the ion exchange which uses electrostatic interactions of the sample with the packing material as a means of separation. This method is particularly used for the separation of proteins.[16]

Regarding the analysis of photosynthetic pigments, dozens of different methodologies have been developed which lead to the separation of substances and allow their quantification within organisms as well as the study of their properties outside the biological system from which they originate.[17,18]

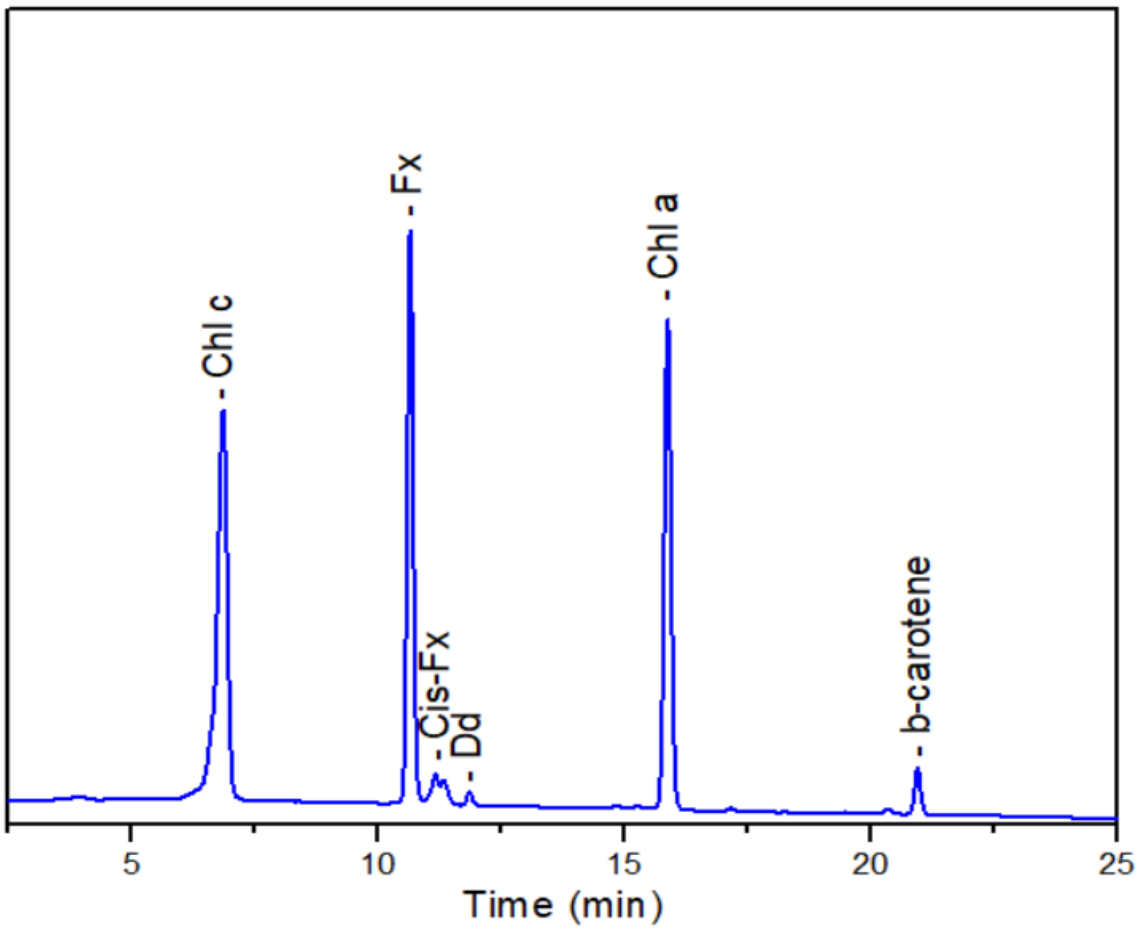

Figure 26: HPLC chromatogram of Frag. sp FCP illustrating the major pigments at their elution time.

3.2. Experimental Techniques

3.2.1. Diatom Growth

The cultures of the diatoms P. Tricornutum (CCAP 1052/1A) and Frag. sp (CCAP 1029/24) have been received from the CCAP (Culture Collection of Algae and Protozoa) center and were maintained by continuous subcultures in the f/2+Si (Guillard's medium). Initially, 5 solutions are prepared which contain the necessary substances for the growth of the diatoms as shown below.[19]

1) $NaNO_3$ 75g/L

2) $NaH_2PO_4.2H_2O$ 5.65g/L

3) Trace elements

Na_2EDTA	4,15g/L
$FeCl_3.6H_2O$	3.15g/L
$CuSO_4.5H2O$	0.01g/L
$ZnSO_4.7H_2O$	0.02g/L
$CoCl_2.6\ H_2O$	0.01g/L
$MnCl_2.4\ H_2O$	0.18g/L
$Na_2MoO_4.2\ H_2O$	6 mg/L

4) Vitamins

Cyanocobalamin (Vitamin B_{12})	0.5mg/L
Biotin	0.5mg/L
Thiamine HCL (Vitamin B_1)	0.1g/L

5) $Na_2SiO_3.9\ H_2O$ 30g/L

Subsequently, for the preparation of the medium, 1ml of each solution is added to 1L of seawater and the pH is adjusted to 8 using 1M NaOH or 1M HCl. The medium as well as the containers in which the diatoms will be grown are sterilized using an autoclave (15min/120°C). All cultivations are carried out in a sterile environment to avoid the growth of other microorganisms inside the containers.

Diatom cultures are grown in glass containers and their volume can be varied depending on the needs of the experimental procedure. The cultures used for the experiments of this thesis had a volume of 30-500 ml. Diatom culture is carried out by transferring a quantity of an existing active culture into a container containing sterile biomass in order to multiply the cells. The volume of the active culture is usually 10% of the final volume of the new culture. In all cases, LED (Light Emitting Diode) lamps were used as a light source, which operated for 12 hours per day, providing the cultures with cycles of 12 hours of light and 12 hours of darkness. The emission spectrum from the lamps used (white, blue and red light) is presented in Figure 27.

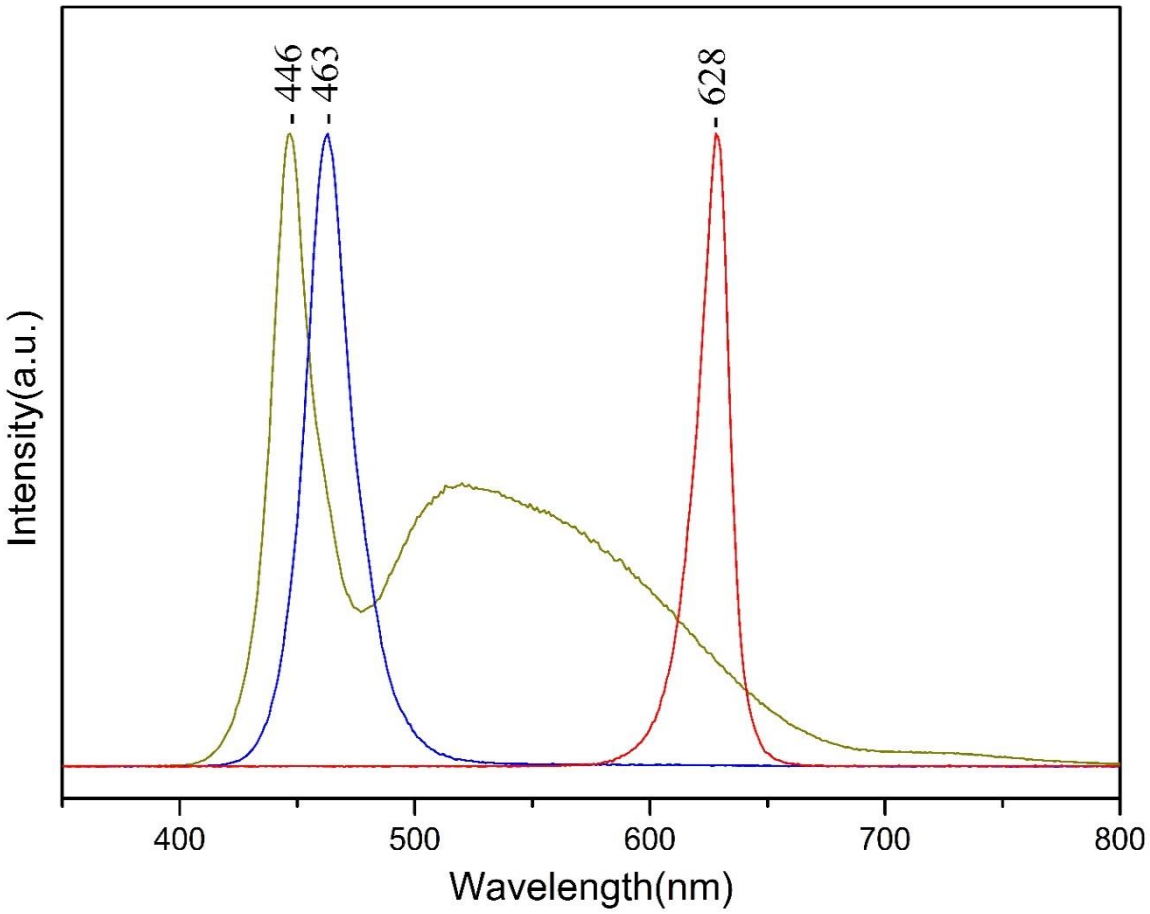

Figure 27: Emission spectrum of LED light sources white (yellow), blue (blue line) and red (red line) light.

The light intensity in the culture for the experiments carried out had values of 15, 150 and 350 μmol photons m^{-2} s^{-1}. The intensity measurement was made using a LightMeter LX-1118, the values reported were measured at the distance from the light source where the cultures were placed. The growth temperature of the diatoms in all cases was 20 °C.

The growth rate of the organisms was monitored by measuring the optical density (OD) at 750nm, which is an indicator of cell proliferation and increases depending on the number of diatoms present in the sample.[20] . A typical growth curve of a diatom is shown in Figure 28.

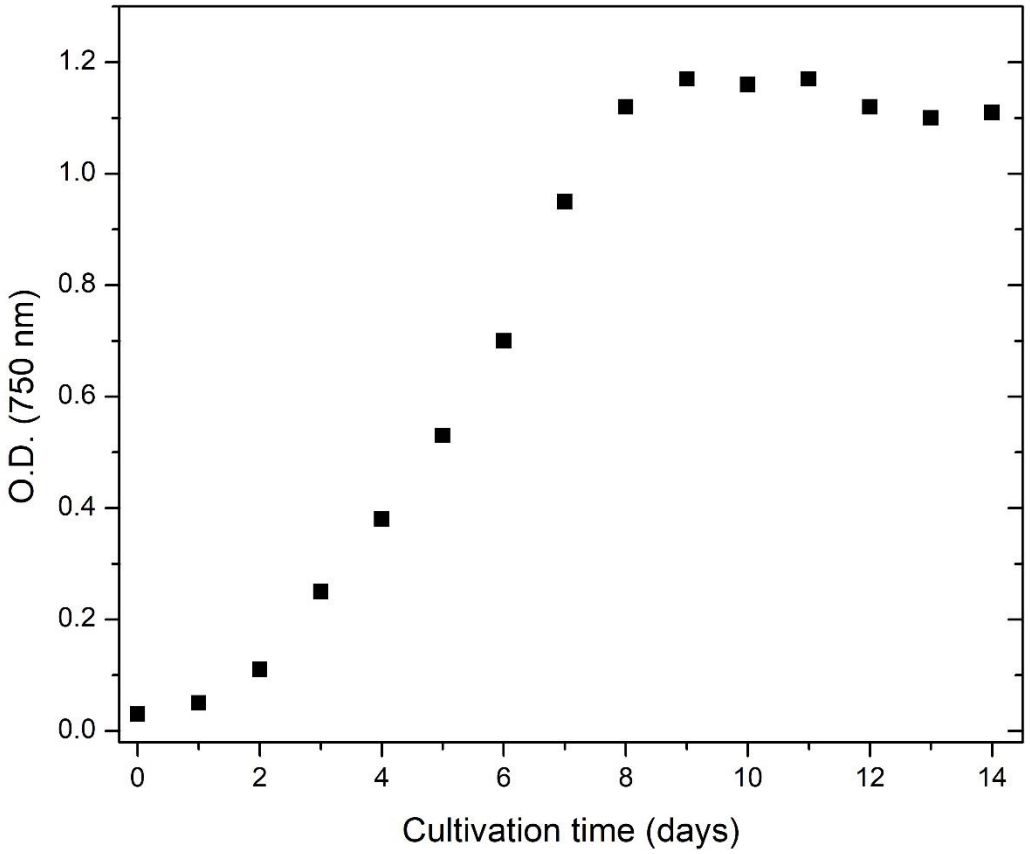

Figure 28: A typical growth curve of a diatom.

The first part of the curve is called the adaptation phase, where no cell division is observed and their mass remains constant. This is followed by the exponential phase where an exponential increase in the number of cells is observed up to approximately 109 cells/ml where the culture now enters the stationary phase. The end of the exponential phase, if there is no other external factor, is due to the lack of nutrients and oxygen from the culture vessel. In this phase the rate of growth and death of cells is equal and thus the population is maintained constant. Finally, the death phase occurs where the growth rate has become smaller than the death rate and the cell population decreases exponentially.

3.2.2. FCPs Isolation

Cells from the diatom were harvested by centrifugation (8000 revolutions per minute (rpm), 30 min, 4°C), and the supernatant medium was removed. The cells were resuspended in 20 mM Tris buffer and sonicated in an ice bath for 20 min. Thylakoids were then solubilized with the addition of β-1,4-dodecyl maltoside (β-DDM, 30 mg, 4 mM) in the resuspended cells while they were shaken for 20 min on ice. The supernatant was collected after centrifugation for the FCP separation. Separation of solubilized proteins was carried out on an ion exchange column (HiPrepQ HP 16/10, 20 mL) in 25 mM Tris, 2 mM KCl, and 0.4 mMβ-DDM at pH 7.4 using a Shimadzu LC-20AD with an SPD-20A detector with two-wavelength detection. The samples were loaded in a column, and fractions were eluted using agradient from 0 to 750 mM KCl in a buffer made of 25 mM Tris buffer, 750 mM KCl, and 0.4 mM β-DDM, pH 7.4 at a flow rate of 3 mL/min. Fractions were pooled and concentrated using Amicon filtration devices with a cutoff of 10 kDa and characterized, spectroscopically and chromatographically. The rest of the fractions were stored at −80 °C until further use.

Table 1: Detailed description of the HPLC low pressure gradient FCPs isolation protocol.

	------- Solvents -------		
Time (min)	A	B	Flow rate (ml/min)
0	100	0	3
2	85	15	3
5.9	70	30	3
12.7	60	40	3
19.6	55	45	3
26.5	45	55	3
31.4	35	65	3
37.2	100	0	3
50	100	0	3

3.2.3. Ultraviolet-Visible spectroscopy

For the acquisition of UV spectra, the Cary 60 Uv-vis instrument (Agilent Technologies, USA) was used and the measurements were performed in a quartz cell. (Hellma fluorescence cuvettes, quartz, spectral range 200-2500 nm, pathlength 3x3 mm, chamber volume 45 μL)

3.2.4. Fluorescence spectroscopy

The Cary Eclipse Fluorescence Spectrophotometer (Agilent Technologies, USA) was used for recording the Fluorescent spectra. The slit widths for the excitation and emission monochromators were set at 10.0 nm and 5.0 nm respectively. The measurements were performed in a quartz cell (Hellma fluorescence cuvettes, quartz,

spectral range 200-2500 nm, pathlength 3x3 mm, chamber volume 45 μL)

3.2.5. Raman Spectroscopy

Raman spectra were obtained using the LabRam system (Horiba, Jobin Yvon, Japan) which is equipped with a CCD detector (1800grooves/mm grating). The spectral resolution was $5cm^{-1}$. The radiation for all measurements came from a KIMMON He-Cd Laser with a wavelength of 405nm and 442nm and its power on the sample was 10mW. For samples that required measurements at low temperature, a temperature-controlled cell (Linkam) was used and the sample was cooled using liquid nitrogen. The duration of the measurements is reported separately for each spectrum presented below.

3.2.6. FTIR Spectroscopy

FTIR spectra were recorded with 4 cm^1 spectral resolution on a Bruker Vertex 80V spectrometer equipped with a photovoltaic MCT detector (Kolmar Technologies KV100-1B-7/190). A vacuum pump was used to evacuate the interferometer compartment to a final pressure of 3.2 mbar and the scan were taken under nitrogen environment. The FTIR spectrometer was placed on a Newport VH optical vibration isolation table to ensure that vibrational background noise from environmental sources was avoided. Approximately 5 μL of sample was deposited on the crystal and allowed to dry for ~10 min until a film layer was formed prior to the measurement. A background spectrum against air was recorded before each sample spectrum. The background and sample spectra were acquired at 4 cm−1 resolution with 32 scans from 4000 to 400 cm−1.

3.2.7. Pigment analysis using HPLC

The collection of cells was done during the exponential growth phase of the organisms in all cases. The initial volume of cells used was 3ml which after centrifugation at 5000 rpm for 3 minutes were collected and the supernatant biomass was removed and replaced with 100 μL of methanol. The following steps were carried out in a room with very low lighting and intermediate placement of the sample on ice in order to avoid damage in the sample due to high temperature or lighting. The sample was subjected to agitation for 30 seconds and then placed in an ultrasonic bath for the same period of time. These steps were repeated 5 times and then the sample was centrifuged for 1 minute at 8000 rpm. The supernatant which contained the pigments of the diatom cells

was collected and stored at a temperature of -20 °C until its analysis. The analysis of the pigments was performed using HPLC. (Shimadzu-Nexera 40 system equipped with a SPD-M40 detector (Photodiode Array Detector)). The column used was Zorbax SB-C18 reverse phase (Agilent). The solutions used were the following: A) 0.5M Ammomium Acetate in methanol/water (85:15 v/v), (B) Acetonitrile and water (90:10, v/v) and (C) 100% Ethyl Acetate. The separation was done by gradient elution as shown in Table 2.

Table 2: Detailed description of the HPLC low pressure gradient pigment separation protocol.

	----------	**Solvents**	----------	
Time (min)	A	B	C	Flow rate (ml/min)
0	60	40	0	0.8
2	0	100	0	0.8
7	0	80	20	0.8
17	0	50	50	0.8
21	0	30	70	0.8
28.5	0	30	70	0.8
29.5	0	100	0	0.8
30.5	60	40	0	0.8

The identification of the various pigments was done using the literature and the absorption spectrum of each substance.[21] The stoichiometry of each sample compared to the chl a concentration was estimated from the area of each peak using the corresponding absorption coefficients.[22]

References

1. Harris DC. *Quantitative Chemical Analysis*. 7th ed, 3rd printing. W. H. Freeman; 2007.

2. Diffey BL. Sources and measurement of ultraviolet radiation. Methods. 2002 Sep;28(1):4–13.

3. Picollo M, Aceto M, Vitorino T. UV-Vis spectroscopy. Physical Sciences Reviews. 2018;14;4(4).

4. Perkampus H. UV-VIS Spectroscopy and Its Applications. Berlin-Heidelberg: Springer-Verlag; 1992.

5. Atkins PW, De Paula J, Keeler J. Atkins' Physical Chemistry. 8th ed. Oxford: Oxford University Press; 2006.

6. Lakowicz J. Principles of fluorescence spectroscopy. 3rd ed. Baltimore, Maryland, USA: Springer; 1983.

7. Albani J. Principles and Applications of Fluorescence Spectroscopy. Lille, France: Blackwell Publishing; 2007.

8. Bates J. Fourier Transform Infrared Spectroscopy. American Association for the Advancement of Science. 1976;191(4222):31-37.

9. Berthomieu C, Hienerwadel R. Fourier transform infrared (FTIR) spectroscopy. Photosynthesis Research. 2009;101(2-3):157-170.

10. Paré J, Belanger J. Instrumental methods in food analysis. Amsterdam: Elsevier; 1997.

11. Farrukh M. Advanced Aspects of Spectroscopy. Rijeka: InTech; 2012.

12. John Ralph Ferraro, Kazuo Nakamoto, Brown CW. Introductory Raman spectroscopy. Amsterdam Etc.: Academic Press; 2009.

13. Gall A, Pascal AA, Robert B. Vibrational techniques applied to photosynthesis: Resonance Raman and fluorescence line-narrowing. Biochimica et Biophysica Acta (BBA) - Bioenergetics. 2015;1847(1):12–8.

14. Papageorgiou M, Charalampos Tselios, Constantinos Varotsis. Photoreduction of carotenoids in the aerobic anoxygenic photoheterotrophs probed by real time Raman spectroscopy. Journal of Photochemistry and Photobiology B Biology. 2020 Oct 24;213:112069.

15. Llansola-Portoles MJ, Pascal AA, Robert B. Electronic and vibrational properties of carotenoids: from in vitro to in vivo. Journal of The Royal Society Interface. 2017 Oct 11;14(135):20170504.

16. Andreou C, Charalampos Tselios, Ioannou A, Constantinos Varotsis. Probing the Fucoxanthin-Chlorophyll a/c-Binding Proteins (FCPs) of the Marine Diatom Fragilariopsis sp. by Resonance Raman Spectroscopy. The Journal of Physical Chemistry B. 2023;127(42):9014–20.

17. Sabir AM, Moloy M, Bhasin PS. HPLC METHOD DEVELOPMENT AND VALIDATION: A REVIEW. International Research Journal of Pharmacy. 2016 Nov 21;4(4):39–46.

18. Zapata M, Rodríguez F, Garrido J. Separation of chlorophylls and carotenoids from marine phytoplankton:a new HPLC method using a reversed phase C8 column and pyridine-containing mobile phases. Marine Ecology Progress Series. 2000;195:29–45.

19. Guillard, R.R.L. Culture of phytoplankton for feeding marine invertebrates. pp 26-60. In Smith W.L. and Chanley M.H (Eds.) Culture of Marine Invertebrate Animals. Plenum Press, New York, USA;1975.

20. Jensen EL, Yangüez K, Carrière F, Gontero B. Storage Compound Accumulation in Diatoms as Response to Elevated CO2 Concentration. Biology. 2019;9(1):5.

21. Kraay GW, Zapata M, Marcel J.W. Veldhuis. SEPARATION OF CHLOROPHYLLS c1c2, AND c3 OF MARINE PHYTOPLANKTON BY REVERSED-PHASE-C18-HIGH-PERFORMANCE LIQUID CHROMATOGRAPHY1. J Phycol. 1992;28(5):708–12.

22. Jeffrey SW, Mantoura RFC. Phytoplankton Pigments in Oceanography. Paris, France: Unesco; 1997.

4. Probing the Fucoxanthin-Chlorophyll a/c-binding proteins (FCPs) of the Marine Diatom Fragilariopsis sp by resonance Raman spectroscopy

Herein, we report resonance Raman spectra of the light-harvesting FCPs of the Marine Diatom Frag. sp The Raman shifts in the ^{15}N-isotope enriched diatom provide the first spectroscopic evidence for the characterization of the C_a-N marker bands, and thus, of the penta- and hexacoordinated states of chls a/c in the FCPs. Under 405 and 442 nm Raman excitations, all the marker bands of Chl a/c are observed, and the isotope-based assignments provide new information concerning the structure of the Chls a/c in the FCPs and their interactions with the protein environment. Therefore, the Raman spectrum at 405 nm originates from the $\pi-\pi*$ transitions of Chl a/c and not from a different, $\pi-\pi*$ non-electronic transition, as previously reported (BBA-Bioenergetics, 2010, 1797, 1647-1656). Based on the ^{15}N isotope shifts of the C_a-N and in conjunction with other marker bands two distinct conformations of five and six-coordinated Chl a and Chl c are observed. In addition, two keto carbonyls were observed at 1679 (strong H-bonded) and at 1691 cm^{-1} (weak H-bonded) in both the 405 and 442 nm Raman spectra. Collectively, the results provide solid evidence for the nature of the vibrational modes of the active Chl a/c photosynthetic pigments in the FCPs.

4.1. Introduction

Marine Diatoms are involved in major photosynthetic biochemical cycles, in oxygenic photosynthesis and carbon fixation.[1-3] They contain the light-harvesting pigment systems FCPs to collect light energy in the blue-green region that is also available under water, and transfer the trapped energy to the reaction centers where the primary electron transfer reactions convert energy into an electrochemical gradient.[4-5] The photoacclimation strategy of species growing under variable light conditions enables the efficient regulation of photosystem structures to the amount of absorbed energy.[6] Specific interactions of the pigment molecules in the protein environment and pigment-pigment interactions account for spectral and excitation energy transfer efficiency to Chl a.[7-9] The structural differences in Chl a versus Chl c lead to modified photophysical properties between the different types of macrocycles which have been selected as the active pigments in marine photosynthesis.[10-12]

Resonance Raman spectroscopy has been applied extensively to characterize the structure of chlorophyll containing proteins.[13-18] The goal of these investigations was to determine the relationship between the protein control of electronic and molecular structure at the chlorophylls and the physiological properties of the macromolecule. A satisfactory interpretational framework is not yet available despite a wealth of published data. The correct assignment of the marker bands of Chl a/c is of pivotal importance in understanding the molecular basis of their function since they display a wide range of frequencies depending on the protein properties. In order to fully utilize the potential of resonance Raman scattering, it is essential to assign the normal modes of the Chl a/c in the FCPs. Raman spectroscopy has been applied in isolated FCPs from the centric diatom C. meneghiniana cells under frozen conditions (77K) with variable excitations from 406.7 nm to 476.5 nm.[15] It was reported that under 441, 457.9 and 476.5 nm excitation two distinct Chl c2 C131 keto carbonyls were observed at 1675 (strong H-bonded) and at 1690 cm^{-1} (weak H-bonded) associated by the presence of two C_a-N breathing modes of Chl c at 1355 and 1362 cm^{-1} indicating the presence of two conformers. Furthermore, it was reported that under 406 and 413 nm excitation there is no evidence for the presence of the C_a-N stretching modes and the C131 keto carbonyl modes of Chl c2 and the C_a-N breathing modes of Chl a are absent. It was suggested that the 406 and 413 nm excitation Raman spectra originate from a different, non π-π^* electronic transition. This suggestion is overly simplistic, but suggests that the origin of the Raman modes observed under 406 and 413 nm excitation is still unknown and raises the possibility that other vibrations despite the fact that are not conjugated into the π-system of the macrocycle could gain Raman activity. Vibrational assignments of Chl a/c based on isotopically enriched ^{15}N-FCPs are not available, yet. Resonance Raman of ^{15}N-enriched Chl a/c under 406 and 441 nm excitation are needed to establish a set of vibrational assignments of Chl a/c in the FCPs that will clarify their separate contributions in this energetic blue region. In the work presented here, we have extended our work in diatoms and employed 405 and 442 nm Raman excitation to probe the Fx-Chl a/c pigment content in the FCPs from the Marine Diatom Frag. sp.[19] The changes in ^{15}N containing Chl a/c bands in the FCP provides the first spectroscopic evidence for the characterization of the structural differences in Chl a versus Chl c that lead to altered photophysical and redox properties between the different classes of macrocycles which are crucial for light harvesting and energy transfer processes. Based on the criteria that the Raman bands associated with large shifts upon ^{15}N-substitution

are related to the C_a-N stretching, where those that do not are related to the carbon-oxygen and carbon-carbon and/or the carbon-hydrogen we have made the assignments of all Chl a/c modes. The 1361(-5) and 1354 (-5) cm^{-1} modes observed in both the 405 and 442 nm excitation Raman spectra originate from the pyrrole breathing C_a-N modes of two conformations of Chl c and those at 1377 (-5) and 1346 (-4) cm^{-1} to the C_a-N of Chl a. There are also additional vibrational modes affected by the ^{14}N to ^{15}N substitution in the macrocycles of Chls a/c. Two keto carbonyls were observed at 1679 (strong H-bonded) and at 1691 cm^{-1} (weak H-bonded) in both the 405 and 442 nm Raman spectra.

4.2. Materials and methods

4.2.1. Diatoms Growth

The culture of Frag. sp (CCAP 1029/24) was obtained from CCAP (Culture Collection of Algae and Protozoa). Cultures were grown in f/2-Si medium containing either $Na^{14}NO_3$ or $^{15}NH_4NO_3$ as nitrogen source, at 19 °C in a dark-light cycle (12h:12h) under white LED light. The light intensity used for the growth of the cell cultures was 150 μmol photons m^{-2} s^{-1}.

4.2.2. FCPs Isolation

Cells from Frag. sp diatom were harvested by centrifugation (8000 rpm, 30 min, 4°C), and the supernatant medium was removed. The cells were resuspended in 20 mM Tris buffer and sonicated in an ice bath for 20 min. Thylakoids were then solubilized with the addition of β-1,4-dodecyl maltoside (β-DDM, 30 mg, 4 mM) in the resuspended cells while they were shaken for 20 min on ice. The supernatant was collected after centrifugation for the FCP separation. Separation of solubilized proteins was carried out on an ion exchange column (HiPrepQ HP 16/10, 20 mL) in 25 mM Tris, 2 mM KCl, and 0.4 mMβ-DDM at pH 7.4 using a Shimadzu LC-20AD with an SPD-20A detector with two-wavelength detection. The samples were loaded in a column, and fractions were eluted using agradient from 0 to 750 mM KCl in a buffer made of 25 mM Tris buffer, 750 mM KCl, and 0.4 mM β-DDM, pH 7.4 at a flow rate of 3 mL/min. Fractions were pooled and concentrated using Amicon filtration devices with a cutoff of 10 kDa and characterized, spectroscopically and chromatographically. The rest of the fractions were stored at −80 °C until further use. A 2:1:1 Chla:Chlc:Fx stoichiometry was determined.

4.2.3. Raman Spectroscopy

Raman data were collected by a confocal LabRAM (HORIBA Jobin Yvon, Kyoto, Japan) equipped with a CCD detector and 1800 grooves/mm grating, and an Olympus BX41 microscope. The spectral resolution was 5 cm^{-1}. The 405 nm excitation was provided by a Coherent Laser, and the laser power incident on the sample was 10 mW. The 442 nm excitation was provided by a KIMMON He-Cd Laser, and the laser power incident on the sample was 10-15 mW. For the Raman measurements the temperature of the samples was kept at -70 °C by using a Linkam cell with a liquid Nitrogen cryostat. Absorption spectra were recorded by a Cary 60 UV–Vis spectrometer (Agilent Technologies, USA).

4.3. Results and Discussion

Figure 29, shows the UV spectra of FCP from Frag. sp at room temperature, pH 8. The transitions at 440 (Soret), 588, 621 (Qx) and 673 (Qy) nm are attributed to Chl a, and at 457 (Soret), 588 (Qx) and 637(Qy) nm to Chl c.[15,19] The broad transition in the 500-560 nm range has been attributed to red Fxs, whereas blue Fx absorb in the 420-470 nm region. The pigment analysis, of the present FCP contains Chl c_2 possessing a vinyl group at the 8-position conjugated to its porphyrin π-system.

One objective of this work is to identify the C_a-N in chl a/c by isotopic labeling of the chl a/c nitrogen (N). This way, the structure/function and coordination state of the Chl a/c in the FCPs will be determines. In the Chl a/c macrocycles, rings I and II are aligned along the y-axis and modes associated with these rings should be enhanced using lines such as 405 nm excitation. Rings II and IV are aligned along the x-axis and modes associated with these rings should be enhanced using lines such as 441 nm and/or 458 nm close to the B_x axis. Excitation within the B_y absorption band using the 406.7 nm line produces a spectrum dominated by totally symmetric Franck-Condon-active modes aligned along the y-axis of the macrocycle. The assignment of the Chl a vibrational modes is still controversial whereas that of Chl c is still limited. The 406.7 nm RR spectra of Chl a in solution obtained by the group of Bocian[13] and those recorded by 457 nm excitation by the group of Koyama[18] in conjunction with ^{15}N isotopes and normal coordinate analysis have been reported. Upon ^{15}N substitution and normal coordinate analysis by the group of Koyama[18] the modes with the largest shift upon

were the $\nu C_aN(II)/\nu C_aNC_a(I)$ at 1138 (-11), $\nu C_bH(IV)$ at 1188 (-8), $\gamma C_bH(IV)$ at 1220 (-5), $\nu C_aN(II, IV)$ at 1284 (-7), $\nu C_aN(IV)$ at 1342 (-6), $\nu C_aN(IV)$ at 1376 (-5) cm^{-1}. In addition, the 1488 (νC_aC_m), 1534 (νC_bC_b)), 1550 ($\nu C_bC_b + C_aC_m(III)$), 1604 ($\nu C_aC_m + C_bC_b$)), and 1698 ($\nu C9=O$) cm^{-1} have been identified.

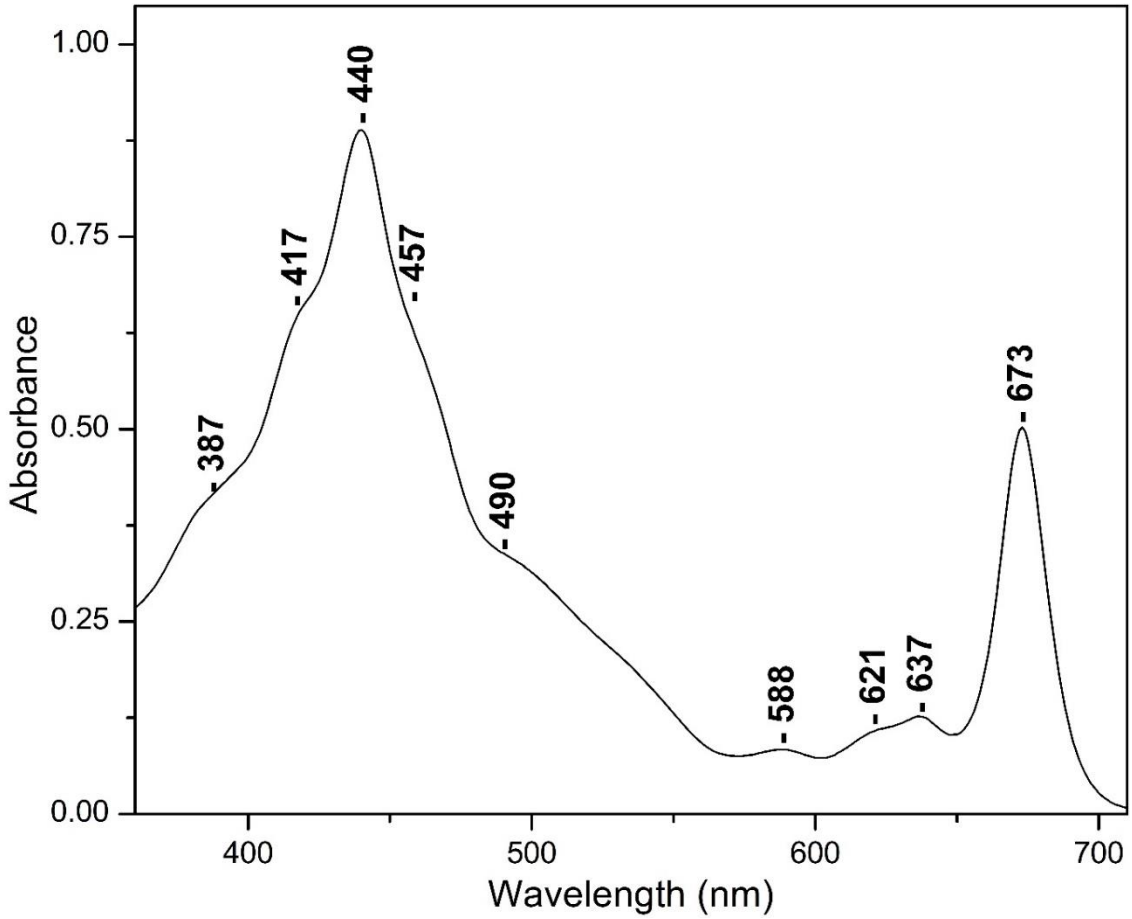

Figure 29: UV absorption spectrum of FCP Fragilariopsis sp at room temperature.

Figure 30 shows the 405 nm excitation Raman spectrum of the FCP from ^{14}N- (trace a) and ^{15}N containing FCP (trace b) at pH 8, 25°C. The assignments of the peaks in traces a are secured via the ^{15}N shifts shown in trace b. The modes with the larger isotopic shift were associated with the C_a-N stretching modes. In trace a, the peaks at 918, 1146, 1138, 1115, 1288, 1361 and 1377 cm^{-1} have contributions from C_aN of Chl a/c and the 1275 and 1346 cm^{-1} from C_mH and C_aN. The clearest indicator of Chl c is the C_a-N mode at 1361 cm-1. Its frequency is similar to that observed for the oxidation state marker band in heme containing protein with the same porphyrin ring structure.[20-21] The five-coordinate Chl a complexes are characterized by modes in the frequency range 1605-1612, 1551-1555 and 1527-1529 cm^{-1} whereas those of six-coordinate are

downshifted to 1596-1600, 1545, 1548 and 1518-1521 cm^{-1}. We assign the peaks at 1609 and 1550 cm^{-1} to five-coordinated Chl a and the 1619 cm^{-1} to the vinyl of Chl c. For the assignments of the 1550, 1656 and 1679 cm^{-1}, see below. The peaks at 965, 1005, 1046, 1160, 1185, 1195, 1490 and 1530 cm^{-1} originate from Fx, in agreement with previous works.[19,22,23]

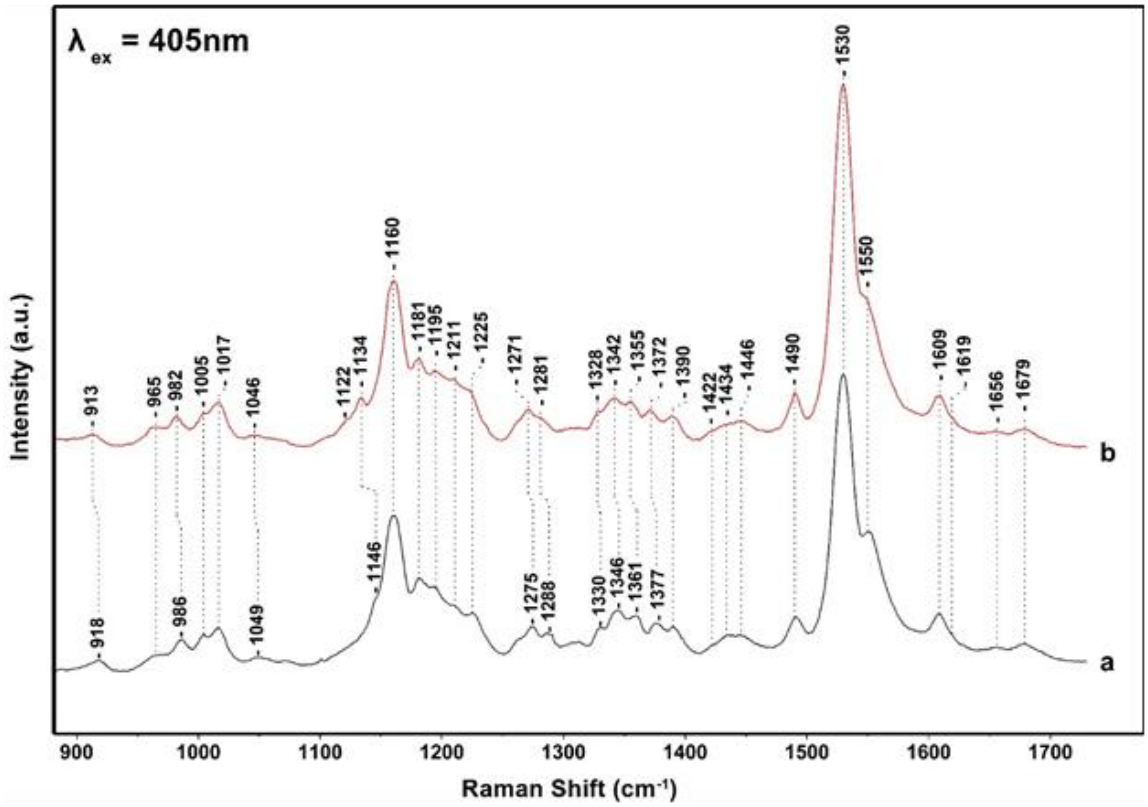

Figure 30: High frequency 405 nm excitation resonance Raman spectra of NA (trace a) and ^{15}N (trace b) FCP from Fragilariopsis sp. The 405 nm excitation laser beam was provided by a Coherent Laser and the laser power incident on the sample was 10 mW. The total accumulation time for each measurement was 1 min. Every spectrum is the average of 10 measurements.

Figure 31 shows the 442 nm excitation Raman spectrum of the FCP from ^{14}N- (trace a) and ^{15}N containing FCP (trace b) at pH 8, 25°C. The assignments of the peaks in traces a are secured via the ^{15}N shifts shown in trace b and via the spectra obtained with 405 nm excitation. The most significant differences in the data presented in Figure 31 and those in Figure 30 are 1) the intensity increase of the 1362 (ν4 of Chl c) and decrease of 1346 (Chl a) modes, 2) the presence of the 1550 cm^{-1} mode observed in the 406 nm excitation and at 1556 cm^{-1} in the 442 nm excitation spectra. The latter indicates that the

1556 cm^{-1} has contributions from the $\nu(C_aC_m+ C_b\text{-}C_b)$ of Chls c whereas the peak at 1550 cm^{-1} originates mostly from the $\nu(C_aC_m+ C_b\text{-}C_b)$ of Chl a. The distinct isotopic shift of the C_a-N modes of Chl a/c in the ^{15}N-labeled FCP confirm in conjunction with the presence of the 1608 and 1586/1593 cm^{-1} modes the presence of five and six-coordinates Chl a. The magnitude of the isotopic shift agrees well with the calculated shift based on empirical normal-coordinate analysis using isotopes of chl a.

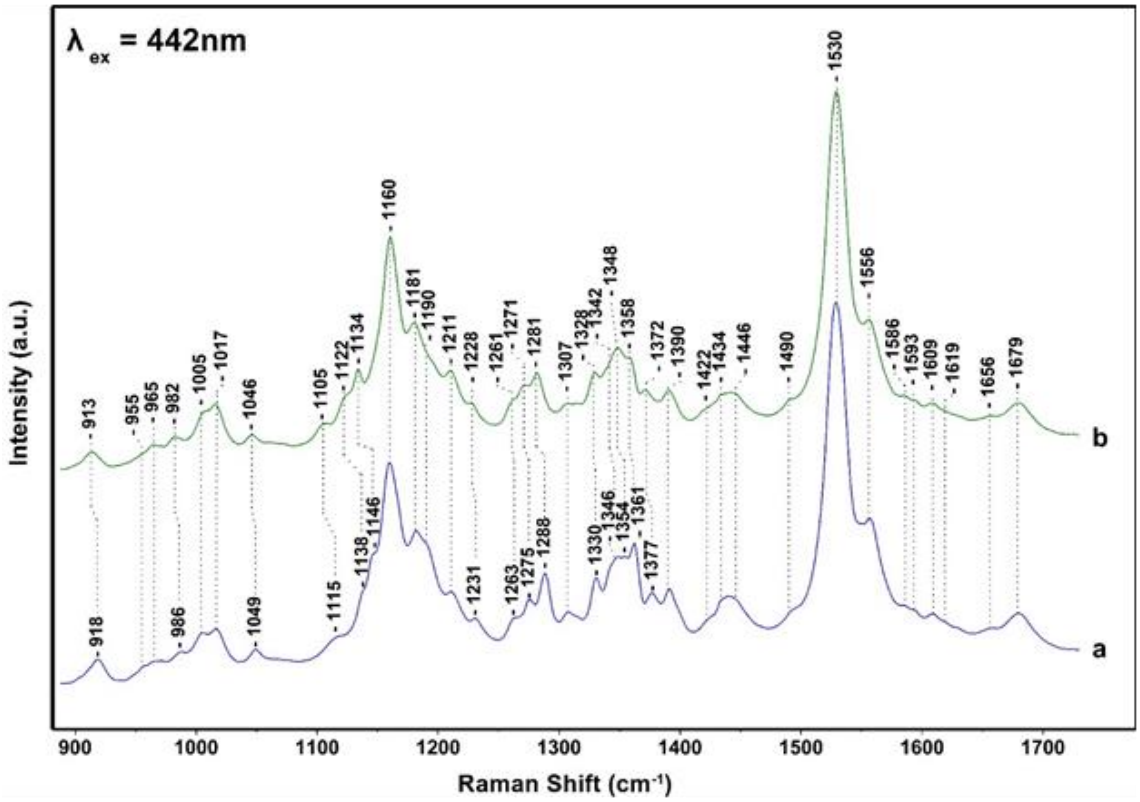

Figure 31: High frequency 442 nm excitation resonance Raman spectra of NA (trace a) and ^{15}N (trace b) FCP from Frag. sp Trace a is the NA FCP and trace b from cell grown in ^{15}N. The 442 nm excitation laser beam was provided by KIMMON He-Cd Laser and the laser power incident on the sample was 10 mW. The total accumulation time for each measurement was 1 min. Every spectrum is the average of 10 measurements.

Expanded frequency and intensity of the 1320-1420 and 1580-1720 cm^{-1} regions of the data presented in Figure 30 and Figure 31 are shown in Figure 32. In the 405 nm excitation spectra, there are three major isotope sensitive bands at 1377 (-5), 1346 (-4), 1330 (-2) cm^{-1} that arise from five and six-coordinated Chl a and two from Chl c at 1361 (-6) and 1354 (-6) cm^{-1} that originate from the two conformations of Chl c, as previously reported.15 However, the two conformations were observed only at 441, 457

and 476 nm excitations but not at 406 or 413 nm excitation. Interestingly, the same authors assigned the 1620 cm^{-1} observed in their 413 nm excitation spectra to the vinyl C31=C32 of Chl c but not the more intense C_aN modes of Chl c. In addition, the C_aN vibrations of Chl a were not reported. It should be mentioned that the Raman spectra in ref.15 were smoothed to recover the Raman spectra with low signal-to-noise ratio (SNR). While this method is effective in reducing the noise signal, it has the undesirable effect of smoothing the underlying Raman features causing significant deviation from the 'true' Raman signals. In the 1580-1720 cm^{-1} region two bands at 1679 and 1691 cm^{-1} are observed and are attributed in agreement with previous assignments, to a medium-strength H-bonded and a weak H-bonded 13-keto C=O mode, respectively. The 1609 cm^{-1} peak arise from the methine bridges of Chls a/c, the frequency of which depends on the coordination state of the central Mg^{2+} ion and the 1630 cm^{-1} from the vinyl group. The coordination sensitive modes in Chl a/c indicate that most Chl a/c molecules are five-coordinated or there certain six-coordinated Chls a/c molecules with weak axial ligands. The observation of the 1355/1361 cm^{-1} of Chl c clearly demonstrate that there is a subset of Chl c molecules that they experience changes in the core size.

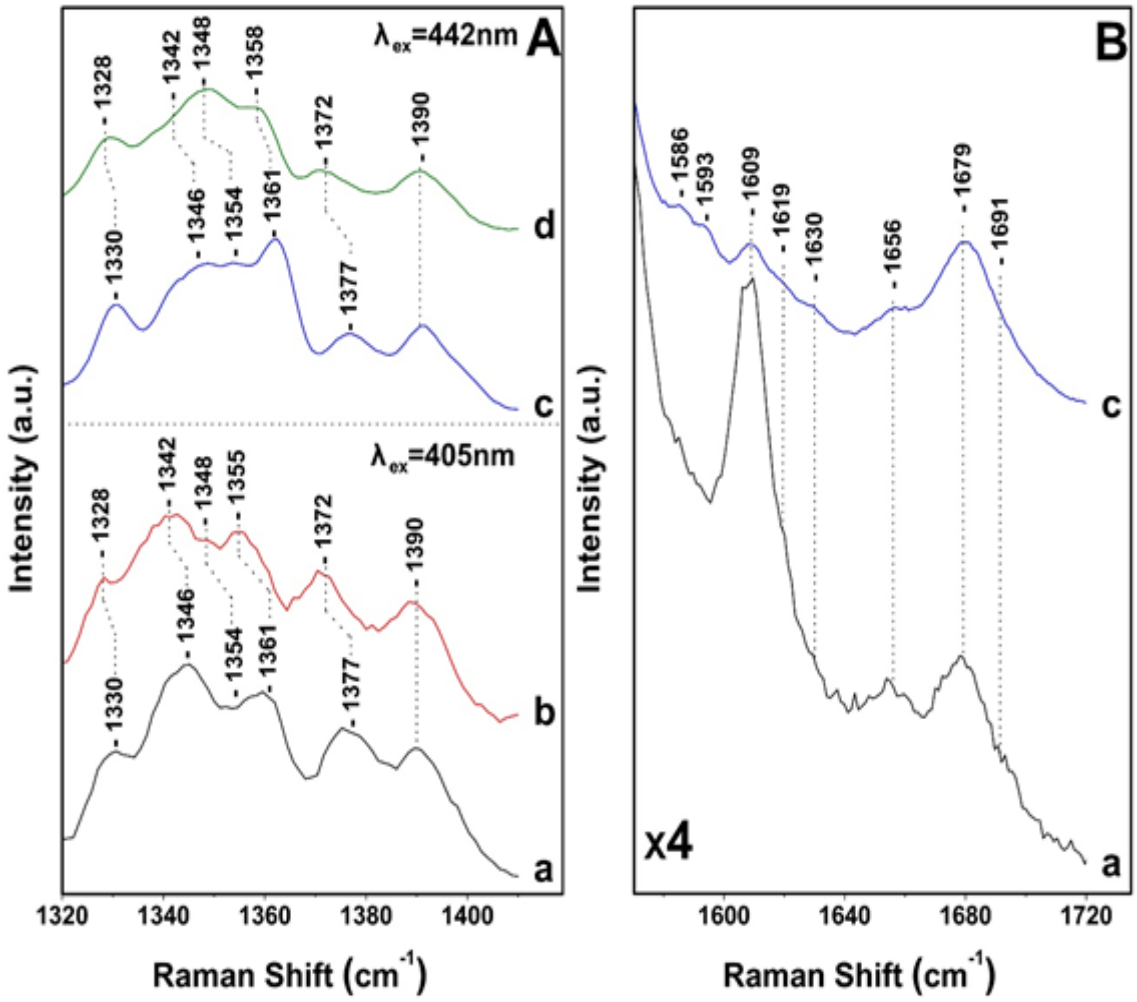

Figure 32: Expanded frequency range of the 405 and 442 nm Raman spectra presented in Figures 2 and 3. The spectra in panel B are x4.

The high-frequency skeletal modes are understood and have been discussed several times with respect to their function as marker bands for oxidation/coordination/spin states sensitivity. Below the ν4 bands in the 1300-1400 cm^{-1} region, assignments of both the Chl a and Chl c have not been reported in the past and are uncertain because of spectral congestion which is due to activation of substituent modes, the Chl a/c out-of-plane modes, the Mg-ligand modes of Chl a/c, and the in-plane skeletal modes.[13] Based on previous reports on Chl a, MgOEP and heme proteins, we tentatively assign the low frequency modes shown in Figure 33 and Figure 34. Figure 33 shows the low-frequency region of the spectra presented in Figure 30, and Figure 34 those of the spectra presented in Figure 31. The spectra presented in Figure 33 revealed ^{15}N isotope bands at 574 cm^{-1} (-3) and at 692 (-2), 717(-2), 736(-6), 746(-4), 756(-2), 764(-20) and 800(-3). In Figure 34, the ^{15}N isotope shifts of a number of bands at 520(-3), 574(-3), 700(-4),

717(-2), 733(-3), 745(-3), 787(-5) and 800(-3) is depicted. The crystal structure of FCP have demonstrated that Chl a/c are coordinated by His, Tyr and H_2O axial ligands. Based on the vibrational analysis of heme and chlorin based assignments we tentatively assign the 214 cm^{-1} mode presented in Figure 34 to the Mg-N symmetrical stretch (His of Chl c) of the five coordinated Chl c and the 338 cm^{-1} to the asymmetrical stretch of the six-coordinated Chl c. The following tentative analysis of the ^{15}N sensitive bands is based on the normal coordinate analysis of Ni-OEP.[24] The 263 (ν9) and 351 (ν8) cm^{-1} modes are pyrrole-substituent bending vibrations. In the 351-400 cm^{-1} region there are unique bending vibrations related to the C-C-C of the acrylate substituents of Chl c_2. There are candidate RR bands for the acrylate moiety in Chl c, at 351-370 and 387-400, modulated by different orientations relative to the porphyrin plane of Chl c. These bands are insensitive to the isotope labeling on the ring. In the 471 to 607 cm^{-1} region there are three ^{15}N sensitive bands at 520 (-3), 564 (-3) and 574 (-3) cm^{-1} that may represent Mg-ligand vibrations. In the 690 to 800 cm^{-1} there are RR bands sensitive to ^{15}N that may have contributions from both Chl c and Chl a. The vibrations are assigned to ν7 (700 cm^{-1}), γ11(717 cm^{-1}), γ5 (733 cm^{-1}), ν15 (745 cm^{-1}), and ν6 (800 cm^{-1}).

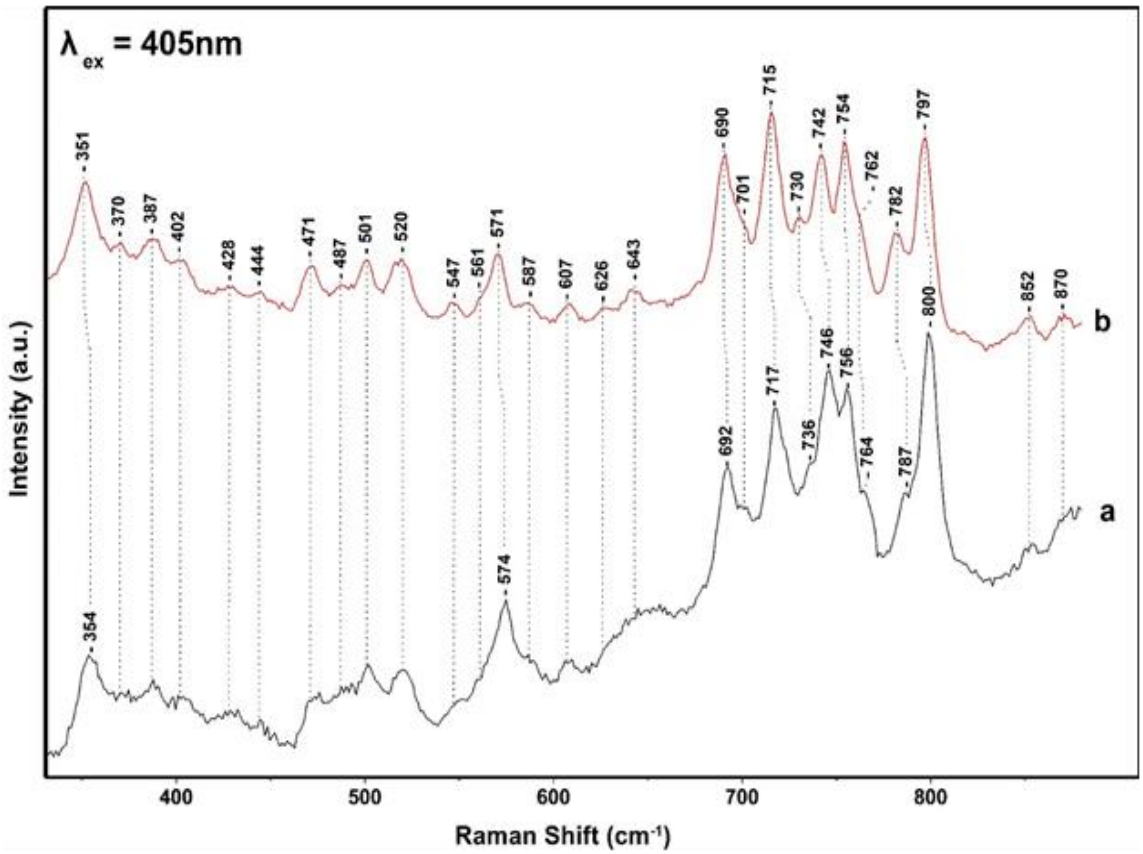

Figure 33: Low frequency 405 nm excitation resonance Raman spectra of NA (trace a) and ^{15}N (trace b) FCP from Frag. sp. The 405 nm excitation laser beam was provided by a Coherent Laser and the laser power incident on the sample was 10 mW. The total accumulation time for each measurement was 1 min. Every spectrum is the average of 10 measurements.

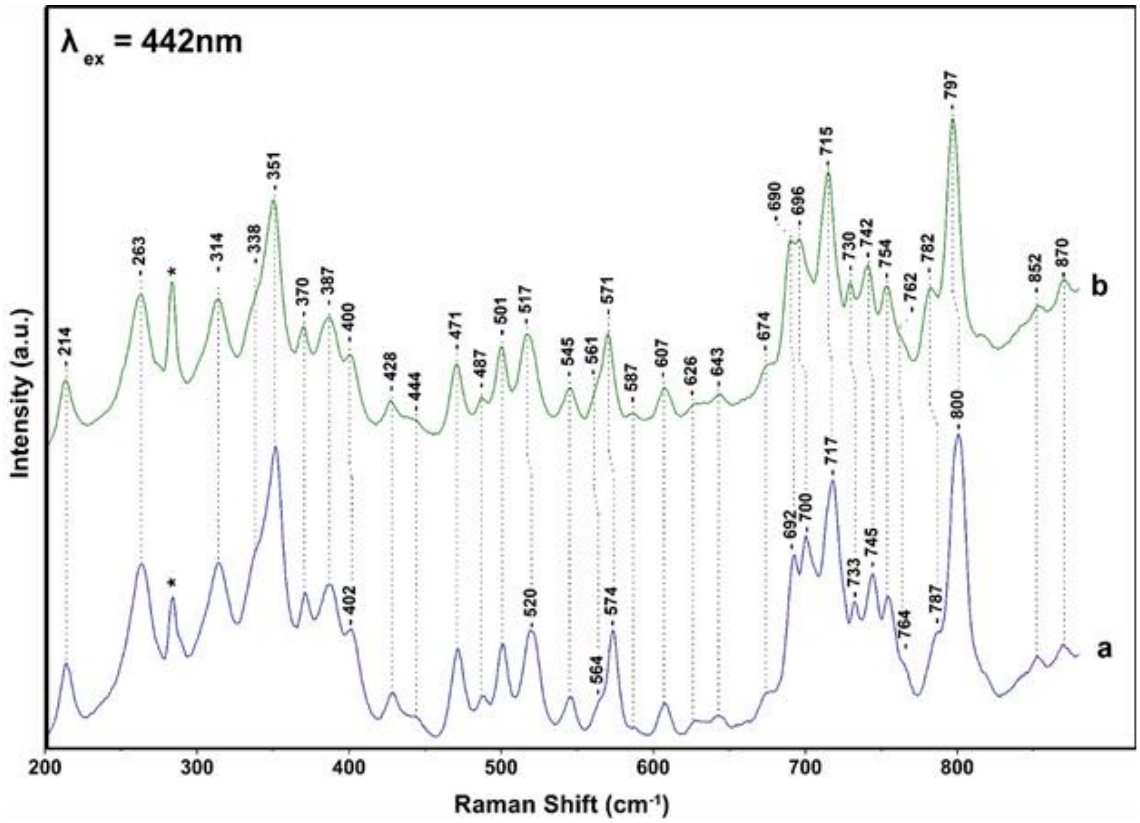

Figure 34: Low frequency 442 nm excitation resonance Raman spectra of NA (trace a) and ^{15}N (trace b) FCP from Frag. sp. Trace a is the NA FCP and trace b from cell grown in ^{15}N. The 442 nm excitation laser beam was provided by KIMMON He-Cd Laser and the laser power incident on the sample was 10 mW. The total accumulation time for each measurement was 1 min. Every spectrum is the average of 10 measurements.

References

1. Büchel C. How diatoms harvest light. Science. 2019;365(6452):447-448.

2. Büchel, C. Advances in Photosynthesis and Respiration (Including Bioenergy and Related Processes), 2020;45, 441-457 Springer, Cham.

3. Büchel, C. Light harvesting complexes in chlorophyll c-containing algae Biochimica et Biophysica Acta – Bioenergetics. 2020;1861(4), 148027.

4. Pi X, Zhao S, Wang W, Liu D, Xu C, Han G, Kuang et al. The pigment-protein network of a diatom photosystem II-light-harvesting antenna supercomplex. Science. 2019;365, 6452.

5. Wang W, Yu LJ, Xu C, Tomizaki T, Zhao S, Umena Y et al. Structural basis for blue-green light harvesting and energy dissipation in diatoms. Science. 2019;363, 6427.

6. Nagao R, Ueno Y, Yokono M, Shen JR, Akimoto S. Alterations of pigment composition and their interactions in response to different light conditions in the diatom Chaetoceros gracilis probed by time-resolved fluorescence spectroscopy. Biochimica et Biophysica Acta – Bioenergetics. 2018;1859(7), 524–530.

7. Oka K, Ueno Y, Yokono M, Shen JR, Nagao R, Akimoto S. Adaptation of light-harvesting and energy-transfer processes of a diatom Phaeodactylum tricornutum to different light qualities. Photosynth. Res. 2020;146, 227– 234.

8. Chrysafoudi A, Maity S, Kleinekathöfer U, Daskalakis V. Robust Strategy for Photoprotection in the Light-Harvesting Antenna of Diatoms: A Molecular Dynamics Study. The Journal of Physical Chemistry Letters. 2021;12 (39), 9626-9633.

9. Ikeda Y, Yamagishi A, Komura M, Suzuki T, Dohmae N, Shibata Y et al. Two types of fucoxanthin-chlorophyll-binding proteins are tightly bound to the photosystem core complex in marine centric diatoms. Biochimica et Biophysica Acta – Bioenergetics. 2013;1827, 529–539.

10. Nagao R, Yokono M, Ueno Y, Shen JR, Akimoto S. High excitation energy quenching in Fucoxanthin chlorophyll a/c binding protein complexes from the diatom Chaetoceros gracilis. J. Phys. Chem. B. 2019;124, 4919-4923.

11. Yamano N, Mizoguchi T, Fujii R. The pH-dependent photophysical properties of chlorophyll-c bound to the light-harvesting complex from a diatom, Chaetoceros calcitrans. Journal of Photochemistry and Photobiology A: Chemistry. 2018;358, 379–385.

12. Tsujimura M, Sugano M, Ishikita H, Saito K. Mechanism of Absorption Wavelength Shift Depending on the Protonation State of the Acrylate Group in Chlorophyll c. J. Phys. Chem. B. 2023;127, 505-513.

13. Zhou C, Diers JR, Bocian DF. Qy-Excitation Resonance Raman Spectra of Chlorophyll a and Related Complexes. Normal Mode Characteristics of the Low-Frequency Vibrations. J. Phys. Chem. B. 1997;101, 9635-9644.

14. Czarnecki K, Diers JR, Chynwat V, Erickson JP, Frank HA, Bocian DF. Comprehensive resonance Raman study of photosynthetic reaction centers from Rhodobacter sphaeroides. Implications for pigment structure and pigment-protein interactions. J.Am. Chem.Soc. 1997;119, 415-426.

15. Premvardhan L, Robert B, Beer A, Büchel C. Pigment organization in fucoxanthin chlorophyll a/c2 proteins (FCP) based on resonance Raman spectroscopy and sequence analysis. Biochimica et Biophysica Acta – Bioenergetics. 2010;1797(9), 1647–1656.

16. Premvardhan L, Bordes L, Beer A, Büchel C, Robert B. Carotenoid structures and environments in trimeric and oligomeric fucoxanthin chlorophyll a/c2 proteins from resonance Raman spectroscopy. Journal of Physical Chemistry B. 2009;113(37), 12565–12574.

17. Lutz M. Antenna Chlorophyll in photosynthetic membranes. A study by resonance Raman spectroscopy. Biochimica et Biophysica Acta;1977, 469, 408-430.

18. Sashima T, Abe M, Kurano N, Miyachi S, Koyama Y. Changes in the Carbon−Carbon and Carbon−Nitrogen Bond Orders in the Macrocycle of Chlorophyll a upon Singlet and Triplet Excitation as Probed by Resonance Raman Spectroscopy of Natural-Abundance and Singly and Doubly Labeled Species with 15N, 13C, and 2H Isotopes. J. Phys. Chem. B. 1998;102, 6903-6914.

19. Tselios C, Varotsis C. Evidence for reversible light-dependent transitions in the photosynthetic pigments of diatoms. RSC Advances. 2022;12, 31555-31563.

20. Pinakoulaki E, Ohta T, Soulimane T, Kitagawa T, Varotsis C. Simultaneous resonance Raman detection of the heme a3-Fe-CO and CuB-CO species in CO-bound ba3-cytochrome c oxidase from Thermus thermophilus: Evidence for a charge transfer Cu-CO transition. J. Biol. Chem. 2004;279, 22791-22794.

21. Pinakoulaki E, Varotsis C. Resonance Raman spectroscopy of nitric oxide reductase and cbb3 heme-copper oxidase. J. Phys. Chem B. 2008;112, 1851-1857.

22. Alexandre MTA, Gundermann K; Pascal A, van Grondelle R, Büchel C, Robert B. Probing the carotenoid content of intact Cyclotella cells by resonance Raman spectroscopy. Photosynthesis Research. 2014;119 (3), 273–281.

23. Llansola-Portoles MJ, Pascal AA, Robert B. Electronic and vibrational properties of carotenoids: from in vitro to in vivo. Journal of the Royal Society, Interface. 2017;14(135), 20170504.

24. Li XY, Czernuszewicz RS, Kincaid JR, Stein P, Spiro TG. Consistent Porphyrin Force Field. 2. Nickel Octaethylporphyrin Skeletal and Substituent Mode Assignments from 15N, Meso-d4, and Methylene-i/16 Raman and Infrared Isotope Shifts. J. Phys. Chem. 1990;94, 47-61.

5. Light harvesting and Photoprotective states in the marine diatom Fragilariopsis sp: Functional implications of Chlorophylls c_1/c_2 in the Fucoxanthin-Chlorophyll a/c-binding proteins (FCPs)

Herein, we report pH/pD-dependent Fluorescence-excitation spectra of the FCPs of the Marine Diatom Frag. sp. There is a reversible 451 to 455 nm Soret transition accompanied by a 588 to 586 nm Q_x transition of chls c_1/c_2 in the pH/pD 4.9-8 range with a pKa = 5.4. The H/D exchangeable site of the 17-acrylate group of chls c_1/c_2 was characterized and from the pH/pD sensitivity of the Soret and Q_y bands we suggest that the chls c_1/c_2-acrylate-H_2O moiety can act as a proton acceptor/donor site. Under high intensity light conditions, the acrylate moiety of chls c_1/c_2 becomes protonated, resembling that observes under acidic conditions. In the photoprotective state, the absorption of chls c_1/c_2 is red shifted and resembles that observed in the reversible transition from light-harvesting to energy-quenching state at acidic pH. The induced ΔpH and that created from the high intensity light, is responsible for the red-shifted chls c_1/c_2 due to the protonation of the acrylate group. We present a model that describes an open and a closed form of the protonated/deprotonated chls c_1/c_2-acrylate-H_2O moiety that controls the proton loading site in the photoprotective and light harvesting state.

5.1. Introduction

Marine Diatoms are involved in major photosynthetic biochemical cycles and carbon fixation.[1] They perform photosynthesis by utilizing light-harvesting chls a/c and Fx located in the plastids and, across their thylakoid membranes, a light induced -proton gradient is formed which is essential for the synthesis of ATP.[1-6] Marine diatoms contain the light-harvesting FCPs to collect light energy in the blue-green region that is also available under water, and transfer the trapped energy to the reaction centers where the primary electron transfer reactions convert energy into an electrochemical gradient.[1-6] In the thylakoid membranes, the pH value of the luminal side decreases upon irradiation until it reaches a steady state under continuous irradiation whereas in the stroma remains unchanged under the same light conditions.[1-3] The photoacclimation strategy of species growing under variable light conditions enables the efficient regulation of photosystem structures to the amount of absorbed energy.[4-7] To protect

against strong light exposure, diatoms have a NPQ photoprotection system, in which the excess absorbed energy is dissipated as heat.[6,7] The main NPQ component called energy-dependent quenching (qE) is triggered by the pH gradient (ΔpH) established between the thylakoid lumen and the stroma during illumination.[8]

The crystal structure of a FCP from the marine P. tricornutum revealed the binding of seven chls a, one chl c_1, one chl c_2, seven Fxs and one Dd in each monomer subunit.[5] Efficient energy pathways between Chls a and Chls c were identified, and each Fx is surrounded by Chls a/c allowing the energy transfer and quenching via Fx.[4-6] In contrast to the His coordination in Chls a/c found in the inner antenna of PSII and PSI core, nine Chls a/c in FCP are coordinated by two His, three Glu, and three Gln residues where Chl a 401 is coordinated by a H_2O molecule.[5] Hydrophilic groups are present in the tetrapyrrole rings of the two Chls c_1/c_2 which are coordinated by His and Gln and are in close interactions with two Chls a. These structural characteristics make Chls c_1/c_2 an efficient harvester of blue-green and even yellow light. Chl c_2 possesses a conjugated to the porphyrin ring at the 8-position vinyl (-CH=CH_2) group, and Chl c_1 an ethyl group at the same position resulting in a red shifted Chl c_2 Soret band.[5] The close distances of all Fxs with Chls a/c indicates that the excess energy absorbed by Chls can dissipated quickly and efficiently through Fxs.[5] Additional structure-function information related to Chls c has been reported, recently.[6] Specific interactions of the pigments with the protein environment, in addition to pigment-pigment interactions, account for their spectral and redox properties in the FCPs. Among these interactions are the ligands coordinated to Chls a/c as well as the H-bonding interactions of the pigment groups with the polypeptide side chains.

Specific interactions of the pigment molecules in the protein environment and pigment-pigment interactions account for spectral, and excitation energy transfer efficiency to Chl a.[4-9] The structural differences in Chl a versus Chl c lead to modified photophysical properties between the different types of macrocycles which have been selected as the active pigments in marine photosynthesis.[4-20] There is a consensus on the energy transfer pathway that involves Fxs, Chl c and Chl a.[10-12] The energy captured by Fx is transferred to Chl a on a picosecond time scale and that from Chl c to Chl a on a femtosecond time scale providing detailed energy flow channels.[10-12,21] However, there is a conundrum with respect to the time constants of the energy transfer from Fx/Chl c

to Chl a because they are highly dependent on the experimental conditions, and the properties of the FCP under investigation.[10-12] In addition, little information is available related to the dynamics of the pigments and protein residues involved in the transition from light harvesting to photoprotection.[6-14,22-23]

It has been demonstrated that the protonation-deprotonation of 17-acrylate of Chls c_1/c_2 affects their photophysical properties.[17] There are two marker transitions to characterize the dynamics of Chls c_1/c_2 in the FCPs of diatoms. The first is related to the protonation/deprotonation of the acrylate group causing a red shift in the Soret and Q_x bands and the second is the red-shift in the Soret and Q_x/Q_y bands of Chl c_2 with respect to Chl c_1.[17,18,24] The pH 4.9 minus pH 8 Fluorescence-excitation difference spectra observed at 638 nm showed a broad peak around 471 nm representing a mixture of protonated and deprotonated 17-CH=CH-COO^- at a ratio of 3:1 and also a negative peak at 446 nm representing a deprotonated 17-CH=CH-COO^-.[17] On the same line, quantum mechanical/molecular mechanical calculations have shown that the absorption wavelength of the Soret band of protonated Chl c is 25 nm longer than that of deprotonated Chl c, which is due to the delocalization of the lowest (LUMO) and second lowest (LUMO+1) unoccupied molecular orbitals toward the acrylate group.[18] It was suggested that in the FCP, the decrease in pH on the luminal side under high-intensity light (HL) conditions leads to protonation of the acrylate moiety and thereby a red shift in the absorption wavelength. In addition, it was reported that the energy transfer efficiency from Chl c to Chl a is reduced under acidic conditions. It is therefore of pivotal importance to have full characterization of the structure-function relationship of the Chls c in the FCP complex including the properties of the acrylate moiety.

In the work presented here, we have extended our work and employed Fluorescence spectroscopy to probe the pH/pD-dependent Fluorescence-excitation spectra of the light-harvesting FCPs of the Marine Diatom Frag. sp.[25,26] There is a reversible Soret transition from 451 to 455 nm in the pH/pD 4.9-8 range accompanied by a pH/pD sensitive Q_y transition from 588 to 586 nm of Chls c_1/c_2 with a pKa = 5.4. The pH/pD dependent Fluorescence-excitation spectra, revealed H/D exchangeable proton sites in the moiety of the 17-acrylate group of Chls c_1/c_2. In addition, the acidic pH created under HL conditions is also involved in the protonation of the 17-acrylate group of Chl c_1/c_2 that creates the red-shift in the absorption spectrum. We propose a mechanism in

which the exchangeable proton sites in the acrylate moiety of Chl c_1-K136 and Chl c_2-R31 exist in a closed and an opened form. The ion pairs can exist in a fully protonated opened form and/or in a closed form in which the protonated forms of Lysine K136 H^+ and Arginine R31H^+ interact with the deprotonated acrylate moieties of Chl c_1 and Chl c_2, respectively.

5.2. Materials and methods

5.2.1. Diatom Growth

The culture of Frag. sp (CCAP 1029/24) was obtained from CCAP (Culture Collection of Algae and Protozoa). Cells were grown in f/2-Si medium, at 19 °C in a dark-light cycle (12h:12h) under white LED light.[27] The light intensity used for the growth of the cells culture was 150 μmol photons m^{-2} s^{-1} for the low-intensity light (LL) condition and 350 μmol photons m^{-2} s^{-1} for the high-intensity light (HL).

5.2.2. FCPs Isolation

Cells from Frag. sp diatom were harvested by centrifugation (8000 rpm, 30 min, 4 °C) and the supernatant medium was removed. The cells were resuspended in 20 mM Tris and sonicated in an ice bath for 20 minutes. Thylakoid membranes were then solubilized with the addition of β -1,4-dodecyl maltoside (β-DDM, 30 mg, 4 mM) in the resuspended cells while they were shaken for 20 minutes on ice.[28] Separation of solubilized FCPs was carried out on an ion exchange column (HiPrep Q HP 16/10, 20 mL) in 25 mM Tris, 2 mM KCl and 0.4 mM β-DDM at pH 7.4 using a Shimadzu LC 20AD with a SPD-20A detector with two-wavelength detection. The samples were loaded in a column, and fractions were eluted using a gradient from 0 to 750 mM KCl in a buffer made of 25 mM Tris, 750 mM KCl and 0.4 mM β-DDM, pH 7.4 at a flow rate of 3 mL/min. Fractions were pooled and concentrated using Amicon filtration devices with a cutoff of 10 kDa and characterized spectroscopically. The rest of the fractions were stored at -80 °C until further use.

5.2.3. Preparation of pH and D_2O Buffers

A series of buffer solutions with different pH values were prepared using 25 mM of MES-NaOH (pH 4.9–6.4) or Tris-HCL (pH 8) at room temperature. The buffer prepared in D_2O was measured assuming pD=pH (observed) + 0.4. For hydrogen/deuterium

studies, solutions of the FCP were exchanged three times in 99.9% D_2O.

5.2.4. UV and Fluorescence Spectroscopy

Absorption spectra were recorded at room temperature with a Cary 60 UV−vis spectrometer (Agilent Technologies, USA). Fluorescence and fluorescence-excitation spectra were measured in a 3 mm cuvette, at room temperature, with a Cary Eclipse Fluorescence Spectrophotometer (Agilent Technologies, USA). The excitation and emission bandwidth slits were 10.0 nm and 5.0 nm, respectively

5.3. Results

Figure 35, panel A, shows the UV spectra of a fraction of solubilized FCPs of Frag. sp at room temperature in the pH range 4.9-8. The transitions at 440 (Soret), 621 (Q_x) and 673 (Q_y) nm accompanying pH changes are attributed to Chl a, and at 457 (Soret), 588 (Q_x) and 637(Q_y) nm to Chls c_1/c_2.[8,17,25,26] The broad transition in the 500-560 nm range has been attributed to red Fxs, as blue Fxs absorb in the 420-470 nm region.[8,25] The inset depicts the pH dependent behavior of the Soret band as the pH is decreased from 8 to 4.9 with isosbestic point at 457 nm. Panel B shows the difference spectra obtained from the subtraction of the pH 8 spectrum from the respective spectra in the pH order 4.9, 5.1, 5.4, 5.9, 6.4. A peak/trough at 474/444 nm is formed as the pH decreases from 8 to 4.9. This clearly demonstrates the transformation of one species to another in a first order equilibrium, as a change of pH. We attribute the observed changes, in agreement with previous work[17], to protonation (17-CH=CH-COOH) and deprotonation (17-CH=CH-COO^-) of the acrylate moiety of Chls c_1/c_2 in the FCP. In panel C, the absorbances of the FCP at 444 (black line) and at 474 (blue line) were plotted against the pH in the 4.9 to 8 range and a pKa =5.4 was determined. The changes in the absorption of 444 and 474 nm are attributed to the acid-dissociation of Chl c_1/c_2. Obviously, the 17-acrylate group of Chls c_1/c_2, as it is in the case of the FCP from Chaetoceros calcitrans (C. calcitrans), controls the acidic and basic forms of Chls c_1/c_2 and from the analysis of the fluorescence data presented below, reversibly.[17]

Determination of the relative concentration of protonated Chls c

In an acid-dissociation equilibrium, the Henderson–Hasselbalch equation defines pH

using the pKa and the concentrations of both the starting acid and the conjugated base: pH = pKa + log ([RCOO]/[RCOOH]), where pH is the negative logarithm of $[H^+]$, pKa is the acid dissociation constant, and [RCOO] and [RCOOH] are the concentrations of the conjugate base and acid, respectively. Applying the relation of [RCOO] + [RCOOH] = N, where N is a constant value, the concentration of the starting acid is written as:

$[RCOOH] = N/\{1 + 10^{pH-pKa}\}$.

$[RCOOH] = 100/\{1 + 10^{4.9-5.4}\}$.

$[RCOOH] = 75.97 \approx 76\%$

By using the determined pKa value of 5.4 from

Figure 35, Panel C, the relative concentration of protonated Chls c_1/c_2 (17-CH=CHCOOH) was calculated to be 76% and 0% at pH 4.9 and 8, respectively. Consequently, the Fluorescence excitation spectrum at pH 8 represents absorbance of the deprotonated form of Chl c_1/c_2 (17-CH=CH-COO-) and that at pH 5 consists of absorbances from protonated and deprotonated Chls c_1/c_2 at a ratio of 3:1.

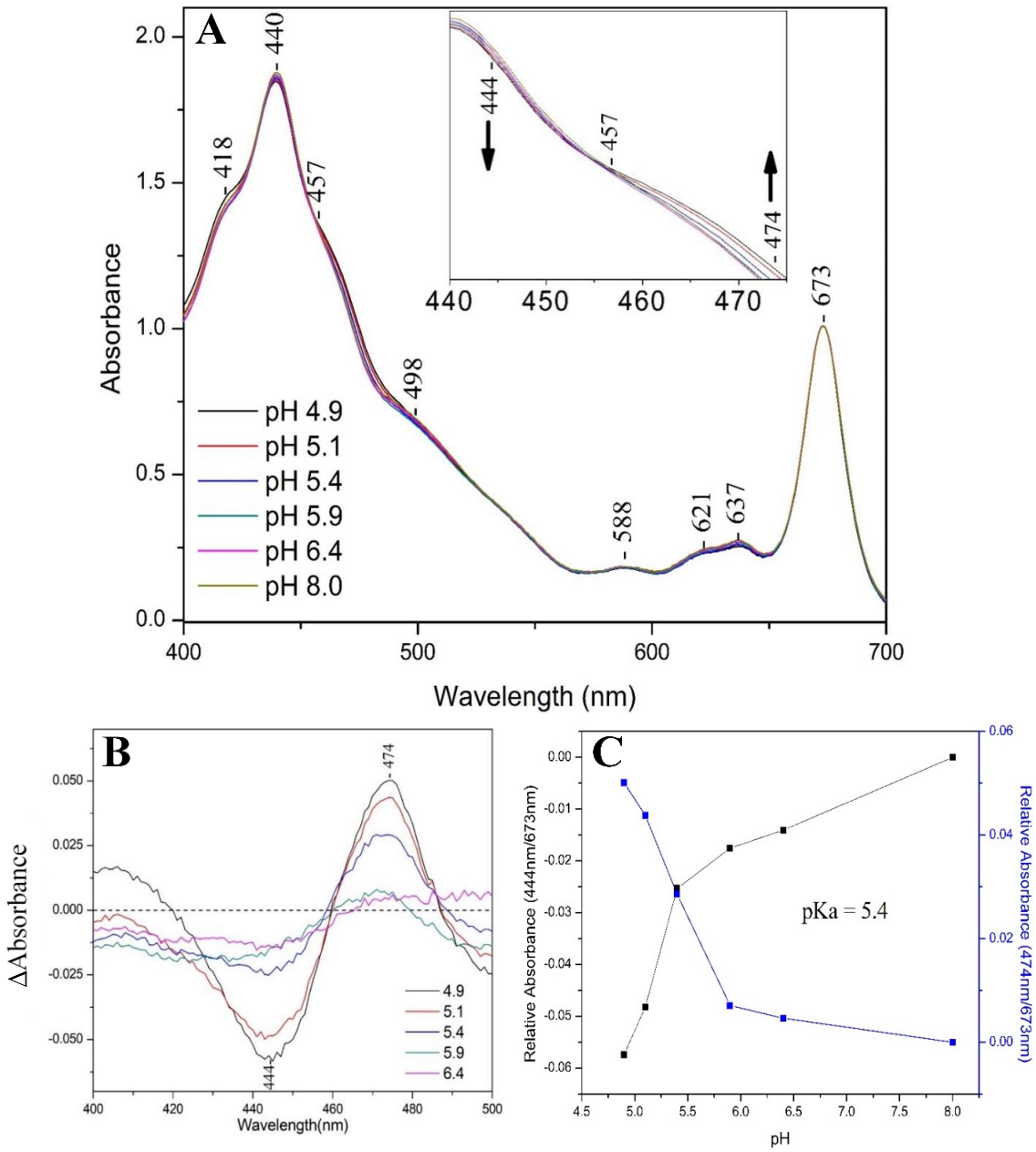

Figure 35: Panel A. Absorption spectra of FCPs of Frag. sp normalized at 673 nm. The inset shows the enlarged spectra highlighting the isosbestic point. Panel B. Difference absorption spectra obtained by subtracting the spectra measured at pH 8 from those with pH values designated in the figure. Panel C. Absorbance at 444 nm (black squares) and 474 nm (blue squares) relative to that at 672 nm against the pH values. The pKa value was determined from the graph.

Figure 36 shows the Fluorescence excitation spectra at 677 nm (blue line) from a fraction of solubilized FCP of Frag. sp, and for comparison the Absorption spectrum (black line) at pH 8 (Panel A) and pH 4.9 (panel B). The Fluorescence excitation spectra at 677 nm show that there is good agreement with the absorptivity, and sufficient energy transfer to Chls a takes place when Chls c_1/c_2 and Fxs were excited. In particular, the 508, 522 and 536 nm peaks are due to the lower energy red Fxs exhibiting different interactions with nearby residues whereas that at 478 nm has contributions from both Fx and Chls c_1/c_2. These observations are in good agreement with those previously reported UV and Fluorescence excitation spectra for FCPs from different diatoms grown under LL conditions where it was shown that there is a strong coupling between Fxs and Chls a, as well as, between Chls c_1/c_2 and Chls a.[25] In panel B, the pH 4.9 Fluorescence excitation spectra at 680 nm and the Absorption spectra are similar to those at pH 8 presented in panel A.

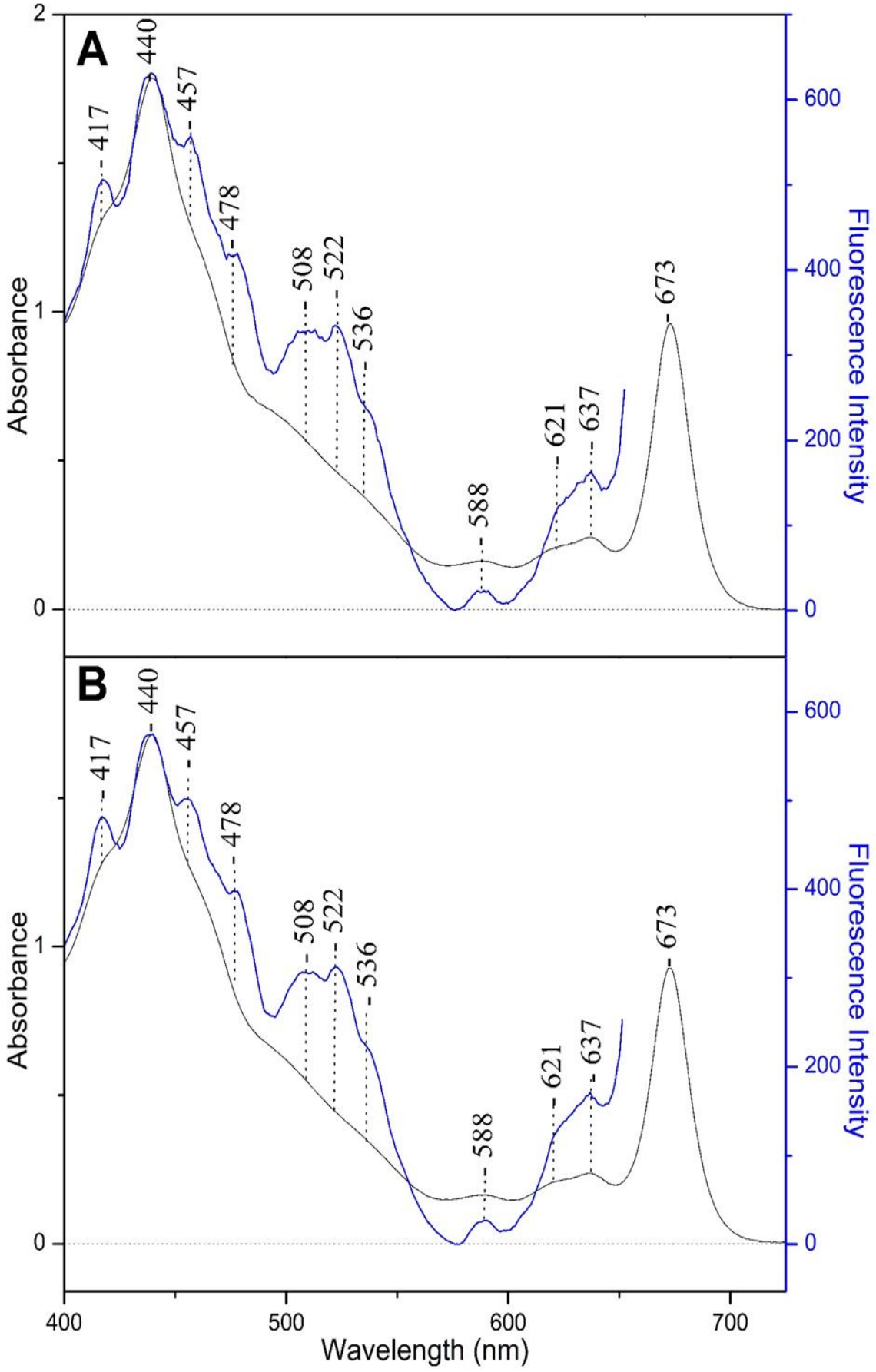
A
B
Absorbance
Fluorescence Intensity
Wavelength (nm)
417
440
457
478
508
522
536
588
621
637
673
0
1
2
200
400
600
500
700

Figure 36: Panel A. Fluorescence excitation from the spontaneous emission at 677 nm (blue line) and absorbance spectrum (black line) of a fraction of FCPs of Frag. sp at pH 8. Panel B. Fluorescence excitation from the spontaneous emission at 677 nm (blue line) and absorbance spectrum (black line) at pH 4.9. The spectra were normalized at the maxima.

Figure 37, panel A, shows the Fluorescence spectra of FCP at pH 4.9 (blue solid line) and at pH 8 (blue broken line) excited at 457 nm and the absorption spectra at pH 4.9 (black solid line) and at pH 8 (black broken line). Both Fluorescence spectra show a peak at 676 nm that originate from the Q_y transition of Chl a bound to FCP and a broad band at 733 nm in agreement with those reported for C. gracilis and C. calcitrans.[17,21] In addition, there is a broad peak at 642 nm indicating the spontaneous emission from the Q_y transition of Chls c_1/c_2, which is also in agreement with previous results.[17-21] The Q_y absorption of Chl a at 672 nm is identical at pH 4.9 and pH 8. In panel B, the Fluorescence excitation spectra from the spontaneous emission from Chl c_2 at 640 nm at pH 8 (black line) and pH 4.9 (red line) are presented. The blue line spectrum is from a sample that was original at pH 8 and subsequently was reduced to 4.9 reproducing the original (red line) spectrum, and finally re-adjusted back to pH 8 reproducing the original (black line) spectrum obtained at pH 8. This observation demonstrates that the pH 8 to pH 4.9 transitions are reversible. The spectra were normalized at maxima. Three distinct transitions at 451, 455 and 418 nm are observed. The spectral shape of the spectra in Panel B are well matched with those obtained in ref. 17 and demonstrate that originate from the Soret transitions of Chls c_1/c_2 bound to FCP. Therefore, the spectra observed at 640 represent the absorption spectra of Chls c_1/c_2. In the spectrum at pH 4.9, the weak peak at 418 nm and that at 451 nm have lost intensity and there is a 3-4 nm red-shifted inhomogeneous broadening of the peak centered at 455 nm. We assign the reversible 451 to 455 nm pH-dependent transition of Chls c_1/c_2 to the deprotonation/protonation of the 17-acrylate group, in agreement with previous work on C. calcitrans.[17] The blue-shifted pH-sensitive transition at 418 nm is also observed and it was also present in the Fluorescence excitation spectra of C. calcitrans but not reported in ref.17. The pH 4.9 and pH 8 spectra were normalized at maxima. The pH 4.9 minus pH 8 spectrum presented in Panel C shows a positive band at 470 nm and negative bands at 445 and 418 nm. The origin of the blue shifted Chls c_1/c_2 at 418 nm is not certain. Modifications of the peripheral groups, the coordination, ligand binding to Mg and H-bonding interactions with the protein environment can cause the observed

shift at 418 nm. In panel D, the Fluorescence excitation spectra at 640 nm of Q_x of Chls c_1/c_2 at pH 4.9 (black line) and pH 8 (red line) are presented and further support the pH sensitivity of Chls c_1/c_2. In panel E, the Fluorescence excitation spectra from the spontaneous emission from Chls c_1/c_2 at 640 nm at pD 8 (black line) and pD 4.9 (red line) are presented. The blue line spectrum is from a sample at pD 8 that it was subsequently reduced to pD 4.9 reproducing the original (red line) spectrum, and finally it was re-adjusted back to pD 8 reproducing the original (black line) spectrum obtained at pD 8. This observation demonstrates that the pD 8 to pD 4.9 transitions are reversible in agreement with the pH experiments presented in panel B. The spectra were normalized at maxima. It should be noted that the sample at pD 4.9 was made from a sample of pH 8, in which the acrylate is deprotonated and subsequently it was reduced to pD 4.9. This implies that that the observed differences are due to the deuterated acrylate group of Chl c_2. Panel F shows the difference pD 4.9 minus pD 8 spectrum, and finally panel G depicts the Emission at 640 nm of Q_y of Chls c_1/c_2 at pD 4.9 (black line) and pD 8 (red line).

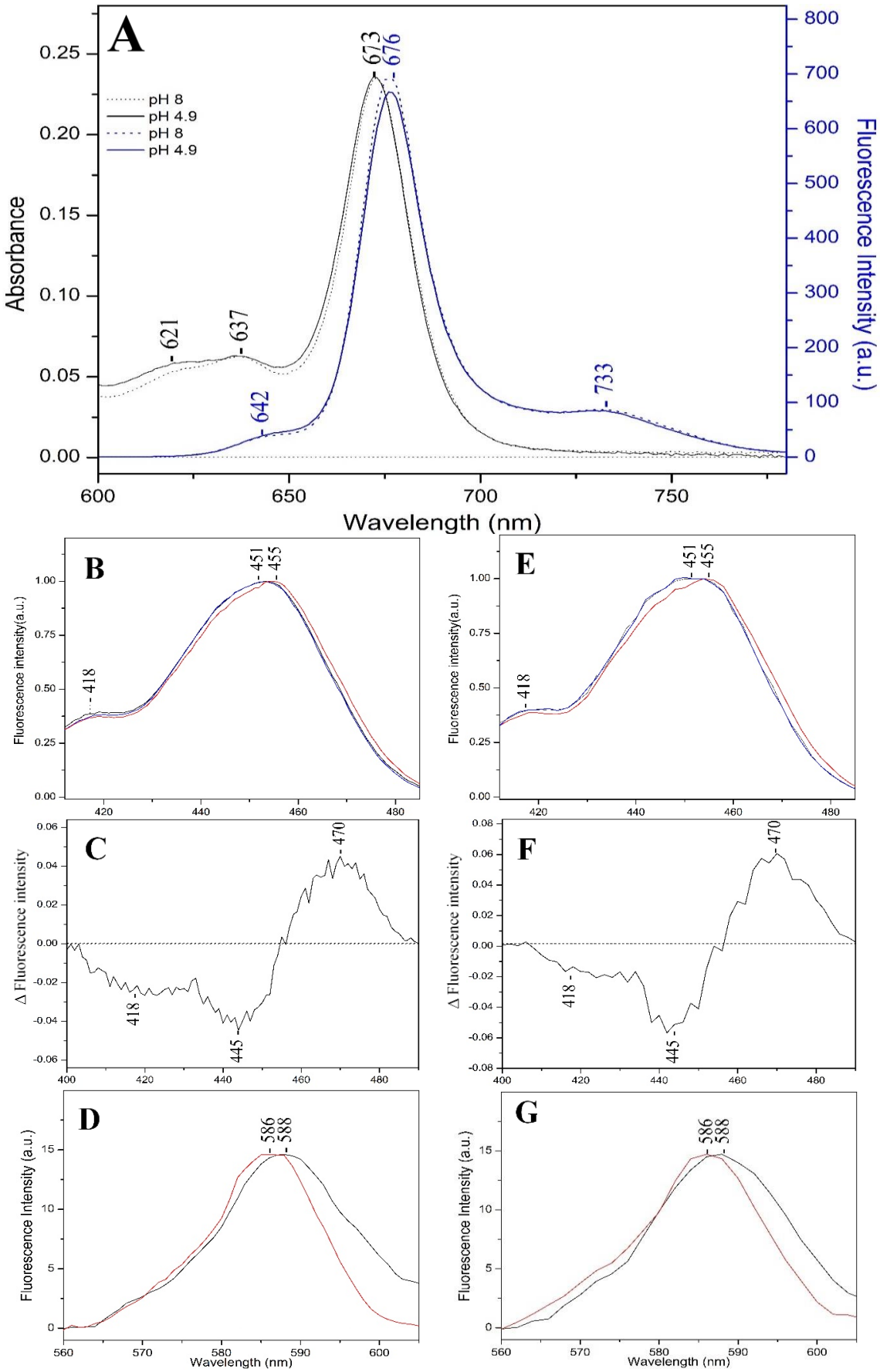
A
pH 8
pH 4.9
pH 8
pH 4.9
673
676
621
637
642
733
Absorbance
Fluorescence Intensity (a.u.)
Wavelength (nm)
B
451
455
418
Fluorescence intensity(a.u.)
E
451
455
418
Fluorescence intensity(a.u.)
C
470
418
445
Δ Fluorescence intensity
F
470
418
445
Δ Fluorescence intensity
D
586
588
Fluorescence Intensity (a.u.)
Wavelength (nm)
G
586
588
Fluorescence Intensity (a.u.)
Wavelength (nm)

Figure 37: Panel A. Absorption (black line) and Fluorescence spectra (blue line) of FCPs of Frag. sp at pH 8 (broken line) and 4.9 (solid line) excited at 457 nm. Panel B. Fluorescence excitation spectra from the spontaneous emission from Chl-c1/c2 at 640 nm at pH 8 (black line) and pH 4.9 (red line). The blue line spectrum is from a sample that was original at pH 8 and subsequently was reduced to 4.9 reproducing the original (red line) spectrum, and finally re-adjusted back to pH 8 reproducing the original (black line) spectrum obtained at pH 8. The spectra were normalized at maxima. C) Difference pH 4.9 minus pH 8 spectrum. D). Emission at 640 nm of Qx of Chl-c1/c2 at pH 4.9 (black line) and pH 8 (red line). E) Fluorescence excitation spectra from the spontaneous emission from Chl c1/c2 at 640 nm at pD 8 (black line) and pD 4.9 (red line). The blue line spectrum is from a sample that was original at pD 8 and subsequently was reduced to pD 4.9 reproducing the original (red line) spectrum, and finally re-adjusted back to pD 8 reproducing the original (black line) spectrum obtained at pD 8. The spectra were normalized at maxima. F) Difference pD 4.9 minus pD 8 spectrum. G) Emission at 640 nm of Qx of Chl-c1/c2 at pD 4.9 (black line) and pD 8 (red line).

Figure 38 compares the Emission at 640 nm of the FCP of Frag. sp at pH 8 (black line) and at pH 5 (red line) under LL growth condition with that observed under HL growth condition (blue line). The Inset depicts the pH 8 species grown under high intensity light minus the pH 8 species grown under low intensity light. The comparison of the difference spectra between the inset in Figure 38 and the Figure 37C demonstrates, that under high intensity light conditions, the absorption of chls c_1/c_2 is red shifted and resembles that observed in the reversible transition from light-harvesting to energy-quenching state at acidic pH in which the acrylate moiety of chls c_1/c_2 is protonated, resembling that observed under acidic conditions.

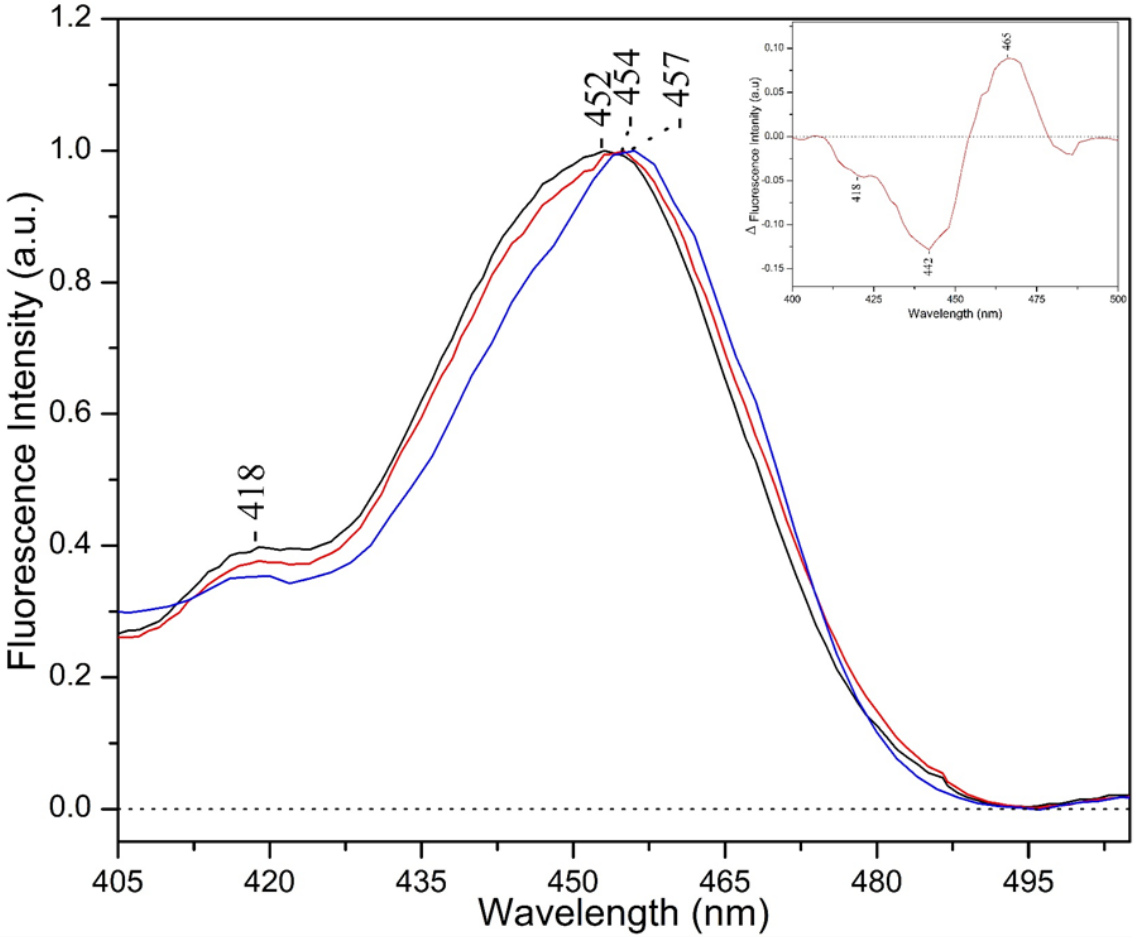

Figure 38: Fluorescence excitation spectra from the spontaneous emission from Chl-c1/c2 at 640 nm of Frag. sp FCP at low intensity light pH 8 (black), pH 4.9 (red) and high intensity light pH 8 (blue) normalized at maxima. The inset shows the difference of the emission spectra 640 nm between the high intensity light at pH 8 minus the low intensity light at pH 8.

5.4. Discussion

The observation of three Soret absorption bands of Chls c_1/c_2 in the protein environment of Frag. sp and their similarities with those observed in C. calcitrans gives a new insight into the photosynthetic properties of the bound Chls c_1/c_2 to FCPs. Of particular note is the observation that at pH 4.9 there is an increase in the Fluorescence intensity at 642 nm resembling that observed in cells from Thalassiosira Pseudonana grown under HL.[25] Therefore, Chls c_1/c_2 in the isolated FCPs and those embedded in the thylakoid membranes have similar interactions with the protein environment leading to the observed decrease in energy transfer efficiency to Chl a. On this line, it is well known that in the thylakoid membranes, the pH value of the luminal side decreases upon

irradiation.[1-6,18] The peaks/troughs shown in Figure 37, panels C and F, are not only unaffected by the pH/pD exchanges in the 4.9-8 range but also demonstrate that all the processes are reversible indicating that the acrylate moiety is easily accessible to H_2O/D_2O exchanges. A sequential or concerted H-bonded connectivity between the environments sensed by the Chl c_2-acrylate-R31-H_2O and Chl c_1-acrylate-K136 could have an activation energy for proton motion that leads to the identification of a proton channel and H_2O molecules. The presence of H_2O/D_2O molecules in the Chls c_1/c_2 acrylate moieties in addition of being able to transfer a proton across a prearranged water array can also induce Chls c_1/c_2-linked ionization phenomena. We suggest that a change in the acrylate environments can be communicated to both the distal and proximal environment of Chls c_1/c_2, causing a modification of the H-bonding status of the proximal and distal coordinated ligands (His 39) to Mg of Chl c_2 and Gln143 to Mg of Chl c_1. This way, the optical transition will shift to higher energy as a result of the increased splitting of the d orbitals and the energy of the antibonding π^* orbitals. The data for heme-copper oxidases and for the peroxidase class of enzymes show that such heme-linked ionization phenomena exist.[29]

Exchangeable protons

The QM/MM-optimized structures of deprotonated acrylate Chls c_1/c_2 showed similar distances (2.8 Å) between the acrylate and Arginine R31 (Chl c_2) and Lysine K136 (Chl c_1).[18] In the protonated forms of Chls c_1/c_2 the distance between acrylate and R31 (Chl c_2) is 7.7 Å whereas that of acrylate and K136 (Chl c_1) is 4.2 Å. In Figure 39 we report a model in which for simplicity we show only the protonated and deprotonated forms of Chl c_2 that interact with H_2O molecules and R31 forming an open and a closed gate, forms. The corresponding Chl c_1-H_2O-K136 interactions are not shown. Water molecules between redox chromophores can affect the electron transfer as well as the triplet-triplet energy transfer. The interaction of intervening H_2O molecules, as well undetectable by x-ray crystallography mobile H_2O molecules, located in hydrophobic cavities can play a crucial role in transferring protons from amino acid residues involving a redox state-dependent switch in the orientation of these water molecules and/or forming H-bonding networks with other protein residues. The close proximity of the R31 residue with the acrylate moiety provides a gate for H^+/H_2O motion, and suggests that they form an ion pair. Dissociation of the pair is expected to raise the pKa

of the acrylate substantially, and lower the pKa of R31. We propose that the pH sensitivity has an effect on the pKa of specific groups resulting in changes in the protonation pattern, which in turn affects local structure via changes in hydrogen-bonding pattern and H_2O motion that affects the energy transfer under acidic conditions.The protonation/deprotonation events in the 17 acrylate-R31/H_2O site are fundamental to the function of diatoms because pH and water molecules play an important role in the water transfer that affects the triplet-triplet energy transfer properties and thus, the switch of the FCP from light-harvesting to energy-quenching state. The abovementioned analysis is also suggested to occur in the vicinity of Chl c_1-H_2O-K136 but to a lesser extend due to the shorter 17-acrylate-K136 distance (4.2 Å) in the protonated form (see below).

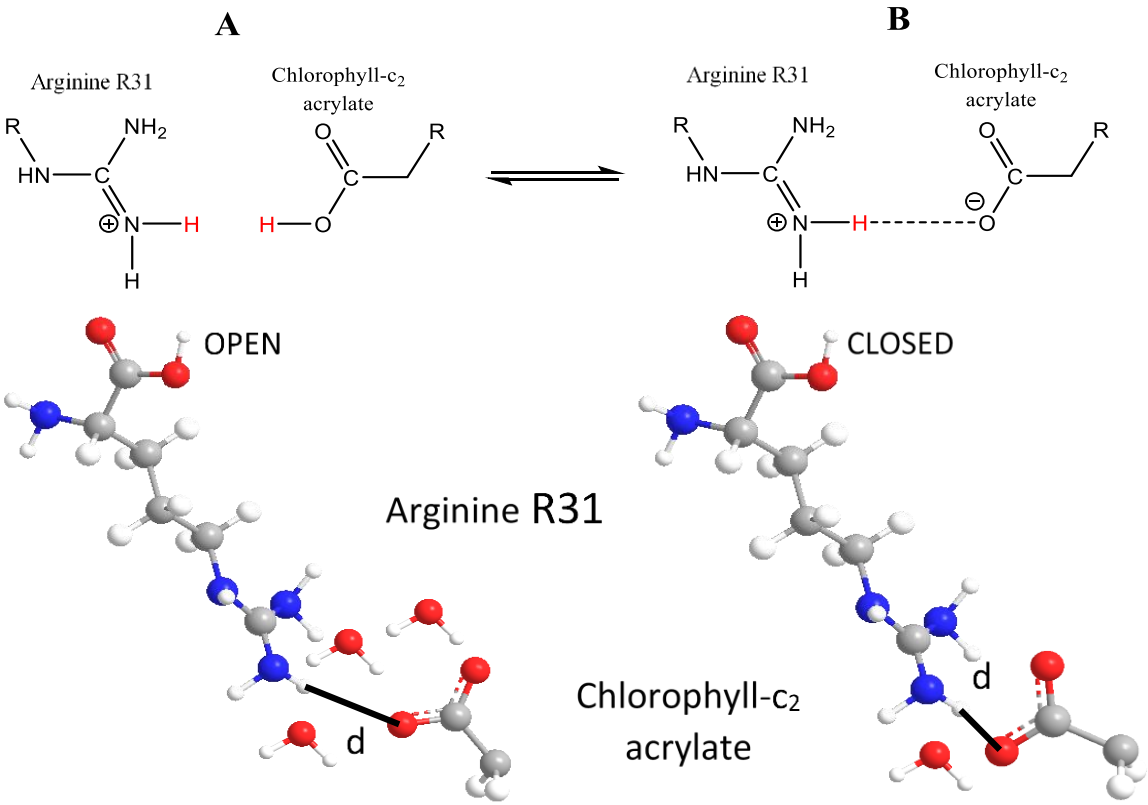

Figure 39: Schematic view of the protonic connectivity between the arginine R31 and chl c_2 acrylate moiety during pH changes. Two forms (open and closed) of the R31/Chl-c2 acrylate ion pair. The closed form is on the right with a short distance, marked d, between the hydrogen of the arginine and the oxygen of the chl c_2 acrylate. The open gate form is shown on the left.

Based on QM/MM optimized structures of FCP the optimized geometry showed that salt bridges form between the acrylate moiety of Chl c_2 and R31 and, Chl c_1 and K136 when Chl c_1 and Chl c_2 are deprotonated, respectively.[18] In addition, it was reported that an increase in the calculated absorption wavelength upon the protonation of Chls c_1/c_2 is also observed in the absence of the FCP environment. Thus, the absorption wavelength shift of Chls c_1/c_2 predominantly originates from the change in the protonation state of the acrylate moiety instead of the protein environment. Of note, is the calculated difference in the increase of the absorption wavelength between the protonated and deprotonated forms of Chl c_1 (+ 31 nm) and Chl c_2 (+18 nm). Our data suggest that the protonated/deuterated form is not influenced by the pH/pD exchanges in the 4.9-8 range. We suggest that the presence of H_2O/D_2O molecules in the moiety of R31-Chl c_2- and K136-Chl c_1 acrylate controls the deprotonated (i.e. salt bridge) to protonated transition of acrylate (i.e. in the absence of salt bridge) is highly dependent of the protein environments. On this line, the dissociation of the ion pair can create a transient proton loading site. The optimized QM/MM structures of the FCP showed an increase in the R31 to 17-acrylate distance from 2.8 Å in the deprotonated form to 7.7 Å in the protonated form whereas the corresponding Chl c_1-acrylate to K136 increased from 2.7 to 4.2 Å, only[18]. This suggests that the protein environment of Chl c_1 is more difficult to protonate/deuterate the acrylate moiety than the corresponding protein environment of Chl c_2. In this scenario, we suggest that the acrylate of Chl c_2 403 in conjunction with H_2O molecules and/or proton channels is the predominant proton loading site providing a protonic switch that is part of the regulation from the light harvesting to the photoprotective states. The data suggest that at low pH there is an overload of H_2O molecules, as compared to high pH, that control the open and closed forms. This emphasizes the importance of balance in the dynamics of water presence in the R31-acrylate moiety to retain the gate in the open form, photoprotective mode. Chls c have been identified in both the stromal side and in the luminal side of PSII-FCP.[22,23] Furthermore, the release of protons to the luminal side of the thylakoid membrane in the chloroplasts results in lowering the pH and depends on the light intensity. Under LL conditions Chls c_1/c_2 are deprotonated whereas under HL conditions the pH is decreased and becomes protonated. Although not included in the model, the nearby Fx (Fx306) residue, based on the crystal structure, interacts through H-bonding with Chl c_2.[5,18] This way, the role of the specific positioning of Fx304 in the crystal structure, is to fix Chl c_2 in a certain configuration and distance from R31.[5] This way, the pH induced changes

between the deprotonated (closed form) and protonated (open form) Chl c_2 403 at the acrylate moiety controls the Chl c_2-R31 distance. There is consensus that the pH-triggered activation of the rapidly inducible thermal dissipation of excess absorbed energy (qE) should be conserved in diatoms.[30] We suggest that the H-bonding of the acrylate moiety of Chls-c_1/c_2 to the red Fxs 307/306 residues could play an important role in proton motion in a water pool, as it has been demonstrated in the oxidative or reductive phases in cytochrome oxidase that contains H_2O channels and maintain a transmembrane proton gradient (ΔpH).[31-34]

References

1. Büchel C. How diatoms harvest light. Science. 2019;365(6452):447–448.

2. Büchel, C. Advances in Photosynthesis and Respiration (Including Bioenergy and Related Processes), 2020;45, 441-457 Springer, Cham.

3. Büchel, C. Light harvesting complexes in chlorophyll c-containing algae Biochimica et Biophysica Acta – Bioenergetics. 2020;1861(4), 148027.

4. Pi X, Zhao S, Wang W, Liu D, Xu C, Han G, Kuang et al. The pigment-protein network of a diatom photosystem II-light-harvesting antenna supercomplex. Science. 2019;365, 6452.

5. Wang W, Yu LJ, Xu C, Tomizaki T, Zhao S, Umena Y et al. Structural basis for blue-green light harvesting and energy dissipation in diatoms. Science. 2019;363, 6427.

6. Feng Y, Li Z, Li X, Shen L, Liu X, Zhou C et al. Structure of a diatom photosystem II supercomplex containing a member of Lhcx family and dimeric FCPII. Sci Adv. 2023;9, 1-13.

7. Nagao R, Ueno Y, Yokono M, Shen JR, Akimoto S. Alterations of pigment composition and their interactions in response to different light conditions in the diatom Chaetoceros gracilis probed by time-resolved fluorescence spectroscopy. Biochimica et Biophysica Acta – Bioenergetics. 2018;1859(7), 524–530.

8. Buck, JM, Kroth PG, Lepetit B. Identification of sequence motifs in LHcx proteins that confer qE-based photoprotection in the diatom Phaeodactylum tricornutum. The Plant Journal. 2021;108, 1721-1734.

9. Wang W, Zhao S, Pi X, Kuang T, Sui SF, Shen J-R. Structural features of the diatom photosystem II-light harvesting antenna complex. FEBS J. 2020;287, 2191-2200.

10. Gelzinis A, Butkus V, Songaila E, Augulis R, Gall A, Büchel C et al. Mapping energy transfer channels in fucoxanthin–chlorophyll protein complex. Biochimica et Biophysica Acta (BBA) - Bioenergetics. 2015;1847(2):241-247.

11. Nagao R, Ueno Y, Yokono M, Shen J, Akimoto S. Effects of excess light energy on excitation-energy dynamics in a pennate diatom Phaeodactylum tricornutum. Photosynthesis Research. 2019;141(3):355-365.

12. Papagiannakis E, van Stokkum I, Fey H, Büchel C, van Grondelle R. Spectroscopic characterization of the excitation energy transfer in the fucoxanthin-chlorophyll protein of diatoms. Photosynth. Res. 2005;86, 241-250.

13. Oka K, Ueno Y, Yokono M, Shen JR, Nagao R, Akimoto S. Adaptation of light-harvesting and energy-transfer processes of a diatom Phaeodactylum tricornutum to different light qualities. Photosynth. Res. 2020;146, 227– 234.

14. Chrysafoudi A, Maity S, Kleinekathöfer U, Daskalakis V. Robust Strategy for Photoprotection in the Light-Harvesting Antenna of Diatoms: A Molecular Dynamics Study. The Journal of Physical Chemistry Letters. 2021;12 (39), 9626-9633.

15. Ikeda Y, Yamagishi A, Komura M, Suzuki T, Dohmae N, Shibata Y et al. Two types of fucoxanthin-chlorophyll-binding proteins are tightly bound to the photosystem core complex in marine centric diatoms. Biochimica et Biophysica Acta – Bioenergetics. 2013;1827, 529–539.

16. Nagao R, Yokono M, Ueno Y, Shen JR, Akimoto S. High excitation energy quenching in Fucoxanthin chlorophyll a/c binding protein complexes from the diatom Chaetoceros gracilis. J. Phys. Chem. B. 2019;124, 4919-4923.

17. Yamano N, Mizoguchi T, Fujii R. The pH-dependent photophysical properties of chlorophyll-c bound to the light-harvesting complex from a diatom, Chaetoceros calcitrans. Journal of Photochemistry and Photobiology A: Chemistry. 2018;358, 379–385.

18. Tsujimura M, Sugano M, Ishikita H, Saito K. Mechanism of Absorption Wavelength Shift Depending on the Protonation State of the Acrylate Group in Chlorophyll c. J. Phys. Chem. B. 2023;127, 505-513.

19. Nagao R, Yokono M, Tomo T, Akimoto S. Control mechanism of Excitation Energy Transfer in a complex consisting of Photosystem II and Fucoxanthin Chlorophyll a/c-Binding Protein. Phys. Chem. Let. 2014;5, 2983-2987.

20. Nagao R, Yokono M, Ueno Y, Shen J, Akimoto S. Acidic pH-Induced Modification of Energy Transfer in Diatom Fucoxanthin Chlorophyll a/c-Binding Proteins. The Journal of Physical Chemistry B. 2020;124(24):4919-4923.

21. Nagao R, Yokono M, Akimoto S, Tomo T. High Excitation Energy Quenching in Fucoxanthin Chlorophyll a/c-Binding protein complexes from the Diatom Chaetoceros gracilis. J. Phys. Chem. B. 2013;117, 6888-6895.

22. Nagao R, Kato K, Kumazawa M, Ifuku K, Yokono M, Suzuki T. et al. Structural basis for different types of hetero-tetrmeric light-harvesting complexes in a diatom PSII-FCPII supercomplex. Nat Commun. 2022;13, 1764.

23. Nagao R, Kato K, Ifuku K, Suzuki T, Kumazawa M, Uchiyama I et al. Structural basis for assembly and function of a diatom photosystem I-light-harvesting supercomplex. Nature Communications. 2020;11, 2481.

24. Faqley MW. Separation of Chlorophylls c1 and c2 from Pigment Extracts of Pavlova gyrans by Reversed-Phase High Performance Liquid Chromatography. Plant Physiol. 1988;86, 76-78.

25. Tselios C, Varotsis C. Evidence for reversible light-dependent transitions in the photosynthetic pigments of diatoms. RSC Advances. 2022;12, 31555-31563.

26. Andreou C, Tselios C, Ioannou A, Varotsis, C. Probing the Fucoxanthin-Chlorophyll a/c-Binding proteins (FCPs) of the Marine diatom Fragilariopsis sp. by Resonance Raman spectroscopy. J. Phys. Chem. B. 2023;127, 9014-9020.

27. R.R. Guillard, in Culture of Marine Invertebrate Animals, ed. W. L. Smith, M. H. Chanley, Springer, Boston MA, 1975, Culture of Phytoplankton for Feeding Marine Invertebrates, p. 29–60.

28. Beer A, Gundermann K, Beckmann J, Büchel C. Subunit Composition and Pigmentation of Fucoxanthin−Chlorophyll Proteins in Diatoms: Evidence for a Subunit Involved in Diadinoxanthin and Diatoxanthin Binding. Biochemistry. 2006;45(43):13046-13053.

29. Pinakoulaki E, Pfitzner U, Ludwig B, Varotsis, C. Direct Detection of Fe(IV)=O Intermediates in the Cytochrome aa3 Oxidase from Paracoccus denitrificans/H2O2 Reaction. J. Biol. Chem. 2023;278, 18761-18766.

30. Buck JM, Sherman J, Río Bártulos C, Serif M, Halder M, Hankel J et al. Lhcx proteins provide photoprotection via thermal dissipation of absorbed light in the diatom Phaeodactylum tricornutum. Nat Commun. 2019;10, 4167.

31. Schelvis JPM, Deinum G, Varotsis CA, Ferguson-Miller S, Babcock GT. Low-Power Picosecond Resonance Raman Evidence for Histidine Ligation to Heme a3 after Photodissociation of CO from Cytochrome c Oxidase J. Am. Chem. Soc. 1997;119, 8409-8416.

32. Stavrakis S, Pinakoulaki E, Urbani A, Varotsis, C.Fourier Transform Infrared Evidence for a Ferric Six-Coordinate Nitrosylheme b3 Complex of Cytochrome cbb3 Oxidase from Pseudomonas Stutzeri at Ambient Temperature J. Phys. Chem. B. 2002;106, 12860-12862.

33. Koutsoupakis C, Soulimane T, Varotsis C. Docking site dynamics of ba3-cytochrome c oxidase from Thermus thermophiles J. Biol. Chem. 2003;278, 36806-36809.

34. Vamvouka M, Varotsis C. Resonance Raman and FTIR Studies of Carbon Monoxide-Bound Cytochrome aa3-600 Oxidase of Bacillus subtilis. J. Phys. Chem. 1999;103, 3030-3034.

6. Ultrafast Dynamics of Frag. sp and P. Tricornutum FCPs by Transient Absorption Spectroscopy

The objective of this investigation is to analyze the transient absorption spectra of Frag. sp and P. Tricornutum FCPs at different light intensities and wavelengths at specific time traces. The spectra exhibit a negative band located at approximately 437 nm, attributed to the ground-state bleaching (GSB) of chlorophylls and carotenoids present in the FCPs. Furthermore, positive bands at 482 nm, 510 nm, and 545 nm are observed, indicating the excited-state absorption (ESA) transition of Fx, Dd and Dt. Additionally, slight negative peaks appearing at 588 nm, 615 nm, and 635 nm are attributed to the GSB/SE of Chl c, Chl a and Chlide a. Finally, the negative peak observed at 672 nm is assigned to the Qy band of Chl a/ Chlide a. moreover, global analysis exhibited in the data are presented in here with two Evolution-associated difference spectra (EADS).

6.1. Introduction

Diatom photosynthesis begins with the capture of solar radiation, which is achieved through FCPs, which contain the chls a and c and the carotenoids Fx and Dd. Fx and chl c enable FCPs to capture the blue-green sunlight that penetrates the sea bed.[1-3] The captured radiation is then transferred from Fx and chl c to chl a and from there to the reaction center for the photosynthesis reactions to take place. Dd and Dt are the main photoprotection pigments of the diatom system against high radiation intensity, as the conversion of Dd to Dt through an epoxidation reaction converts excess light energy in the form of heat.[1-6]

Herein, FCPs isolated from the diatoms Frag sp. and P. Tricornutum were studied using the Ultrafast Time-Resolved Laser Spectroscopy technique. This technique provides information on the kinetics of the molecules, which will lead to the identification of their excitation-de-excitation mechanisms. The advantage of this technique is that the duration of the perturbation is very short, due to the use of an ultrashort pump pulse, providing the possibility of detecting ultrafast processes while avoiding overlap by the perturbation process. Given this, the temporal resolution is improved because the response time of the system is limited to the pulse duration.[7]

6.2. Materials and Methods

6.2.1. Diatoms Growth

The culture of *Fragilariopsis.sp* (CCAP 1029/24) and *P.Tricornutum* (CCAP 1052/1A) were obtained from CCAP (Culture Collection of Algae and Protozoa). Cells were grown in f/2-Si medium,[8] at 19 °C in a dark-light cycle (12h:12h) under white or red LED light. The light intensity used for the growth of the cells culture was 150 μmol photons m^{-2} s^{-1} for the low-intensity light (LL) condition and 350 μmol photons m^{-2} s^{-1} for the high-intensity light (HL).

6.2.2. FCP Isolation

Cells from diatoms were harvested by centrifugation (8000 rpm, 30 min, 4 °C) and the supernatant medium was removed. The cells were resuspended in 20 mM Tris and sonicated in an ice bath for 20 minutes. Thylakoid membranes were then solubilized with the addition of β -1,4-dodecyl maltoside (β-DDM, 30 mg, 4 mM) in the resuspended cells while they were shaken for 20 minutes on ice.[9] Separation of solubilized FCPs was carried out on an ion exchange column (HiPrep Q HP 16/10, 20 mL) in 25 mM Tris, 2 mM KCl and 0.4 mM β-DDM at pH 7.4 using a Shimadzu LC 20AD with a SPD-20A detector with two-wavelength detection. The samples were loaded in a column, and fractions were eluted using a gradient from 0 to 750 mM KCl in a buffer made of 25 mM Tris, 750 mM KCl and 0.4 mM β-DDM, pH 7.4 at a flow rate of 3 mL/min. Fractions were pooled and concentrated using Amicon filtration devices with a cutoff of 10 kDa and characterized spectroscopically. The rest of the fractions were stored at -80 °C until further use.

6.2.3. Pigment analysis using HPLC

The FCP or the free pigments (FP) were extracted in 100% methanol buffered with 2% ammonium acetate. The following steps were carried out in a room with very low lighting and intermediate placement of the sample on ice in order to avoid changes in the sample due to high temperature or lighting. The sample was subjected to agitation for 30 seconds and then placed in an ultrasonic bath for the same period of time. These steps were repeated 5 times and then the sample was centrifuged for 1 minute at 8000 rpm. The supernatant which contained the pigments of the diatom cells was collected

and stored at a temperature of -20 °C until its analysis. The analysis of the pigments was performed using HPLC. (Shimadzu-Nexera 40 system equipped with an SPD-M40 detector (Photodiode Array Detector)). The column used was Zorbax SB-C18 reverse phase (Agilent). The solutions used were the following: A) 0.5M Ammomium Acetate in methanol/water (85:15 v/v), (B) Acetonitrile and water (90:10, v/v) and (C) 100% Ethyl Acetate.[10] The separation was done by gradient elution as shown in Table 2.

6.2.4. Ultrafast time–resolved laser spectroscopy

The experimental setup employed has been mentioned previously.[11] Briefly, the output of an amplified titanium-sapphire laser system with central wavelength at λ = 790 nm, repetition rate 1 kHz and τ_{pulse} > 30 fs were used to perform the pump-probe experiments. As a pump source, the second harmonic laser frequency (395 nm), was used. White–light supercontinuum generation was produced by focusing the laser beam into a cuvette containing distilled water and used for differential absorption signal probing. All samples were contained in a 2 mm spinning cell. The transmitted signal from the probe beams was collected into the entrance slit of a 0.0200 cm spectrograph, which offered spectral coverage in the range of 423 - 735 nm. Anisotropy effects were suppressed by setting the polarization of the probe beam at “magic angle” (54.7°) with respect to that of the pump. The samples’ OD was adjusted to OD_{550}=0.5 and the energy delivered to each sample per area was equal to F= 2 mJ/cm^2. All measurements were performed at room temperature and the accumulation time was 10 iterations /hour.

6.3. Results

Using the HPLC for isolating the FCP proteins of Frag. sp, seven unique fractions with different pigment composition were isolated. Under different spectroscopic and chromatographic techniques, we concluded that fraction 3, as shown in Figure 40, was the nearest fraction towards the FCPs appeared in the bibliography.[9,12-14] This was due to its pigment molarity ratio, UV absorbance and fluorescence emission. Fractions 4-7 were closer to fraction 3 however, fraction 3 yielded more product and was stable under light exposure. Furthermore, fraction 1 was mainly consisted of FP which were photolabile under Raman spectroscopy and high intensity light. This characteristic made it hard for spectroscopic analysis however, due to its high Dd and Dt pigment composition percentage, fraction 1 could be the ideal sample to investigate the Dd cycle

and photoprotection system of diatoms. Fraction 2 was a mixture of fraction 1 and 3 according to its UV spectra and was not ideal for further study. The UV spectra of the seven fractions is illustrated in Figure 41.

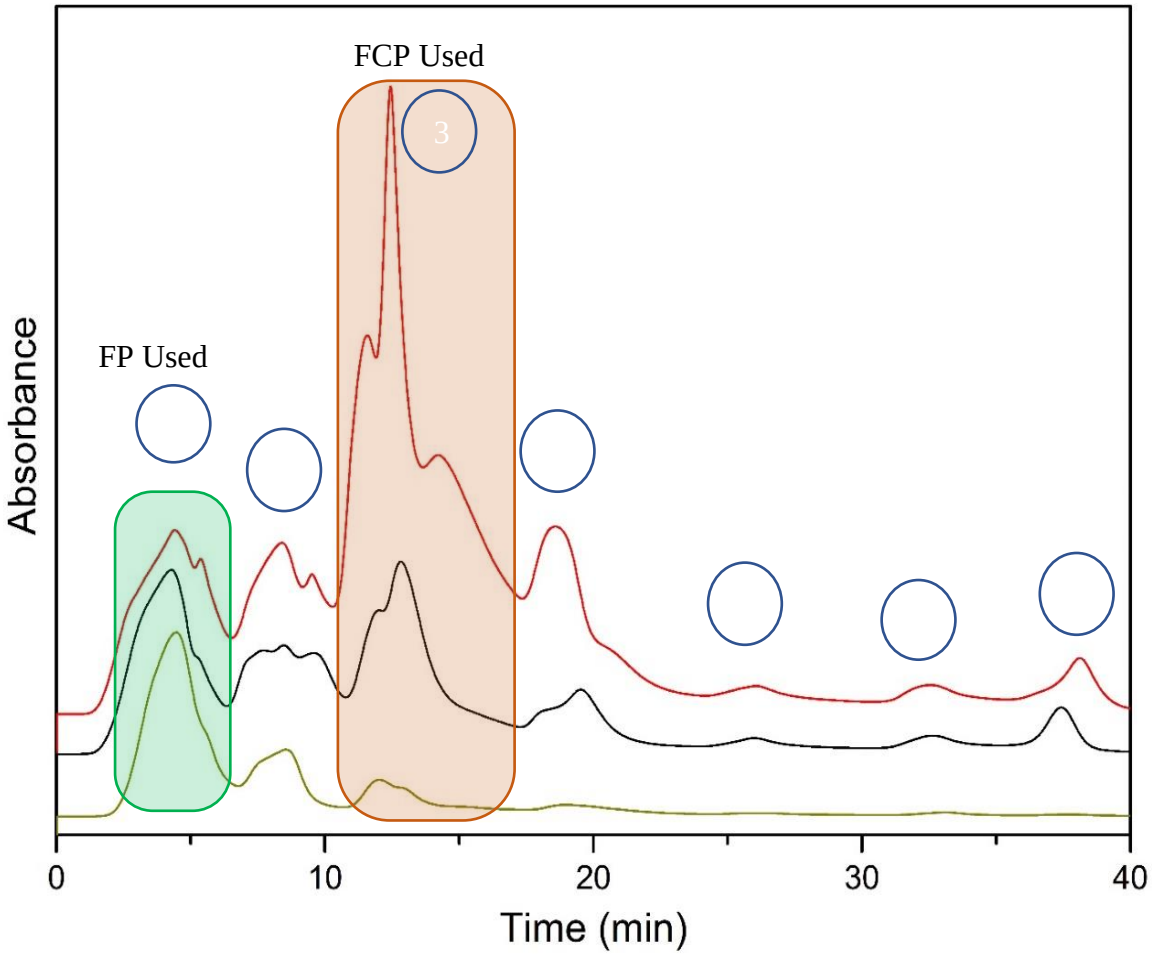

Figure 40: HPLC Chromatogram from the FCPs isolation method illustrating the FP and the FCPs used for the experiments. The isolations from HL, LL and RL are represented by yellow, black and red line, respectively.

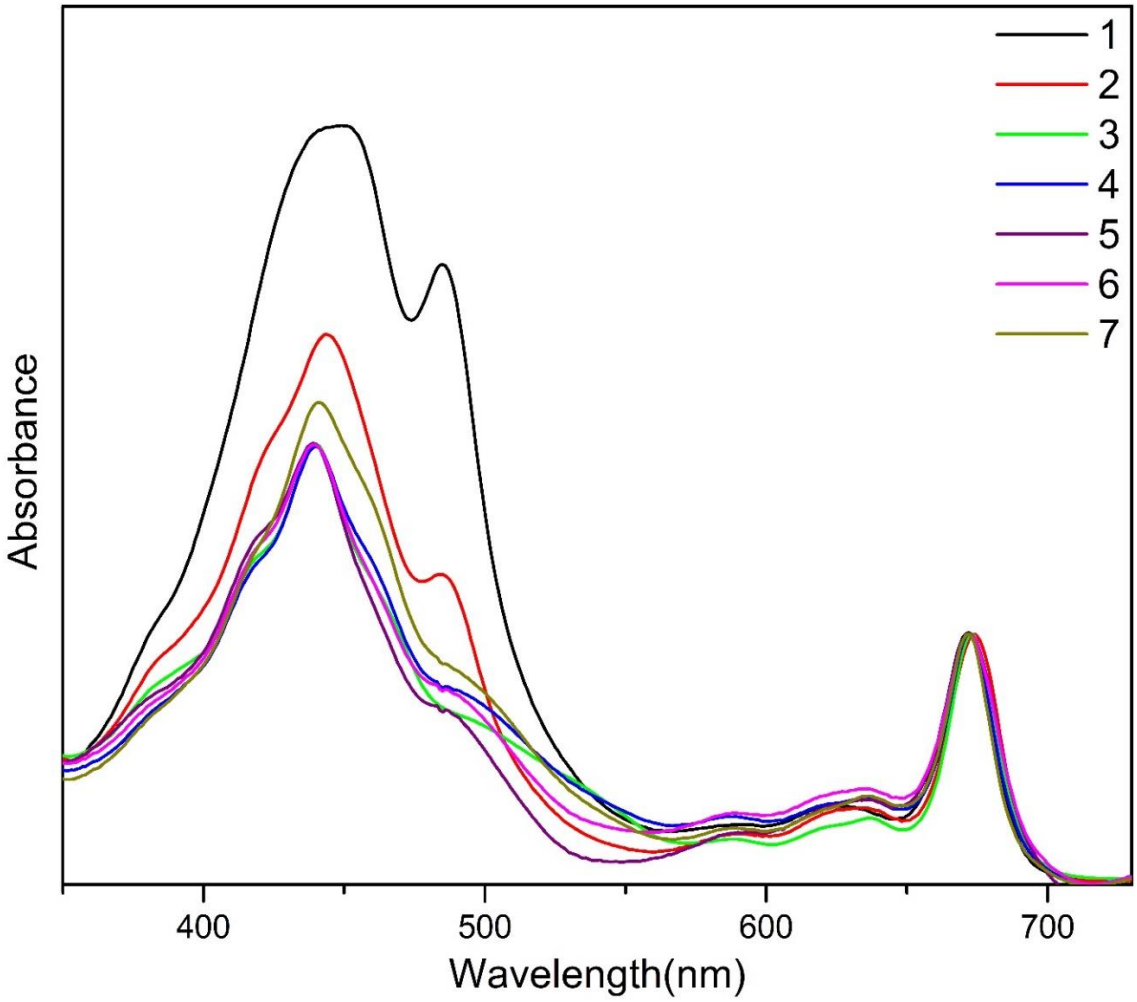

Figure 41: UV spectra of the seven fractions isolated from Frag. sp.

6.3.1. Fragilariopsis sp FCP Low Light

Using the HPLC method for FCPs isolation, many FCPs were isolated from the organism Frag. sp however, the third fraction was chosen for further analysis and its pigments composition contained, was clarified. The HPLC method for pigments identifications was used to clarify the composition of the pigments in the FCPs, revealing that the Frag. sp FCP LL sample has as main pigments Fx and chl a and c as shown in Figure 42. This particular sample represents a typical FCP, as those reported in the literature. [9,12-14]

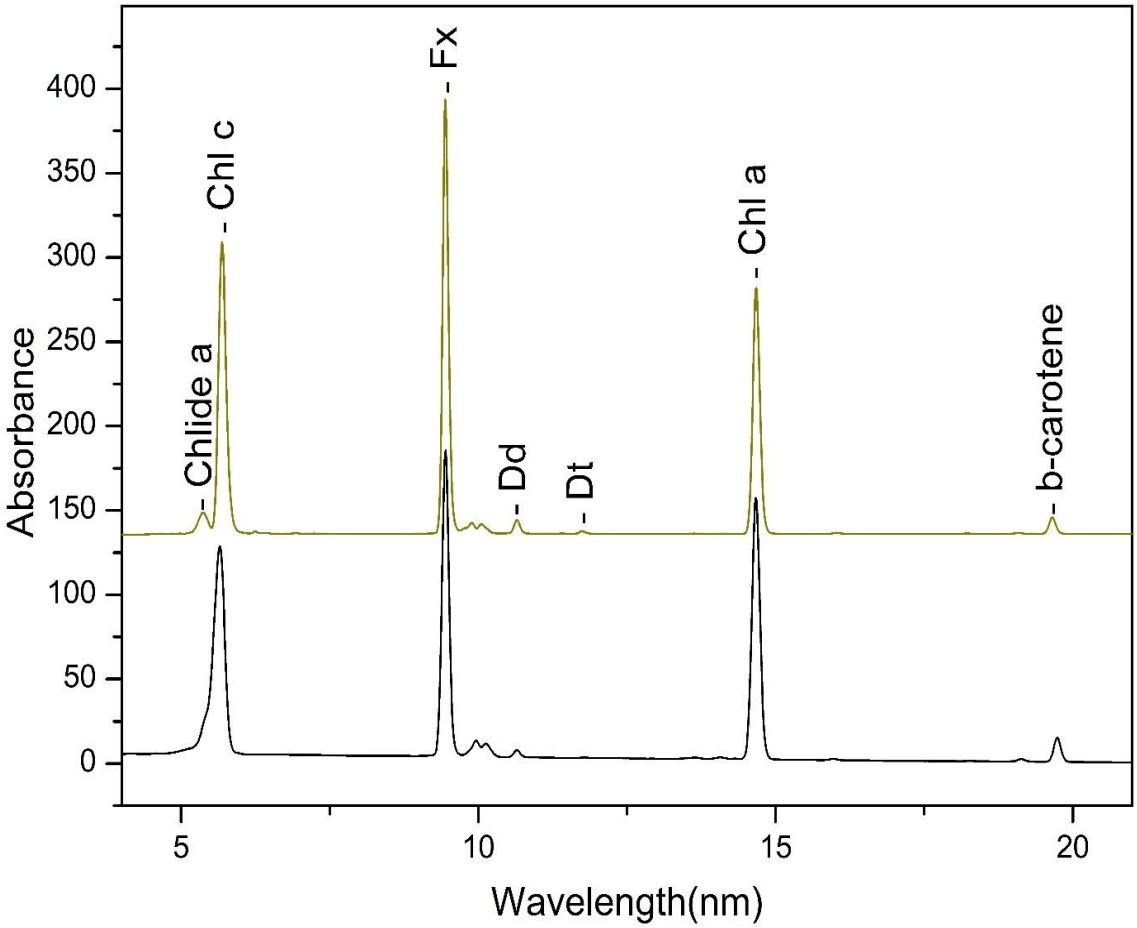

Figure 42: HPLC chromatogram of Frag. sp FCP illustrating the major pigments at their elution time. Yellow line illustrates the HL growth and black line shows the LL growth.

The study of the Frag. sp FCP LL sample using time-resolved laser spectroscopy and the use of a pump pulse with a wavelength of 400 nm resulted in the excitation of all pigments (Fx, Chl-a and Chl-c) within the FCP to the S2 state and the yield of transient absorption spectra, which are depicted in Figure 43. In the spectral range from λ = 420 nm to λ = 470 nm, the S0→S2 (Ground State Bleaching-GSB) transitions of Chl-a, Chl-c and Fx are observed. The appearance of the negative peak at λ = 437 nm is mainly attributed to the GSB of Chl-a. However, the intensity of this peak is enhanced by the S0→S2 (GSB) transitions of Chl-c (λ = 460 nm) and Fx (λ = 400-560 nm) despite the fact that it was not possible to distinguish the maximum wavelengths of these peaks in the present spectrum. In the spectral range from λ = 570 nm to λ = 700 nm, the signal of the Excited-state-absorption (ESA) transition of Fx is observed with maxima at λ = 510 nm and λ = 547 nm. At the same time, in the same region at λ = 482 nm, the ESA of Chl-a appears, as well as the GSB/SE (Stimulated Emission-SE) of Chl-a and Chl-c at λ = 615 nm, 672 nm and λ = 588 nm, 635 nm, respectively.

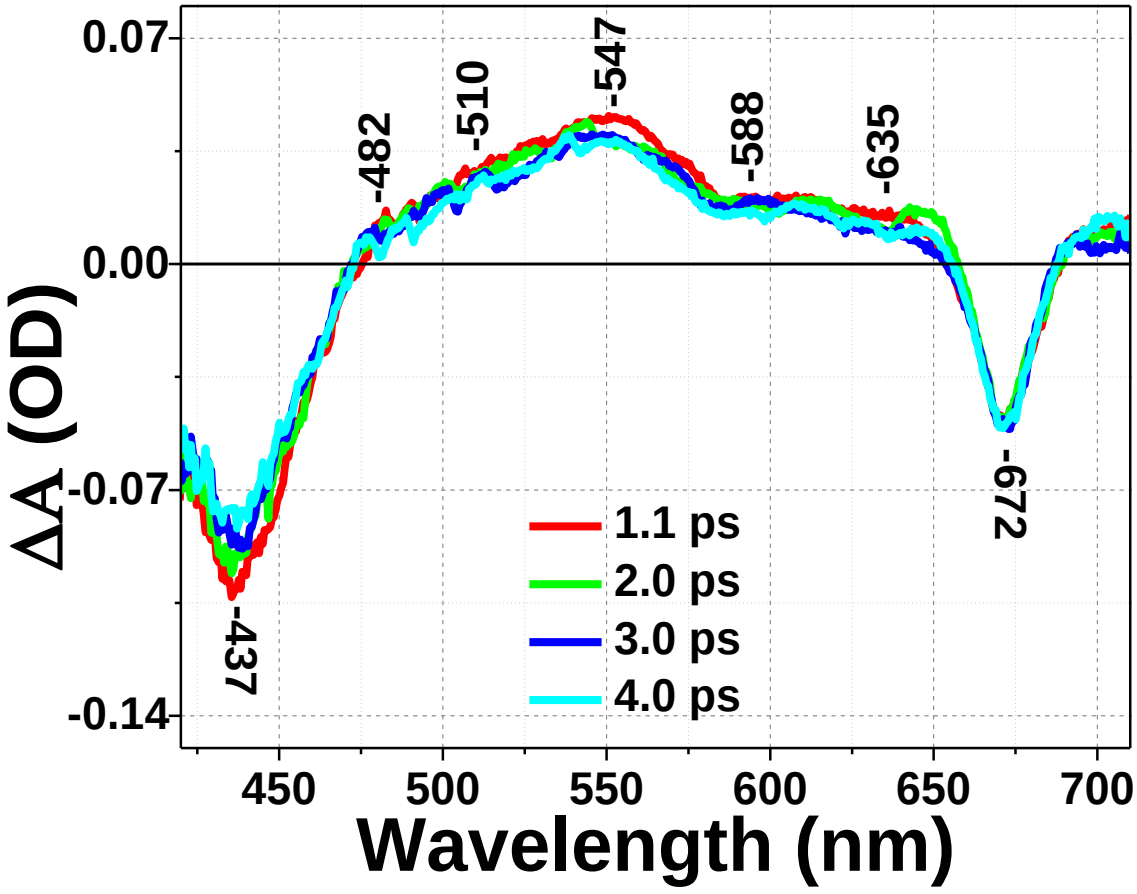

Figure 43: Transient absorption spectra of sample Frag. sp FCP LL.

6.3.1. Fragilariopsis sp FCP High Light

The growth of the organism Frag. sp under conditions of high intensity white light results in a change in the composition of FCPs. In the Frag. sp FCP HL sample, it was found that the main pigments present were Fx, chls a and c, and chlorophyllide-a (Chlide-a). Ultrafast time-resolved laser spectroscopy was used to study the Frag. sp FCP HL sample and the pump pulse with λ = 400 nm caused the excitation of all FCP pigments in the S2 state. The differential absorption spectra of the Frag-HL-Fraction-3 sample are depicted in Figure 44.

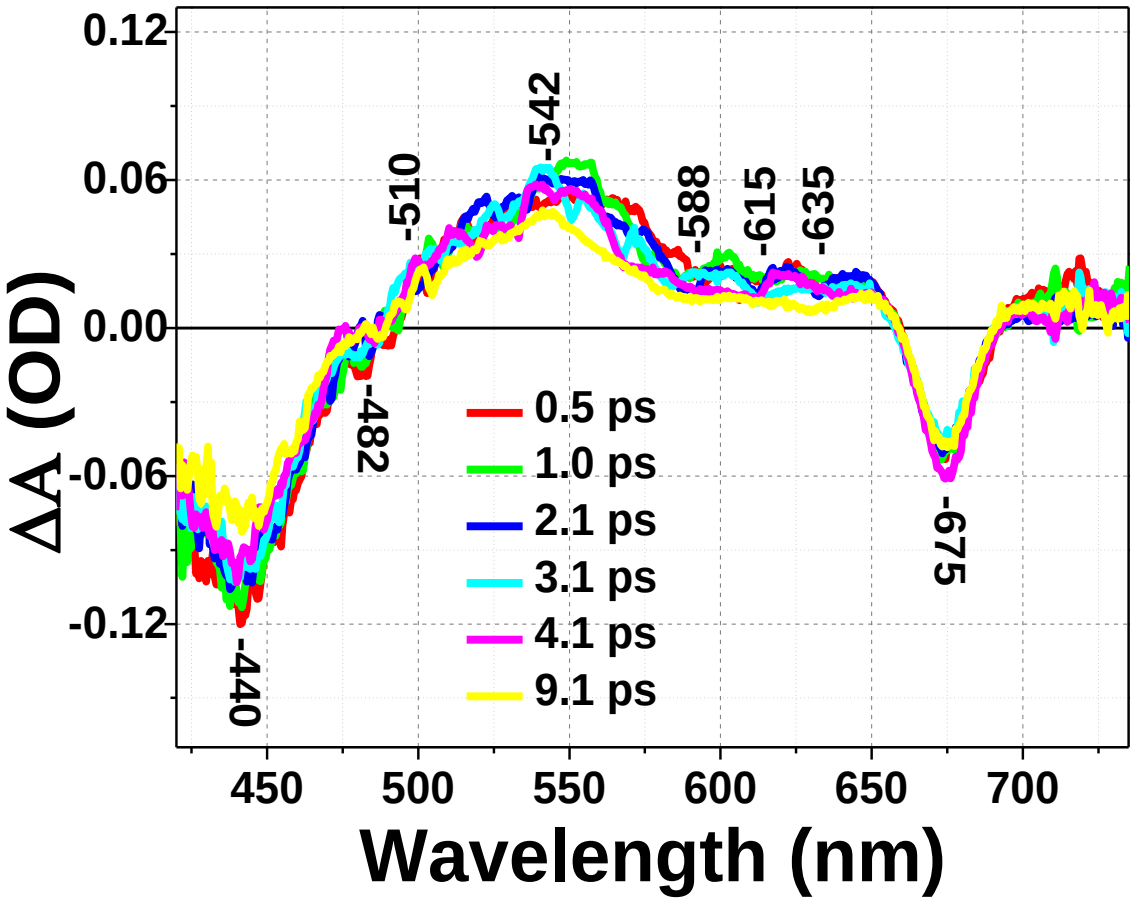

Figure 44: Transient absorption spectra of sample Frag. sp FCP HL.

In the spectral range from λ = 420 nm to λ = 500 nm, the GSB transitions from the S2 state of all pigments within the FCP (Fx, Chl-a, Chl-c and Chlide-a) are observed. The characteristic peak at λ = 440 nm is attributed to Chl-a and Chlide-a, while the negative peak at λ = 482 nm is due to Fx. In addition, the ESA transition of Chl-a appears in the region around λ = 482 nm, which results in the formation of a positive peak. Since the amount of Fx is greater than that of Chl-a within the sample (2:1), the negative peak of Fx is more prominent in the differential absorption spectrum, rather than the positive peak of Chl-a. The broad spectral band from λ = 570 nm to λ = 700 nm is attributed to the ESA transition of Fx. In this spectral region, the peaks at λ = 510 nm and λ = 542 nm appear, which are attributed to transitions from different vibrational levels of S1 to the Sn state of Fx. In the differential absorption spectra, the GSB/SE transitions from the S1 states of Chl-a at λ = 615 nm, λ = 672 nm and of Chl-c at λ = 588 nm, λ = 635 nm are observed. The EADS spectra, extracted from the analysis of the experimental data with the global analysis method, are presented in Figure 45.

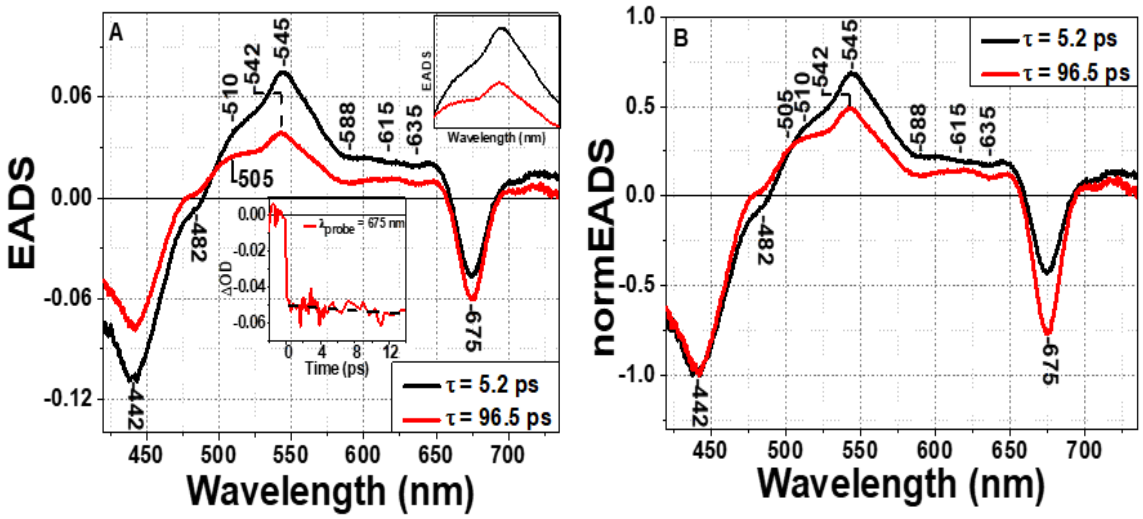

Figure 45: A) EADS spectra and B) Normalized EADS spectra of the Frag. sp FCP HL sample. Insets: a) Kinetic curve for λ_{probe} = 675 nm, b) Gaussian simulation of the peak at λ = 540-550 nm (FWHM $_{black\ line}$ = 21 nm, FWHM $_{red\ line}$ = 18 nm).

The Frag. sp FCP HL sample contains the pigments Dd and chlide a which are barely or no found in Frag. sp FCP LL sample. The change in composition does not affect the function of FCP, as the study of the Frag. sp FCP HL sample via ultrafast time-resolved laser spectroscopy technique resulted in experimental times that are similar to those of the Frag-LL-Fraction-3 sample and are attributed to the same photophysical deexcitation processes of Fx.

Spectrally, the presence of Chlide a is detected, as the characteristic ESA transition at λ = 505 nm is observed when Fx is de-excited. The increase in the ratio of the peak intensities at λ = 542 nm to the peak at λ = 510 nm observed in the Frag. sp FCP HL sample compared to the Frag. sp FCP LL sample comes from the presence of Dd in the Frag. sp FCP HL sample. In the differential absorption spectrum of the Frag. sp FCP HL sample, the peak at λ = 482 nm is negative and not positive as in the spectrum of the Frag. sp FCP LL sample. This phenomenon is due to the increase in carotenoids (Fx, Dd) within the Frag. sp FCP HL sample.

6.3.1. Fragilariopsis sp FCP Red Light

The use of RL for the growth of the organism Frag. sp. resulted in the main pigments of the FCPs being Fx, Chl-a, Chl-c and Chlide-a. The study of the sample Frag. sp FCP RL with the technique of ultrafast time-resolved laser spectroscopy and the use of a pump

pulse at λ = 400 nm resulted in all pigments being excited to the S2 state and the differential absorption spectra of Figure 46 were obtained.

The peaks attributed to the GSB transitions from the S2 state of the pigments (Fx, Chl-a, Chl-c and Chlide-a) within the FCP are observed in the spectral range from λ = 420 nm to λ = 470 nm. The negative peak at λ = 441 nm is mainly attributed to the GSB transition of Chl-a and Chlide-a. The intensity of this peak is enhanced by the S0→S2 (GSB) transitions of Chl-c (λ = 460 nm) and Fx (λ = 400-560 nm) despite the fact that the maxima of these peaks are not distinguishable in the spectrum. The peak at λ = 482 nm is attributed to the ESA transition of Chl-a, the amount of which is comparable to that of Fx, so the superposition of the signals results in the spectrum having a positive absorption at this wavelength. The peaks at λ = 510 nm and λ = 542 nm are attributed to ESA transitions of Fx from a different vibrational level of the S1 state, while the peaks at λ = 615 nm and λ = 672 nm are due to GSB/SE transitions of Chl-a. The peaks at λ = 588 nm and λ = 635 nm are attributed to GSB/SE of Chl-c.

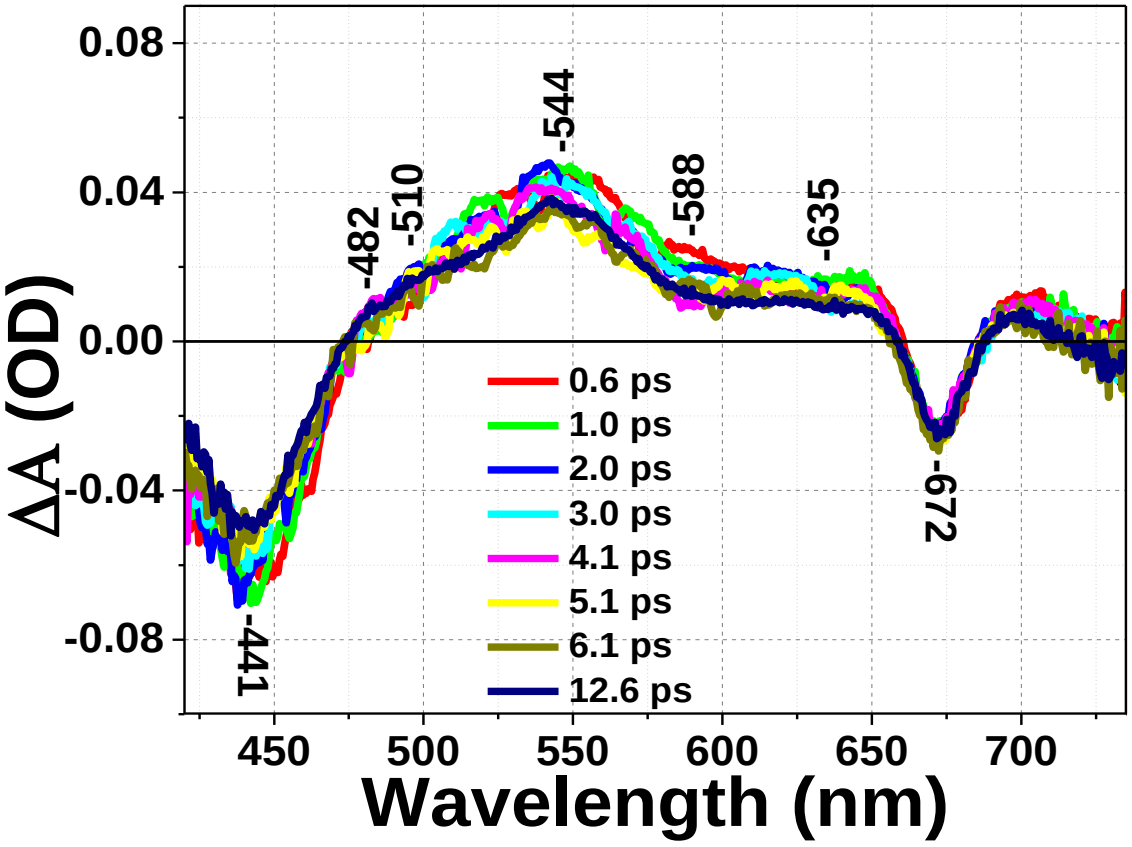

Figure 46: Transient absorption spectra of sample Frag. sp FCP RL.

Frag. sp FCP RL containing the pigments Chl a, Chl c, Fx and Chlide a. As in the Frag. sp FCP HL sample, the presence of Chlide a does not alter the function of the FCP in the Frag. sp FCP RL sample. The presence of Chlide a is detected through the observation of the ESA transition at λ = 505 nm. The Frag. sp FCP RL sample does not contain Dd, so the ratio of the peak intensities at λ = 542 nm and λ = 510 nm is similar to that of the Frag. sp FCP LL sample.

6.3.1. Fragilariopsis sp FP Low Light

Using the HPLC method for FCPs isolation, the first fraction was isolated, containing FP, from the organism Frag. sp and the composition of the pigments contained in it was clarified. Using the HPLC method for pigments identifications, the chlorophylls and the carotenoids were separated as shown in Figure 47. The main pigments contained in the Frag. sp FP LL sample are Fx, Dd and Chlide a, which is a precursor compound of chl a. Chlide a differs structurally from Chl a, as it lacks the phytol group. The transient absorption spectra of the Frag. sp FP LL sample (Figure 48) were obtained after excitation of all dyes within the FCP (Fx, Dd and Chlide a) to the S2 state.

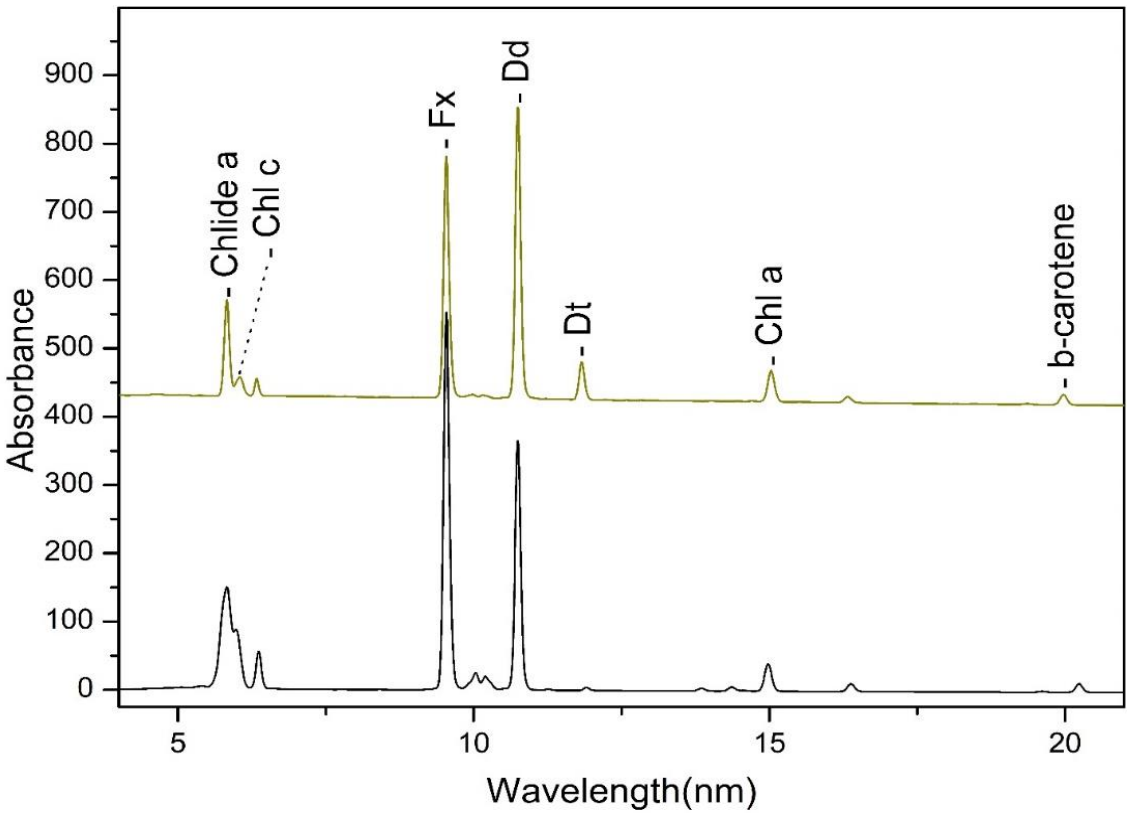

Figure 47: HPLC chromatogram of Frag. sp FP revealing the major pigments at their elution time. Yellow line illustrating the HL growth and black line shows the LL growth.

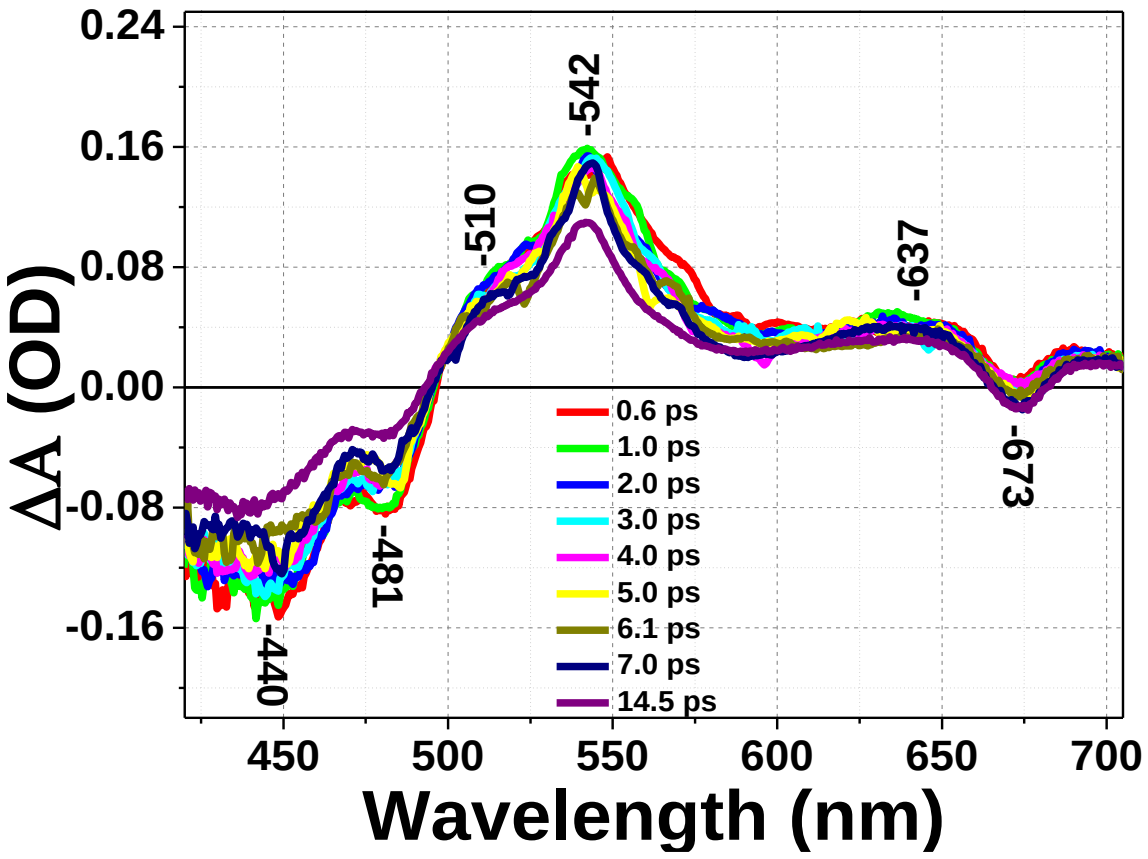

Figure 48: Transient absorption spectra of sample Frag. sp FP LL.

In the spectral range from λ = 420 nm to λ = 490 nm, the GSB transitions of Chlide-a, Dd and Fx from the S2 states are observed. The negative peak at λ = 440 nm is mainly attributed to Chlide-a and the peak at λ = 481 nm to the carotenoids (Dd and Fx). The ESA transition of Fx from the S1 state yields a broad spectral band from λ = 500 nm to λ = 700 nm with maxima at λ = 510 nm, λ = 542 nm and λ = 637 nm. The peaks at λ = 510 nm and λ = 542 nm are due to S1→Sn transitions from different vibrational levels, while the peak at λ = 637 nm originates from the Internal Charge Transfer (ICT) level in the Sn level. At the same time, in the same region (from λ = 500 nm to λ = 600 nm) the ESA transition of Dd appears, which has maxima at λ = 510 nm and λ =542 nm. The peak at λ = 673 nm is attributed to GSB/SE from the S1 state of Chlide-a. The spectroscopic properties of Chlide-a are similar to those of Chl-a, as no change in the position of the peak at λ = 673 nm is observed. This observation is an indication that the phytol group does not alter the properties of the porphyrin ring, even in the presence of a protein environment or nearby neighboring pigments (e.g. Fx). The EADS spectra, extracted from the analysis of the experimental data with the global analysis method, are presented in Figure 49.

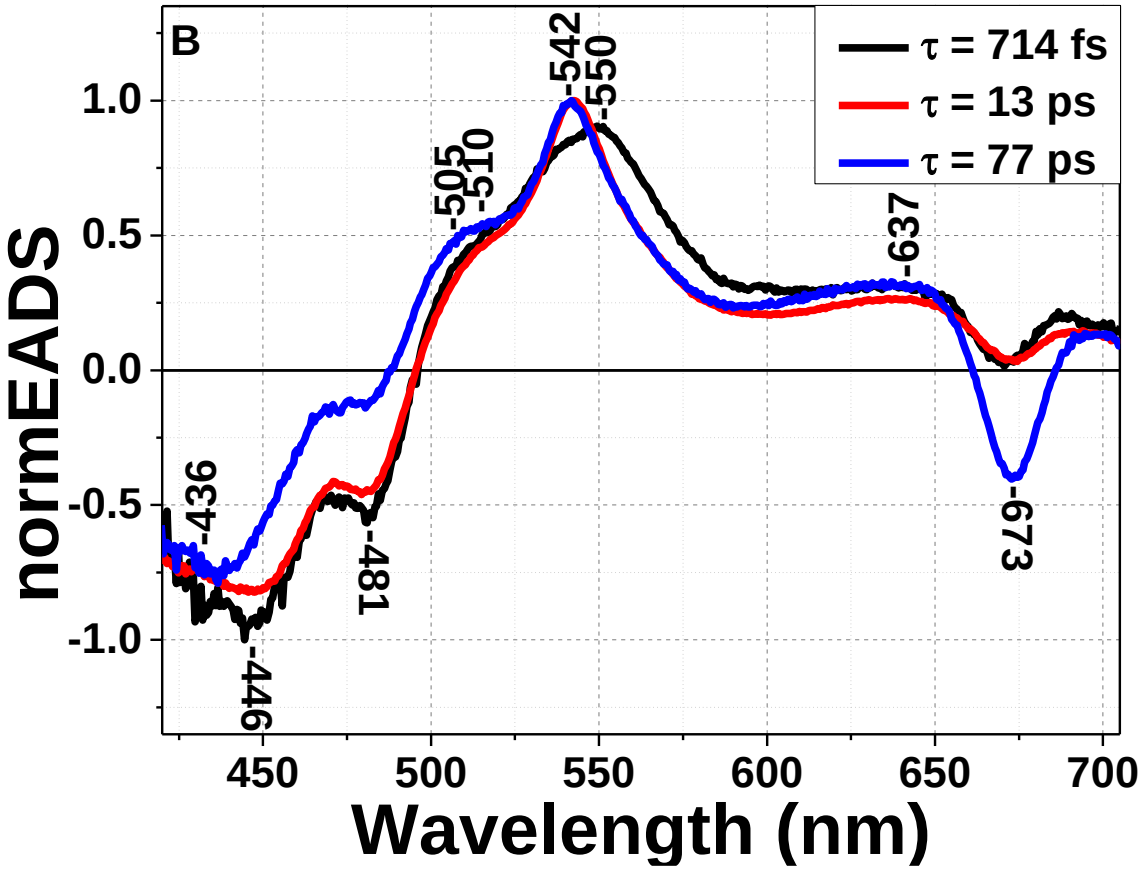

Figure 49: Normalized EADS spectra of the Frag. sp FP LL.

The operation of the FPs of fraction 1 differs from the operation of the FCPs of fraction 3, as revealed by the study of the dynamics of the Frag-LL-Fraction-1 sample. Specifically, the study of the Frag. sp FP LL sample with the ultrafast time-resolved laser spectroscopy technique yielded three characteristic times. The first time, τ = 714 fs, is attributed to the vibrationally excited levels of the S1 states of Dd and Fx and the second time, τ = 13 ps, is due to the S1 state of Dd. The first pathway is the energy transfer from the S1 state of Fx to the S1 state of Chl a and the second pathway is the de-excitation of the S1 state of Fx. Spectrally, the presence of Chlide a is confirmed by the peak at λ = 505 nm, which is attributed to an ESA transition. The presence of Dd in the sample is detected by the increase in the ratios of the peaks at λ = 542 nm and λ = 510 nm. The peak at λ = 482 nm is negative, as the number of carotenoids (Fx, Dd) is increased compared to the Frag. sp FCP LL sample. The negligible amount of Chl-c in the sample does not allow the detection of its spectroscopic characteristics.

6.3.1. Fragilariopsis sp FP High Light

The growth of the organism Frag. sp with high intensity white light resulted in a change in the composition of the FCPs proteins. In the Frag. sp FP HL sample, Fx, Dd, Chlide-a and Dt were found as the main pigments. Dd and Dt are carotenoids that participate in the protection of FCPs proteins from high intensity radiation. The study of the Frag-HL-Fraction-1 sample with time-resolved laser spectroscopy yielded the transient absorption spectra of Figure 50. The pump pulse used to excite the sample was tuned to λ = 400 nm, causing the excitation of all FCP pigments to the S2 state.

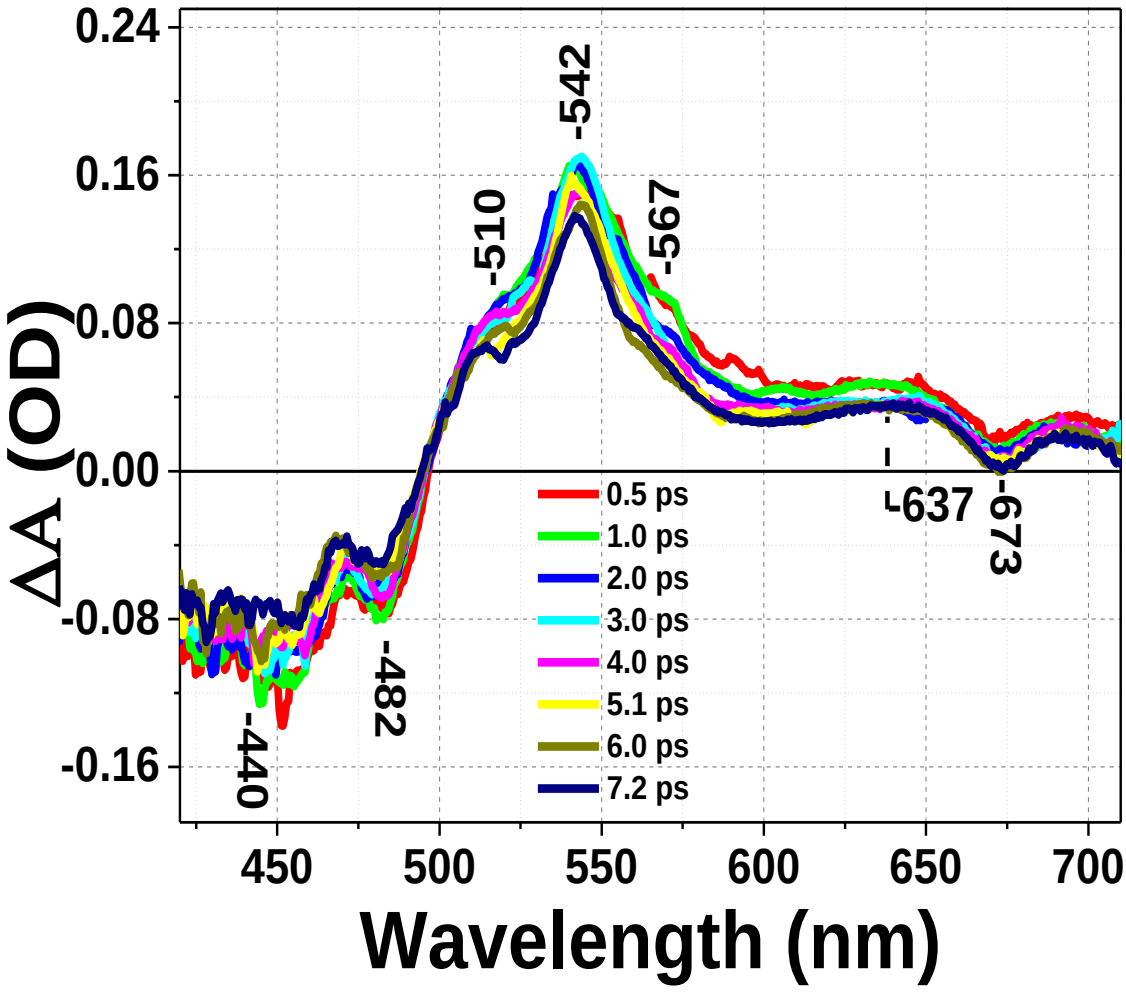

Figure 50: Transient absorption spectra of sample Frag. sp FP HL.

The spectra of the Frag. sp FP HL sample are similar to those of the Frag. sp FP LL sample, showing in the spectral region from λ = 420 nm to λ = 490 nm the GSB transitions of Chlide-a, Dd, Dt and Fx from the S2 states. The peak at λ = 440 nm is

attributed to Chlide-a, while the peak at λ = 482 nm to the carotenoids (Dd, Dt and Fx). The broad spectral band from λ = 500 nm to λ = 700 nm is attributed to the ESA transition of Fx. The peaks at λ = 510 nm and λ = 542 nm are due to S1→Sn transitions from different vibrational levels of Fx and Dd, while the peak at λ = 567 nm is attributed to the S1→Sn transition of Dt. The peak at λ = 637 nm is due to the transition from the ICT level to the Sn level of Fx and the peak at λ = 673 nm is attributed to GSB/SE from the S1 state of Chlide-a. As in the case of the Frag. sp FP LL sample, the observation of spectroscopic features of Chl-c is impossible due to its negligible amount in the sample.

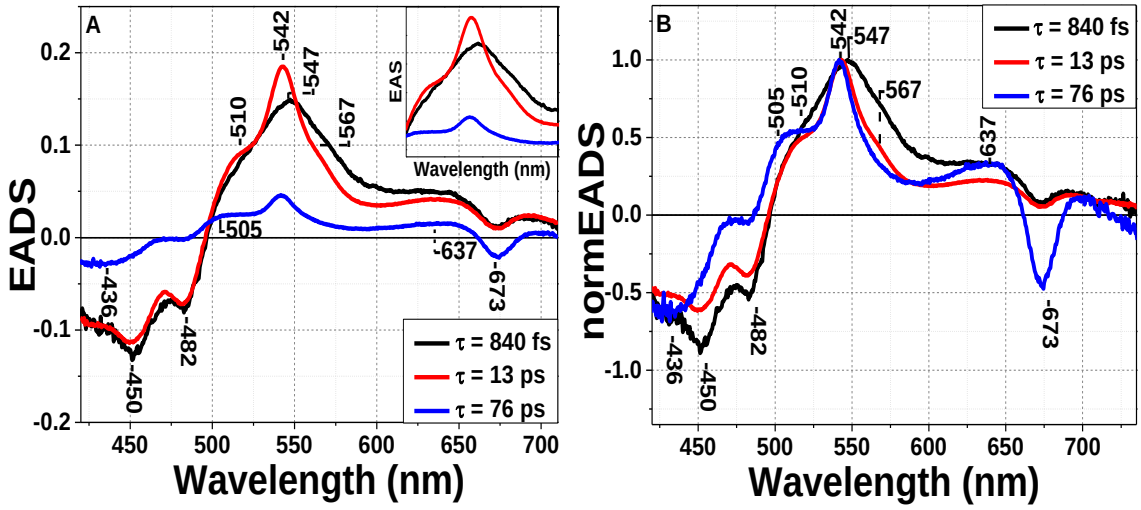

Figure 51: A) EADS spectra and B) Normalized EADS spectra of the Frag. sp. FP HL sample. Inset: Gaussian simulation of the peak at λ = 540-550 nm ($FWHM_{black\ line}$ = 53 nm, $FWHM_{red\ line}$ = 16 nm, $FWHM_{blue\ line}$ = 14 nm).

Frag. sp. FP HL sample contained the following pigments; Fx, Dd, Dt και Chide a. The presence of the Dt does not affect the function of the FPs based on the study of the dynamics of the Frag. sp. FP HL sample. Specifically, the same photophysical processes were observed as those of the Frag. sp. FP LL sample and the lifetimes obtained from the analysis are τ = 840 fs, τ = 13 ps and τ = 76 ps. The transient absorption spectrum of the Frag. sp. FP HL sample is similar to the spectrum of the Frag. sp. FP LL sample. Their difference lies in the presence of a peak at λ = 567 nm in the spectrum of the Frag. sp. FP HL sample. The peak is attributed to an ESA transition of Dt. The Dt peak appears at a longer wavelength than the other two carotenoids (Fx, Dd) due to the additional carbon-carbon double bond in its conjugation and the conformational

distortion of its ring. In the first two EADS spectra of the Frag-HL-Fraction-1 sample (Figure 51), two peaks are observed at λ = 450 nm and λ = 482 nm, which are not observed as strongly in the EADS spectra of the other samples. This differentiation comes from the increased number of carotenoids (Fx, Dd, Dt) that the Frag. sp. FP HL sample presents compared to the other samples. Spectral characteristics of Chl-c are not detected due to its negligible amount in the sample.

6.3.1. Fragilariopsis sp FP Red Light

The use of RL for the growth of the organism Frag. sp. resulted in the FP (Frag. sp FP RL) having as main pigments Fx, Dd and Chlide-a. The Frag. sp FP RL sample has a similar composition to the Frag. sp FP LL sample, so the differential absorption spectra of the Frag. sp FP RL sample (Figure 52) are similar to that of the Frag. sp FP LL sample (Figure 48). The use of a pump pulse with λ = 400 nm caused the excitation of the pigments Fx, Dd and Chlide-a to the S2 state.

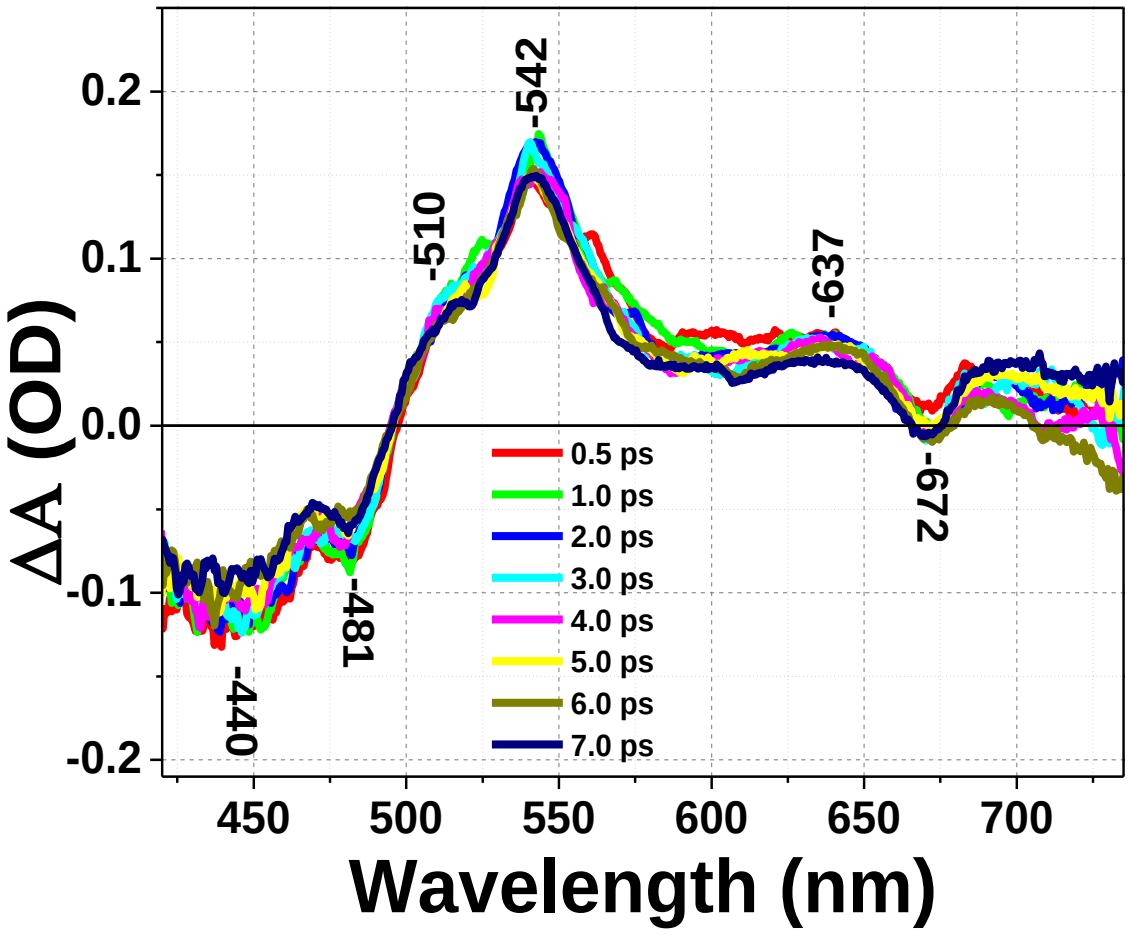

Figure 52: Transient absorption spectra of sample Frag. sp FP RL.

In the spectral range from λ = 420 nm to λ = 490 nm, the GSBs of the carotenoids Fx and Dd are presented, as well as the GSB of Chlide-a. In Chlide-a, the peak at λ = 440 nm is assigned, while in the carotenoids (Fx, Dd) the peak at λ = 481 nm. The broad spectral band from λ = 500 nm to λ = 700 nm is assigned to the ESA transition of Fx. In this spectral range, the peaks at λ = 510 nm and λ = 542 nm are distinguished, which are due to S1→Sn transitions from different vibrational levels of Fx and Dd, and the peak at λ = 637 nm, which is assigned to the ICT→Sn transition. The peak at λ = 673 nm is assigned to GSB/SE from the S1 state of Chlide-a. Spectral characteristics of Chl-c are not detected due to its negligible amount in the sample.

The use of RL in the growth of the organism Frag. sp. did not affect the composition of the FPs of fraction 1, which have Fx, Dd and Chlide-a as the main pigments. The function of the FPs of the Frag. sp FP RL sample is similar to that of the Frag. sp FP LL sample, since the two samples do not differ in terms of their composition.

6.3.2. Phaeodactylum Tricornutum FP Low and Red Light

The samples P. Tricornutum FP LL and RL a similar composition to the corresponding samples isolated from the organism Frag. sp. (FP, LL and RL), so their transient absorption spectra (Figure 53) are similar to those of the organism Frag. sp. (Figure 48 and Figure 52). The pump pulse at λ = 400 nm caused the excitation of the pigments Fx, Dd and Chlide-a to the S2 state.

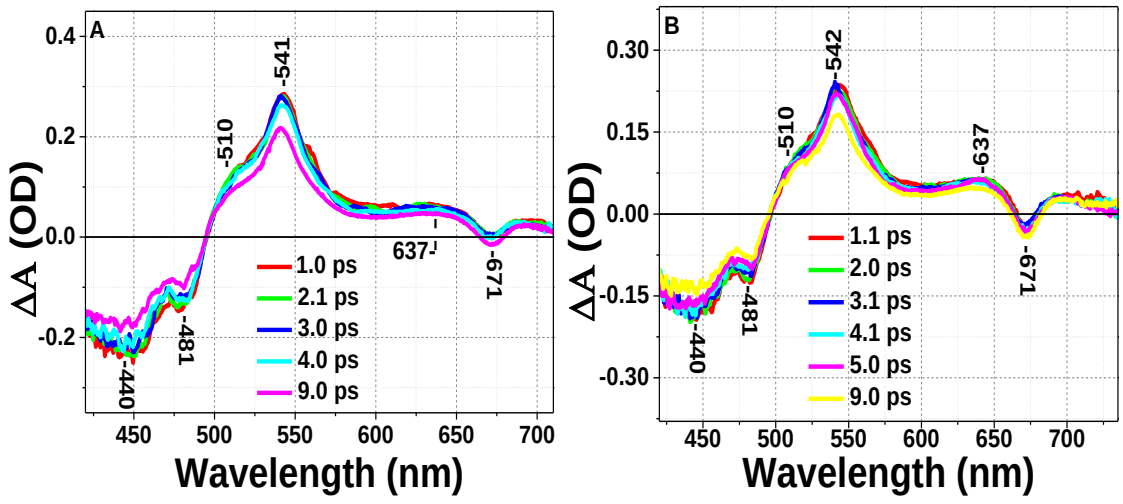

Figure 53: Transient absorption spectra of samples A) P. Tricornutum FP LL and B) P.

Tricornutum FP RL.

In the spectral range from λ = 420 nm to λ = 490 nm, the GSB transitions of Fx, Dd and Chlide-a are presented. The peak at λ = 440 nm is due to Chlide-a, while the peak at λ = 481 nm is due to carotenoids (Fx, Dd). The spectral band from λ = 500 nm to λ = 700 nm is due to an ESA transition of Fx. The peaks at λ = 510 nm and λ = 542 nm are attributed to S1→Sn transitions from different vibrational levels of Fx and Dd and the peak at λ = 637 nm, which is attributed to the ICT→Sn transition of Fx. The peak at λ = 673 nm is attributed to GSB/SE from the S1 state of Chlide-a. Chl-c is not detected spectrally, due to its negligible amount in the sample.

6.4. Discussion

The Diatom Frag. sp possesses different types of FCPs, which are expected to carry out different functions of the organism. In the present work, the FCPs of fraction 3 and the FPs of fraction 1 were isolated and studied. The FCPs of fraction 3 are typical FCPs, as they have Fx, Chl a and Chl c as their main pigments. The study of the dynamics of the FCPs of fraction 3 resulted in two characteristic times, the first, τ = 1.9 ps, is attributed to the vibrationally excited S1 state of Fx and the second time, τ = 61 ps to the S1 state of Fx. The FPs of fraction 1 contain the pigments Fx, Dd and Chlide a. The dynamics of the FPs of fraction 1 differs from the FCPs of fraction 3, as three characteristic times are observed, which are attributed to different photophysical processes. The first lifetime, τ = 714 fs, is attributed to the vibrationally excited levels of the S1 states of Dd and Fx, the second lifetime, τ = 13 ps, is due to the S1 state of Dd, and the third lifetime, τ = 77 ps, is attributed to either the energy transfer from Fx to Chlidea or to the S1 state of Fx.

The differences in the mechanism of action between FCPs and FPs reflect the different functions they perform inside the diatom. In the analysis of the photophysical processes of the FPs of fraction 1, it was reported that the third photophysical process is attributed either to the energy transfer from Fx to Chlide a or to the deexcitation of Fx, which results in the appearance of the characteristic spectrum of Chlide a. Considering the first pathway as the predominant one, it is observed that after being excited by the pump pulse with λ = 400 nm, the FPs of fraction 1 perform energy transfer from Fx to Chlide a, while the FCPs of fraction 3 do not perform the corresponding energy transfer from Fx to Chl a. In the literature, it is known that FCPs, such as fraction 3, carry out energy

transfer processes, however, in these studies the pump pulse was tuned to λ = 500 nm.[15-17] The non-occurred energy transfer in FCPs of fraction 3 is probably due to the fact that the Fxs are fewer than the Chls, so they are not close enough for the phenomenon to occur. Furthermore, it is possible that the protein environment of FCPs of fraction 3 does not contribute to the proximity of the pigments. In contrast, the Fxs are more or equal in quantity to Chlide a in FPs of fraction 1, so it is not excluded that they are in greater proximity, so that the energy transfer phenomenon can occur. Furthermore, it is possible that the protein environment of FPs of fraction 1 favors the interaction of the pigments. Based on the above observations, it is concluded that FPs of fraction 1 may participate in the protection of the diatom, as they possess large amounts of Dd and manage the high-energy radiation of the pump pulse (λ = 400nm) by performing energy transfer processes. FCPs of fraction 3 probably carry out the processes of photosynthesis, since they perform energy transfer processes when excited by pump pulses tuned to longer wavelengths. Assuming that the third photophysical process of FPs of fraction 1 is the deexcitation of Fx, the increase in the intensity of the peak at λ = 673 nm, due to GSB/SE of Chlide-a, comes from the decrease in the intensity of the spectral band, due to the ESA transition of Fx. The intensity of the peak at λ = 673 nm is not observed to change in the transient absorption spectra of FCPs of fraction 3. This difference in the transient absorption spectra is due to the high amount of Fxs compared to Chls, which are present in FPs of fraction 1 and results in the superposition of the signals leading to a positive absorption of the peak at λ = 673 nm. The intensity of the peak at λ = 673 nm takes on negative values as the contribution of Fxs decreases. FCPs of fraction 3 have more Chls compared to Fx, so the peak at λ = 673 nm has a negative absorption, which does not change in the time window of the measurement. Based on these observations, the conclusion is drawn that the pigments of FPs of fraction 1 and fraction 3 are deexcited without interacting with each other, when excited with a pump pulse of wavelength 400 nm. Therefore, the functions of the two different types of FCPs within the diatom Frag. sp. are not clarified.

In this study, the influence of diatom growth conditions on the function of FCPs was examined. Specifically, high-intensity white light was used for the growth of the diatom Fragi sp. and the mechanism of function of FPs of fraction 1 and FCPs of fraction 3 was studied. Through the HPLC method, it was shown that the composition of FPs of fraction 1 had changed, as it additionally contained the pigment Dt, while FCPs of

fraction 3 also contained Chlide-a and Dd. The changes in the composition of FPs or FCPs reflect the activation of the diatom protection mechanism, which is activated when exposed to high-intensity radiation. The study of the photophysical processes of samples Frag. sp. FP HL and Frag. sp. FCP HL revealed that the changes in the composition, induced by high-intensity radiation, do not affect their functions. In the transient absorption spectra of the Frag. sp. FP HL sample, the characteristic peak of Dt was detected at $\lambda = 567$ nm, while in the spectra of the Frag. sp. FCP HL sample, a change in the ratio of the intensities of the peaks at $\lambda = 542$ nm and $\lambda = 510$ nm and the peak at $\lambda = 505$ nm, attributed to Dd and Chlide-a, respectively, was recorded. The use of RL for the growth of Frag. sp. did not cause a change in the composition of the FPs of fraction 1, but it altered the composition of the FCPs of fraction 3. Specifically, the FCPs of fraction 3 contained additional Chlide a. The mechanism of action of the FCPs of fraction 3, isolated from the diatom, which had been grown under RL conditions, was not affected by the presence of Chlide a. In the transient absorption spectrum of the Frag. sp. FCP RL sample, the peak at $\lambda = 505$ nm is recorded, which is attributed to the ESA transition of Chlide a.

References

1. Büchel C. How diatoms harvest light. Science. 2019;365(6452):447–448.

2. Büchel, C. Advances in Photosynthesis and Respiration (Including Bioenergy and Related Processes), 2020;45, 441-457 Springer, Cham.

3. Büchel, C. Light harvesting complexes in chlorophyll c-containing algae Biochimica et Biophysica Acta – Bioenergetics. 2020;1861(4), 148027.

4. Pi X, Zhao S, Wang W, Liu D, Xu C, Han G, Kuang et al. The pigment-protein network of a diatom photosystem II-light-harvesting antenna supercomplex. Science. 2019;365, 6452.

5. Wang W, Yu LJ, Xu C, Tomizaki T, Zhao S, Umena Y et al. Structural basis for blue-green light harvesting and energy dissipation in diatoms. Science. 2019;363, 6427.

6. Feng Y, Li Z, Li X, Shen L, Liu X, Zhou C et al. Structure of a diatom photosystem II supercomplex containing a member of Lhcx family and dimeric FCPII. Sci Adv. 2023;9, 1-13.

7. Rulliere C. Femtosecond Laser Pulses. 2nd ed. New York: Springer; 2005.

8. R.R. Guillard, in Culture of Marine Invertebrate Animals, ed. W. L. Smith, M. H. Chanley, Springer, Boston MA, 1975, Culture of Phytoplankton for Feeding Marine Invertebrates, p. 29–60.

9. Beer A, Gundermann K, Beckmann J, Büchel C. Subunit Composition and Pigmentation of Fucoxanthin−Chlorophyll Proteins in Diatoms: Evidence for a Subunit Involved in Diadinoxanthin and Diatoxanthin Binding. Biochemistry. 2006;45(43):13046-13053.

10. Kraay GW, Zapata M, Marcel J.W. Veldhuis. SEPARATION OF CHLOROPHYLLS c1c2, AND c3 OF MARINE PHYTOPLANKTON BY REVERSED-PHASE-C18-HIGH-PERFORMANCE LIQUID CHROMATOGRAPHY1. J Phycol. 1992;28(5):708–12.

11. Nikoloudakis E, Pigiaki M, Polychronaki MN, Margaritopoulou A, Charalambidis G, Serpetzoglou E. et al. Self-Assembly of Porphyrin Dipeptide Conjugates toward Hydrogen Production. ACS Sustainable Chemistry & Engineering,2021;9(23): 7781-7791.

12. Büchel C. Fucoxanthin-Chlorophyll Proteins in Diatoms: 18 and 19 kDa Subunits Assemble into Different Oligomeric States. Biochemistry. 2003;42(44):13027–34.

13. Gundermann K, Wagner V, Mittag M, Büchel C. Fucoxanthin-Chlorophyll Protein Complexes of the Centric Diatom Cyclotella Meneghiniana Differ in Lhcx1 and Lhcx6_1 Content. Plant Physiology. 2019;179(4):1779–95.

14. Kansy M, Volke D, Sturm L, Wilhelm C, Hoffmann R, Goss R. Pre-purification of diatom pigment protein complexes provides insight into the heterogeneity of FCP complexes. BMC Plant Biology. 2020;20(1)456.

15. Gelzinis A, Butkus V, Songaila E, Augulis R, Gall A, Büchel C et al. Mapping energy transfer channels in fucoxanthin–chlorophyll protein complex. Biochimica et Biophysica Acta (BBA) - Bioenergetics. 2015;1847(2):241-247.

16. Gelzinis A, Augulis R, Büchel C, Robert B, Valkunas L. Confronting FCP structure with ultrafast spectroscopy data: evidence for structural variations. Physical Chemistry Chemical Physics. 2021;23(2):806-821.

17. Agostini A, Büchel C, Di Valentin M, Carbonera D. A distinctive pathway for triplet-triplet energy transfer photoprotection in fucoxanthin chlorophyll-binding proteins from Cyclotella meneghiniana. Biochimica et Biophysica Acta (BBA) - Bioenergetics. 2021;1862(1):148310.

7. Resonance Raman spectroscopy of ^{13}C isotope-enriched Fucoxanthin-Chlorophyll a/c-binding proteins (FCPs) in intact membranes of the Marine Diatom Fragilariopsis sp

Resonance Raman spectroscopy combined with FTIR were employed to investigate the ^{13}C- enriched light-harvesting FCPs in intact thylakoid membranes of the Marine Diatom Frag. sp at physiological room temperature conditions. Two fractions from the solubilized thylakoid membranes were investigated. The first fraction (free pigments) contains photolabile Chl a/c and stable Fx/Dd pigments from degraded FCPs in the thylakoid membranes and the second, stable FCPs. All the ^{13}C-sensitive Raman and amide I/II FTIR have been identified. The ^{13}C shifts of the marker bands of chls a/c and of the carotenoids Fx/Dd provide the first spectroscopic evidence for the characterization of all pigments present in the FCPs which are crucial for light harvesting and energy transfer in the blue region. The dynamics of the pigments in the two fractions are compared and discussed in terms of their configuration and photosensitivity/photostability in the thylakoid membranes.

7.1. Introduction

Marine Diatoms are photosynthetic algae that contribute to global primary productivity. The primary step in photosynthesis involves the absorption of light by proteins which are embedded in the photosynthetic membranes which are composed by the supercomplexes PSI/PSII-specific FCPs.[1-3] The pigments in the FCPs play a crucial role for the light harvesting because more blue-green photons are available under water.[4-5] The specific pigment-pigment interactions in the protein environment account for the spectral and excitation energy transfer to Chl a.[6-9] Chl c does not contain the phytol chain seen in Chl a but instead has a conjugated propionic acid in its protoporphyrin ring.[10-12] The Dd cycle found in the FCP antennae, operate in quenching the excess energy under strong light conditions. The enzymes involved in the deepoxidation/epoxidation are sensitive to pH changes in the lumen providing a high ability for NPQ. The crystal structure of an FCP from the marine P. tricornutum revealed the binding of seven Chls a, two Chls c, seven Fxs and one Dd. Efficient energy pathways between Chl a and c were identified and each Fx is surrounded by Chls allowing the energy transfer and quenching via Fx.[5-6]

Resonance Raman spectroscopy has been applied to characterize the structure of heme and chlorophylls a/c containing proteins.[13-18] Recently, based on the ^{15}N-enriched FCPs the marker bands of the chls a/c including the pyrrole breathing C_a-N modes were identified and two conformations of Chl c and Chl a were observed. The Raman bands that shifted largely upon the ^{15}N-substitution were related to the C_a-N stretching, where those that do not, were related to the carbon-oxygen and carbon-carbon and/or the carbon-hydrogen. In addition, two keto carbonyls were observed at 1679 (strong H-bonded) and at 1691 cm^{-1} (weak H-bonded) in both the 405 and 441 Raman spectra.[19] The Fluorescence excitation spectra of the FCP at pH 8 observed from spontaneous emission of Chl c at 640 nm showed the presence of three Soret bands at 418, 449 and 455 nm. A reversible pH-dependent 447 to 454 nm Soret transition of Chls c was observed, that is attributed in agreement with previous work on C. Calcitrans, to the deprotonation/protonation of the 17-acrylate moiety.[11] The observation of three Soret absorption bands of Chl c in the protein environment of Fragilariopsis sp at 418, 447 and 454 nm gives a new insight into the photosynthetic properties of the bound Chl c to FCPs and in conjunction with the identification of three red provide a framework for all the pigments organization in the FCP complex.

The C-sensitive assignment of the marker bands of Chl a/c as well those originate from carotenoids and the amide I/II is important in understanding the molecular basis of their function since Chl a/c and both Fx and Dd display a wide range of frequencies depending on the protein properties. In order to fully utilize the potential of resonance Raman scattering, it is essential to assign the normal modes of the Chl a/c in the FCPs. Vibrational assignments of Chl a/c based on isotopically enriched ^{13}C-FCPs are not available, yet. Resonance Raman of ^{13}C-enriched Chl a/c and Fx/Dd under 406 nm excitation are needed to establish a set of vibrational assignments of Chl a/c and Fx/Dd in the FCPs that will clarify their separate contributions in this energetic blue region.

In the work presented here, we have employed 406 nm Raman excitation to probe the Fx-Chl a/c pigment content in the FCPs from two different fraction of solubilized thylakoid membranes containing FCPs of the Marine Diatom Frag. sp at physiological room temperature conditions. The changes in ^{13}C containing Chl a/c bands and Fx/Dd provide the first spectroscopic evidence for the characterization of all pigments in the FCPs which are crucial for light harvesting and energy transfer in the blue region. The

406 nm Raman spectrum originates from π-π* transitions related to Chl a/c and from the 0-1 of blue Fxs. Upon the ^{13}C-substitution, the C-C stretching vibrations of Chl a/c shift largely whereas the C-N stretching vibrations shift less. The stable FCP fraction is characterized by isotope ^{13}C sensitive amide I/II at 1654/1548 cm^{-1} with specific frequencies for each type of protein characteristic of a-helix, b-sheet and loop.

7.2. Materials and methods

7.2.1. Culture Growth

The culture of Frag. sp (CCAP 1029/24) was obtained from CCAP (Culture Collection of Algae and Protozoa). Liquid cultures (200 mL) were grown in f/2-Si medium, at 19 °C in a dark-light cycle (12h:12h) under white LED light.[20] The light intensity used for the growth of the cells culture was 150 μmol photons m^{-2} s^{-1}. Cultures were supplemented with 4% v/v of 1 mM sodium bicarbonate ($NaH^{13}CO_3$) or sodium bicarbonate ($NaHCO_3$) (99% enrichment, Sigma-Aldrich), both buffered with 20 mM Tris-NaOH, pH 8.0. Subsequently, the vials containing the cultures were sealed and all the air was removed under the vacuum line. The carbon supplemented cultures were grown anaerobically. Control cultures with no addition of carbon source were grown aerobically. Cultures were grown for a total of 14 days.

7.2.2. FCP Isolation

Cells from Frag. sp. were harvested by centrifugation (8000 rpm, 30 min, 4 °C) and the supernatant medium was removed. The cells were resuspended in 20 mM Tris and sonicated in an ice bath for 20 minutes. Thylakoid membranes were then solubilized with the addition of β -1,4-dodecyl maltoside (β-DDM, 30 mg, 4 mM) in the resuspended cells while they were shaken for 20 minutes on ice.[21] Separation of solubilized FCPs was carried out on an ion exchange column (HiPrep Q HP 16/10, 20 mL) in 25 mM Tris, 2 mM KCl and 0.4 mM β-DDM at pH 7.4 using a Shimadzu LC 20AD with an SPD-20A detector with two-wavelength detection. The samples were loaded in a column, and fractions were eluted using a gradient from 0 to 750 mM KCl in a buffer made of 25 mM Tris, 750 mM KCl and 0.4 mM β-DDM, pH 7.4 at a flow rate of 3 mL/min. Fractions were pooled and concentrated using Amicon filtration devices with a cutoff of 10 kDa and characterized spectroscopically. The rest of the fractions were stored at -80 °C until further use.

7.2.3. FTIR

Absorption spectra were recorded by a Cary 60 UV–Vis spectrometer (Agilent Technologies, USA). FTIR spectra were recorded with 4 cm-1 spectral resolution on a Bruker Vertex 80V spectrometer equipped with a photovoltaic MCT detector (Kolmar Technologies KV100-1B-7/190). A vacuum pump was used to evacuate the interferometer compartment to a final pressure of 3.2 mbar and the scan were taken under nitrogen environment. The FTIR spectrometer was placed on a Newport VH optical vibration isolation table to ensure that vibrational background noise from environmental sources was avoided. Approximately 5 μL of sample was deposited on the crystal and allowed to dry for ~10 min until a film layer was formed prior to the measurement. A background spectrum against air was recorded before each sample spectrum. The background and sample spectra were acquired at 4 cm^{-1} resolution with 32 scans from 4000 to 400 cm^{-1}.

7.2.4. Raman Spectroscopy

Raman spectra were acquired at room temperature using a 640mm focal length Czerny-Turner spectrograph (Horiba, T64000 system operated in single stage), equipped with 1800 g/mm holographic grating and a Horiba Symphony II BIDD1024x256 CCD detector. Samples were placed in a quartz spinning tube to minimize local heating, and scattering was collected in a 90o geometry. The slit width was set to 100 μm. An Ondax SureLock LM-405 laser with an integrated CleanLine ASE filter was used to provide the excitation wavelength at 405 nm, and a Semrock StopLine 405 nm single-notch filter was used to reject Rayleigh scattering. The power incident on the sample was 4 mW and total accumulation time for each spectrum was 10 min. The Raman shifts were calibrated using toluene. Origin software was used for spectra processing and analysis.

7.3. Results and Discussion

Figure 54 shows the absorption of the FP and FCP in the intact thylakoid membrane grown with bicarbonate. For the FCP (blue line), the transitions at 440 (Soret), 588, 621 (Q_x) and 673 (Q_y) nm are attributed to Chl a and at 457 (Soret), 588 (Q_x) and 637(Q_y) nm to Chl c. The broad transition in the 500-560 nm range has been attributed to red Fxs, whereas blue Fx absorb in the 420-470 nm region. In addition, no peak at 485 nm due to Dd is present and the 338 nm peak is due to the cis-Fx. Finally, the 270 nm UV

transition is attributed to a higher lying state of Bu+ symmetry that is typical of all carotenoids. The red line shows the absorption spectrum of a FP characterized by absorption maxima at around 440 and 450 nm, accompanied by a shoulder at 460 nm. The maximum at 440 and the shoulder at 460 nm corresponded to the blue absorption maxima of Chl a and Chl c, respectively, and the pronounced maximum at 485 nm is related to a strong carotenoid absorption in this wavelength region. It corresponded to the third absorption maximum of the absorption spectrum of carotenoid molecules, which typically shows three defined absorption bands in the blue to blue-green part of the spectrum. The first and second absorption bands of the carotenoid absorption spectrum were not visible as defined maxima since they were concealed by the Chl a and Chl c absorption bands. The high absorption in the blue to blue-green part of the spectrum, together with the pronounced carotenoid peak at around 485 nm, demonstrated that Fraction 1 FP was enriched in carotenoids. Since the main carotenoid of diatoms, i.e. fucoxanthin (Fx), is characterized by a rather broad, undefined absorption spectrum, the clear maximum at 485 nm indicates a strong contribution of the xanthophyll cycle pigment (diadinoxanthin) Dd to the absorption of Fraction 1.

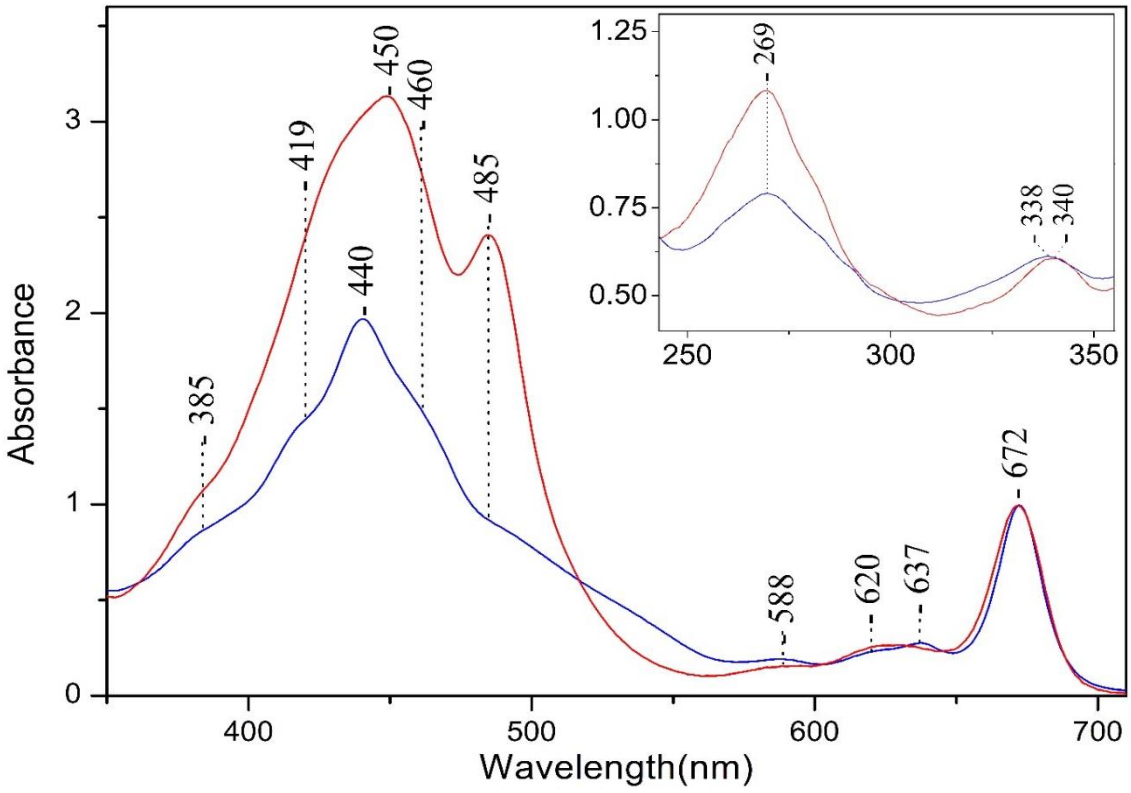

Figure 54: UV absorption spectrum of Fraction 1 FP (red line) and Fraction 3 FCP (blue line).

Figure 55 shows the FTIR spectra of the air-dried and ^{13}C-enriched FCPs. In proteins, the frequency of the amide I band depends on the peptide backbone conformation. The amide I (C=O stretching at about 1654 cm^{-1}) and amide II, (NH bending at 1540cm^{-1}) bands are easily identified. The shoulder at 1515 cm^{-1} on the amide II band is probably due to tyrosine residues. The stable FCP fraction is characterized by the amide I/II at 1654/1548 cm^{-1} with specific frequencies for each type of protein secondary structure with characteristic of a-helix, b-sheet (1631 cm^{-1}) and loop (1598 cm^{-1}). In addition to the amide I and II bands, there are spectral features of the side chain, such as 1515 cm^{-1} from tyrosine. Side chain peaks are critical for the elucidation of protonation and de-protonation states of various amino acids.

Both the amide I band centered at 1654 cm^{-1} together with amide II centered on 1540 cm^{-1} are characteristic features of the α-helix. The weaker amide I band centered at 1631 together with amide II at 1520 cm^{-1} structures are the exact features expected for disordered part of protein structure. The same comment stands for the β-sheet structure with, for amide I, a maximum at 1631 cm^{-1} and a marked shoulder around 1690 cm^{-1} together with amide II at 1533 cm^{-1}.[22] These spectral features are typical of β-sheet structures.[23,24]

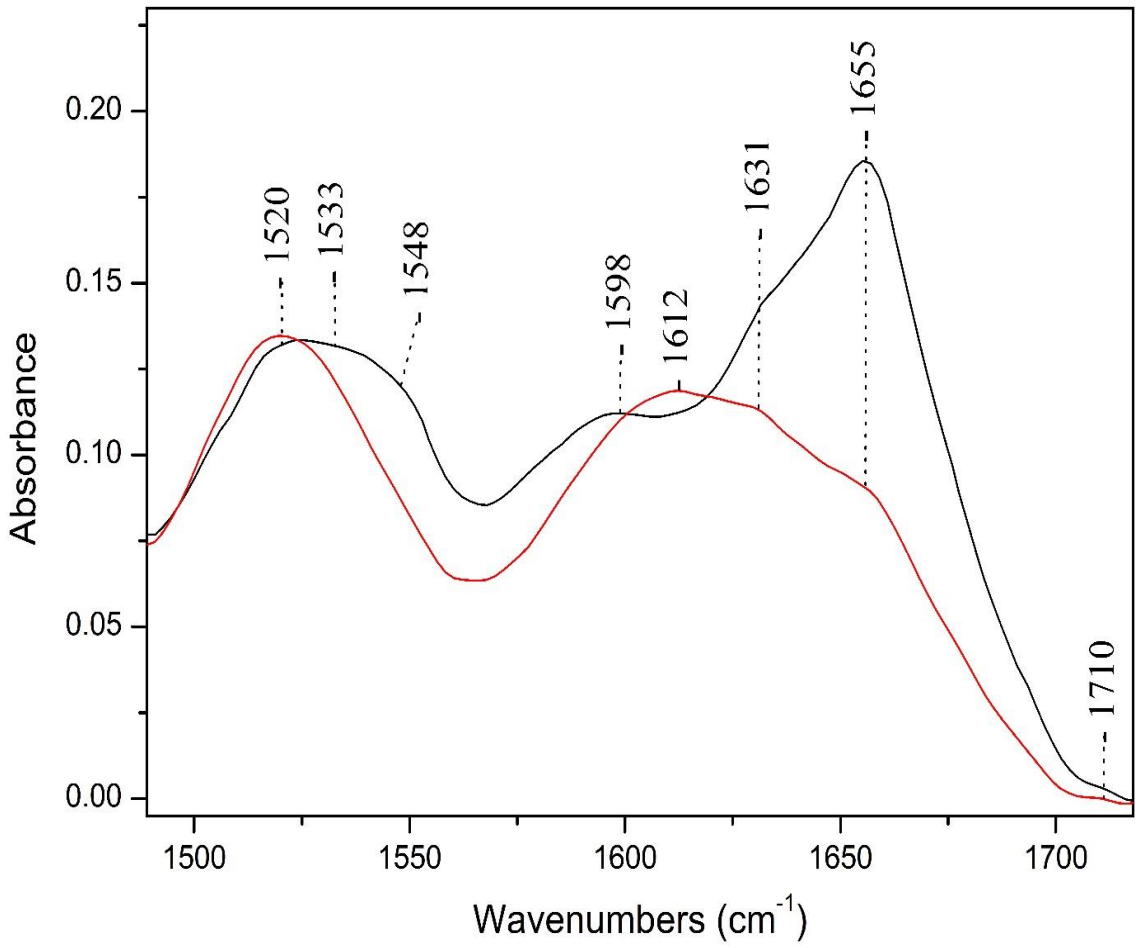

Figure 55: FTIR spectrum of Fragilariopsis sp fraction 3 low light cultured anaerobically with $NaH^{13}CO_3$ supplement (red line) and control cultured anaerobically with $NaH^{12}CO_3$ supplements (black line), respectively.

Figure 56 and Figure 57 shows the 406 nm excitation spectra of the ^{13}C-enriched FCPs at room temperature. Rings I and II are aligned along the y-axis and modes associated with these rings should be enhanced using lines such as 405 nm excitation. Rings II and IV are aligned along the x-axis and modes associated with these rings should be enhanced using lines such as 441 and/or 458 nm close to the Bx axis. Excitation within the B_y absorption band using the 406.7 nm line produces a spectrum dominated by totally symmetric Franck-Condon-active modes aligned along the y-axis of the macrocycle. The assignment of the Chl a vibrational modes is still controversial whereas that of Chl c_2 is still limited.

Figure 56 illustrates the high-frequency 405 nm excitation resonance Raman spectra of control (trace a) and 13C FP (Fraction 1) (trace b) from Frag. sp. at pH 8, 25 °C. The ν1 which appears at approximately 1520 cm^{-1} and is attributed to stretching vibrations of

the C=C double bonds of carotenoids is isotopic shifted from 1529 to 1515 cm^{-1}. The ν2 appears at approximately 1160cm^{-1} and is due to the stretching vibrations of the carotenoids C-C single bonds. The 13C-enriched FP is shifted from 1159 to 1152, from 1192 to 1190 and from 1211 to 1205 cm^{-1}, respectively. The ν3 is due to the in-plane stretching vibrations of the methyl groups attached to the polymer chain in combination with the in-plane C-H bending vibrations and appears at approximately 1005 cm^{-1}. The 13C-enriched FP is shifted from 1013 to 1007 cm^{-1}. Regarding the vibrations originating from chlorophyll molecules, the region between 900-1600 cm^{-1} where vibrations are sensitive to the geometric configuration of the molecules appear, such as the C-N vibrations. This region revealed ^{13}C isotope bands at 1270(-3), 1289(-8), 1314(-3), 1354(-2), 1390(-2) and 1446(-2) cm^{-1}.

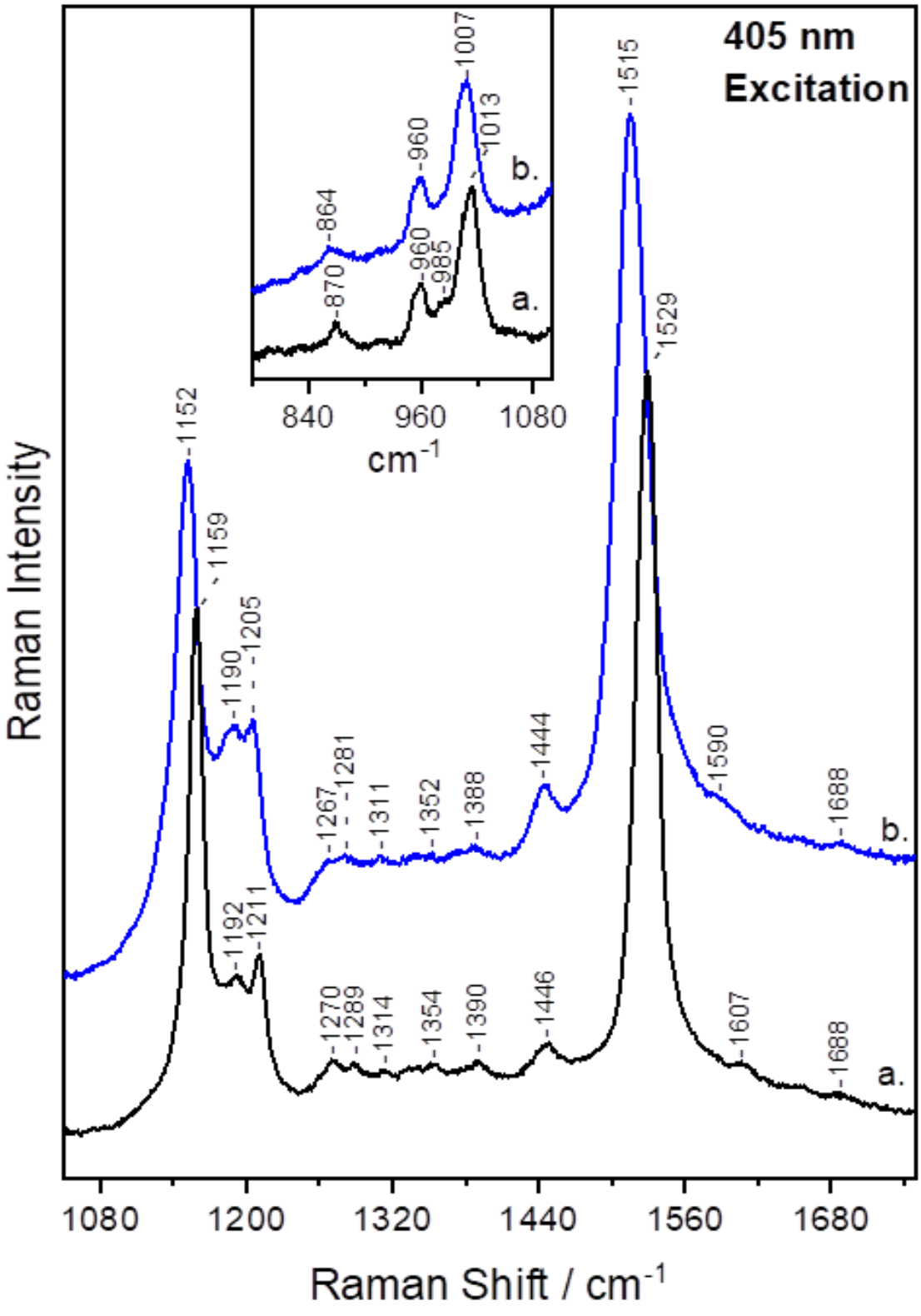

Figure 56: High-frequency 405 nm excitation resonance Raman spectra of control (trace a) and ^{13}C (trace b) FP (Fraction 1) from Frag. sp. The 405 nm excitation laser beam was provided by a Ondax SureLock with an integrated CleanLine ASE filter, and the laser power incident on the sample was 4 mW. The total accumulation time foreach measurement was 10 min.

Figure 57 illustrates the high-frequency 405 nm excitation resonance Raman spectra of control (trace a) and 13C FCP (Fraction 3) (trace b) from Frag. sp. at pH 8, 25 °C. The ν1 is isotopic shifted from 1531 to 1518 cm^{-1}. In ν2, the 13C-enriched FCP is shifted from 1160 to 1153 and from 1182 to 1179 cm^{-1}, respectively. In ν3, the 13C-enriched FCP is shifted from 1017 to 1014 cm^{-1}. The vibrations originating from chlorophyll molecules, revealed ^{13}C isotope bands at 1270(-4), 1289(-8), 1343(-7), 1354(-2), 1375(-3), 1390(-3) and 1449(-5) cm^{-1}.

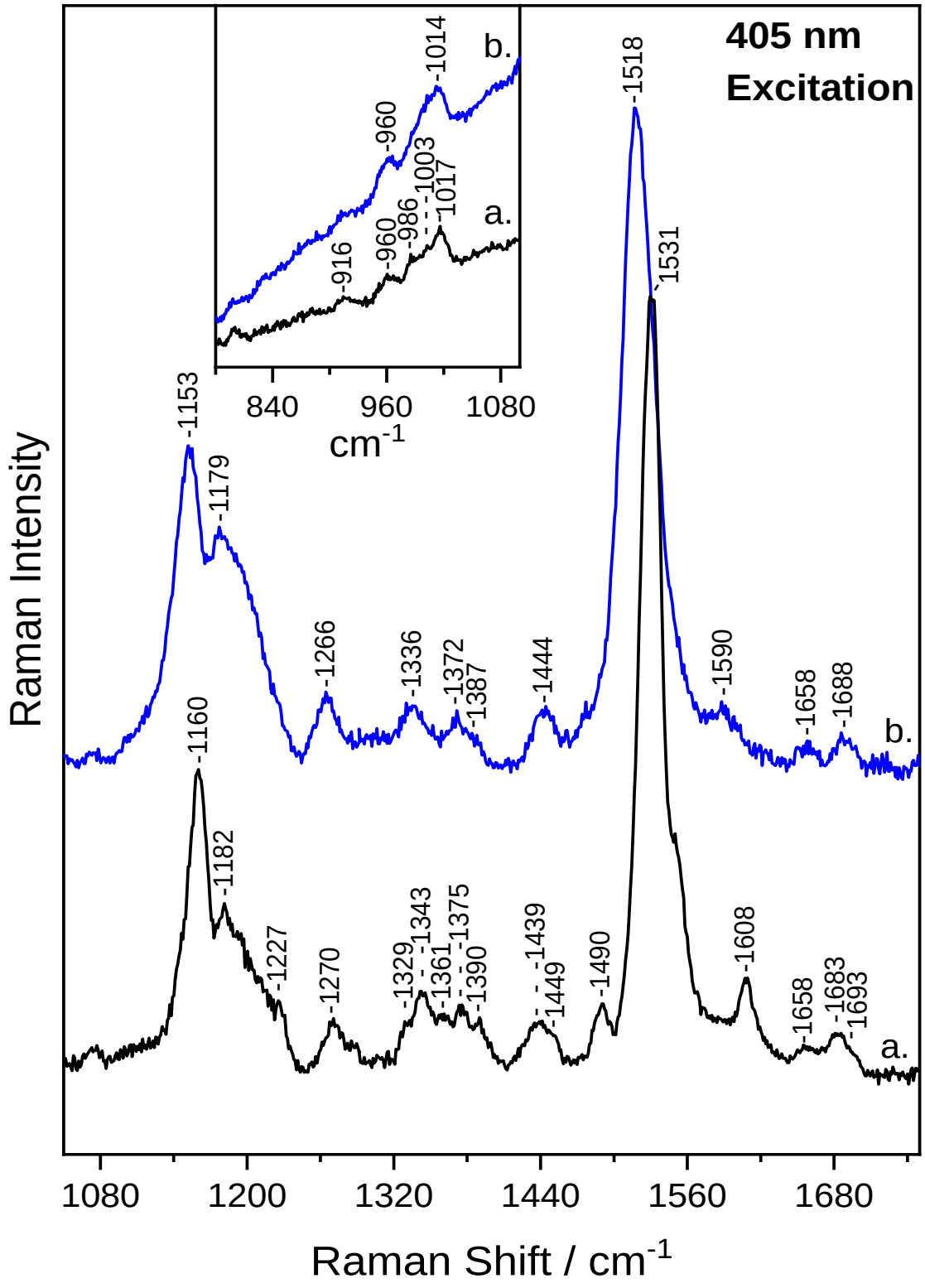

Figure 57: High-frequency 405 nm excitation resonance Raman spectra of control (trace a) and ^{13}C (trace b) FCP (Fraction 3) from Frag. sp. The 405 nm excitation laser beam was provided by a Ondax SureLock with an integrated CleanLine ASE filter, and the laser power incident on the sample was 4 mW. The total accumulation time foreach measurement was 10 min.

References

1. Büchel C. How diatoms harvest light. Science. 2019;365(6452):447-448.

2. Büchel, C. Advances in Photosynthesis and Respiration (Including Bioenergy and Related Processes), 2020;45, 441-457 Springer, Cham.

3. Büchel, C. Light harvesting complexes in chlorophyll c-containing algae Biochimica et Biophysica Acta – Bioenergetics. 2020;1861(4), 148027.

4. Pi X, Zhao S, Wang W, Liu D, Xu C, Han G, Kuang et al. The pigment-protein network of a diatom photosystem II-light-harvesting antenna supercomplex. Science. 2019;365, 6452.

5. Wang W, Yu LJ, Xu C, Tomizaki T, Zhao S, Umena Y et al. Structural basis for blue-green light harvesting and energy dissipation in diatoms. Science. 2019;363, 6427.

6. Nagao R, Ueno Y, Yokono M, Shen JR, Akimoto S. Alterations of pigment composition and their interactions in response to different light conditions in the diatom Chaetoceros gracilis probed by time-resolved fluorescence spectroscopy. Biochimica et Biophysica Acta – Bioenergetics. 2018;1859(7), 524–530.

7. Oka K, Ueno Y, Yokono M, Shen JR, Nagao R, Akimoto S. Adaptation of light-harvesting and energy-transfer processes of a diatom Phaeodactylum tricornutum to different light qualities. Photosynth. Res. 2020;146, 227– 234.

8. Chrysafoudi A, Maity S, Kleinekathöfer U, Daskalakis V. Robust Strategy for Photoprotection in the Light-Harvesting Antenna of Diatoms: A Molecular Dynamics Study. The Journal of Physical Chemistry Letters. 2021;12 (39), 9626-9633.

9. Ikeda Y, Yamagishi A, Komura M, Suzuki T, Dohmae N, Shibata Y et al. Two types of fucoxanthin-chlorophyll-binding proteins are tightly bound to the photosystem core complex in marine centric diatoms. Biochimica et Biophysica Acta – Bioenergetics. 2013;1827, 529–539.

10. Nagao R, Yokono M, Ueno Y, Shen JR, Akimoto S. High excitation energy quenching in Fucoxanthin chlorophyll a/c binding protein complexes from the diatom Chaetoceros gracilis. J. Phys. Chem. B. 2019;124, 4919-4923.

11. Yamano N, Mizoguchi T, Fujii R. The pH-dependent photophysical properties of chlorophyll-c bound to the light-harvesting complex from a diatom, Chaetoceros calcitrans. Journal of Photochemistry and Photobiology A: Chemistry. 2018;358, 379–385.

12. Tsujimura M, Sugano M, Ishikita H, Saito K. Mechanism of Absorption Wavelength Shift Depending on the Protonation State of the Acrylate Group in Chlorophyll c. J. Phys. Chem. B. 2023;127, 505-513.

13. Zhou C, Diers JR, Bocian DF. Qy-Excitation Resonance Raman Spectra of Chlorophyll a and Related Complexes. Normal Mode Characteristics of the Low-Frequency Vibrations. J. Phys. Chem. B. 1997;101, 9635-9644.

14. Czarnecki K, Diers JR, Chynwat V, Erickson JP, Frank HA, Bocian DF. Comprehensive resonance Raman study of photosynthetic reaction centers from Rhodobacter sphaeroides. Implications for pigment structure and pigment-protein interactions. J.Am. Chem.Soc. 1997;119, 415-426.

15. Premvardhan L, Robert B, Beer A, Büchel C. Pigment organization in fucoxanthin chlorophyll a/c2 proteins (FCP) based on resonance Raman spectroscopy and sequence analysis. Biochimica et Biophysica Acta – Bioenergetics. 2010;1797(9), 1647–1656.

16. Premvardhan L, Bordes L, Beer A, Büchel C, Robert B. Carotenoid structures and environments in trimeric and oligomeric fucoxanthin chlorophyll a/c2 proteins from resonance Raman spectroscopy. Journal of Physical Chemistry B. 2009;113(37), 12565–12574.

17. Lutz M. Antenna Chlorophyll in photosynthetic membranes. A study by resonance Raman spectroscopy. Biochimica et Biophysica Acta;1977, 469, 408-430.

18. Sashima T, Abe M, Kurano N, Miyachi S, Koyama Y. Changes in the Carbon−Carbon and Carbon−Nitrogen Bond Orders in the Macrocycle of Chlorophyll a upon Singlet and Triplet Excitation as Probed by Resonance Raman Spectroscopy of Natural-Abundance and Singly and Doubly Labeled Species with 15N, 13C, and 2H Isotopes. J. Phys. Chem. B. 1998;102, 6903-6914.

19. Andreou C, Tselios C, Ioannou A, Varotsis, C. Probing the Fucoxanthin-Chlorophyll a/c-Binding proteins (FCPs) of the Marine diatom Fragilariopsis sp. by Resonance Raman spectroscopy. J. Phys. Chem. B. 2023;127, 9014-9020.

20. R.R. Guillard, in Culture of Marine Invertebrate Animals, ed. W. L. Smith, M. H. Chanley, Springer, Boston MA, 1975, Culture of Phytoplankton for Feeding Marine Invertebrates, p. 29–60.

21. Beer A, Gundermann K, Beckmann J, Büchel C. Subunit Composition and Pigmentation of Fucoxanthin−Chlorophyll Proteins in Diatoms: Evidence for a Subunit Involved in Diadinoxanthin and Diatoxanthin Binding. Biochemistry. 2006;45(43):13046-13053.

22. Arrondo JLR, Muga A, Castresana J, Goñi FM. Quantitative studies of the structure of proteins in solution by fourier-transform infrared spectroscopy. Progress in Biophysics and Molecular Biology. 1993;59(1):23–56.

23. Goormaghtigh E, Véronique Cabiaux, Jean Marie Ruysschaert. Determination of Soluble and Membrane Protein Structure by Fourier Transform Infrared Spectroscopy. Subcell Biochem. 1994;23:329–62.

24. Barth A. Infrared spectroscopy of proteins. Biochimica et Biophysica Acta (BBA) - Bioenergetics. 2007;1767(9):1073–101.

8. Conclusions and Future Work

8.1. Conclusions

From the experimental results presented in the previous chapters, some important conclusions emerge regarding the study of the response of the diatoms under different growth conditions. The main conclusions that emerged from each chapter are the following:

8.1.1. Probing the Fucoxanthin-Chlorophyll a/c-Binding Proteins (FCPs) of the Marine Diatom Fragilariopsis sp. by Resonance Raman Spectroscopy

By reporting resonance Raman spectra of the ^{15}N-isotope-enriched FCPs of Frag. sp we provide the first spectroscopic evidence for the characterization of the C_a-N marker bands and, thus, of the penta- and hexacoordinated states of chlorophylls a/c in the FCPs. The structures of the Chl a/c molecules in the lowest excited singlet and triplet states play key roles in the primary processes of photosynthesis. The studies reported herein for Chl a/c in the FCP provide insight in the key structural element that distinguishes Chl a from Chl c. Comparison of the FCP of Frag. sp to those from other marine diatoms with known crystal structures may provide the means to identify conserved structural features which can be assumed to be involved in basic functions to different classes of FCPs. In contrast, dissimilarities between these FCPs are likely to be involved in the fine-tuning to specific needs demanded by differences in the local protein environment of the FCPs. Furthermore, with the identification of the major coordination marker bands of Chl a/c the changes in the electronic and molecular structure of the macrocycles upon singlet and triplet excitation can also be obtained with more certainty.

8.1.2. Light harvesting and Photoprotective states in the marine diatom Fragilariopsis sp: Functional implications of Chlorophylls c1/c2 in the Fucoxanthin-Chlorophyll a/c-binding proteins (FCPs)

By illustrating the pH/pD-dependent Fluorescence-excitation spectra of the FCPs of the Frag. sp we showed a reversible 451 to 455 nm Soret transition accompanied by a 588 to 586 nm Qx transition of chls c1/c2 in the pH/pD 4.9-8 range. Similar phenomenon

was reproduced under HL growth compared to LL growth of Frag. sp, concluding that the acrylate moiety of chls c1/c2 becomes protonated, under acidic or HL conditions by a similar mechanism. We suggest that Chl c_2 and more specifically the 17-acrylate moiety has a role in the photoprotection in diatoms, which switches the FCP function between light harvesting and energy-dissipation modes depending on the light intensity. We propose that H_2O molecules are involved in controlling the extend of the photoprotection mode which is characterized as the open protonated form with a larger distance between R31 and 17-acrylate $Chlc_2$ 403 as compared to the deprotonated closed form.

8.1.3. Ultrafast Dynamics of Frag. sp and P. Tricornutum FCPs by Transient Absorption Spectroscopy

Herein, a complete time-dynamic study of two different fractions, isolated from the diatoms Frag. sp and P. Tricornutum, was carried out and information was obtained regarding the role of these pigments and proteins in the function of the diatom. Furthermore, the effect of growth light conditions on the composition of the FCPs and their function was investigated. The differences in the mechanism of action between FCPs and FPs reflect the different functions they perform inside the diatom. In the analysis of the photophysical processes of the FPs, it was reported that the third photophysical process is attributed either to the energy transfer from Fx to Chlide a or to the deexcitation of Fx, which results in the appearance of the characteristic spectrum of Chlide a. The FPs perform energy transfer from Fx to Chlide a, while the FCPs of fraction 3 do not perform the corresponding energy transfer from Fx to Chl a. Even though it is known that FCPs, the non-occurred energy transfer in FCPs is probably due to the fact that the Fxs are fewer than the Chls. However, the information obtained from the above studies needs further investigation via, same time, optimization of the data acquisition conditions (stirring, time window and excitation wavelengths). The participation of diatoms in the management of atmospheric pollution and of FCPs in photovoltaic systems, makes them important for the field of biotechnology, so the information obtained in this research is expected to offer important basic knowledge in the specific fields of technological development and applications.

8.1.4. Resonance Raman spectroscopy of ^{13}C isotope-enriched Fucoxanthin-Chlorophyll a/c-binding proteins (FCPs) in intact

membranes of the Marine Diatom Frag. sp

One objective of this work is to identify the Chlorophyll a/c and carotenoids by isotopic labeling. The magnitude of the isotopic shift agrees well with the calculated shift based on empirical normal-coordinate analysis using isotopes of Chlorophyll a/c. The distinct isotopic shift of the C-C and C=C modes of Fx/Dd in the ^{13}C-labeled FCPs confirm their presence in the unstable FP and stable FCP. With the observation of ^{13}C sensitive modes in Chlorophyll a/c, Fx/Dd and secondary structure of the FCPs the dynamic of the protein has been demonstrated.

8.2. Future Work

The use of high light intensity for the growth of organisms has led to observations made for the first time in these species. Thus, it appears that it would be useful to study the response of diatoms to a variation of light intensities as well as different wavelengths that seem to significantly affect the properties of the organism.

In addition to this, spectroscopic studies, using fluorescence spectroscopy and UV to identify changes in energy transfer among the FCP pigments that participate in photosynthesis and photoprotection of diatoms due to different lighting conditions growth will lead to the clarification of energy pathways during stress time or natural conditions.

The use of Raman spectroscopy to study the photosynthetic mechanism of diatoms and especially its structure can provide very important information. The use of more isotopes with the methodology used in this thesis will lead to the characterization of a large number of vibrations that appear in the Raman spectra and will help in drawing conclusions and designing experiments for the further study of diatoms.

Finally, the conducted experiments on FCPs can be repeated again but on lipids isolated from the diatoms. The major carbon storage compound in diatoms is lipids. Lipids are the major constituents of diatom cells as their content in diatoms could achieve up to 25% of dry weight although, the production of lipids in diatoms can vary on culture conditions. these experiments will give as insights of lipids behavior, production and composition during stress period and alternative growth conditions.